Technische Universität München

TUM School of Medicine and Health

Constitutive CXCR4 activation and B-cell targeted Myd88^{L252P} collaborate in lymphoproliferation

Nikita Singh

Vollständiger Abdruck der von der TUM School of Medicine and Health der Technischen Universität München zur Erlangung des akademischen Grades einer

Doktorin der Naturwissenschaften (Dr. rer. nat.)

genehmigten Dissertation.

Vorsitz: Prof. Dr. Susanne Kossatz

Prüfer*innen der Dissertation: 1. apl. Prof. Dr. Robert Oostendorp

2. Prof. Dr. Dirk Haller

Die Dissertation wurde am 05.06.2023 bei der Technischen Universität München eingereicht und durch die TUM School of Medicine and Health am 08.11.2023 angenommen.

Table of Contents

ABBREVIATIONS

α	Alpha
β	Beta
γ	Gamma
µl	Microliter
µg	Microgram
-	Negative Expression
*	Significance
%	Percent
° C	Degree Celsius
+	Positive Expression
ABC-DLBCL	Activated B-Cell-Like Diffuse Large B-Cell Lymphoma
ACK	Ammonium Chloride–Potassium Bicarbonate
AID	Activation-Induced Cytidine Deaminase
AKT	Akt Serine/Threonine Kinase 1
ANOVA	Analysis Of Variance
APL	Acute Promyelocytic Leukemia
APS	Ammonium Persulfate
AS-PCR	Allele-Specific Polymerase Chain Reaction
ASC	Antigen Secreting Cell
BCL6	B-cell Lymphoma 6
BCR	B-cell Receptor
Blimp1	B Lymphocyte Induced Maturation Protein 1
BM	Bone Marrow
BMM	Bone Marrow Microenvironment
bp	Base Pair
BSA	Bovine Serum Albumin
BTK	Bruton'S Tyrosin Kinase
C	Cxcr4C1013G
CBM	Card11–Bcl10–Malt1
CD19	Cd19-Cre
cDNA	Complementary Dna
CLL	Chronic Lymphocytic Leukemia
CLP	Common Lymphoid Progenitors
CM-19	Cxcr4C1013G; Myd88L252P; Cd19-Cre
CM-Aid	Cxcr4C1013G; Myd88L252P; Aidcre
Cre	Causes Recombination, Recombinase From Phage Pi
CSR	Class-Switch Recombination
D	Diversity
DAMPs	Danger-Associated Molecular Patterns
DEG	Differentially Expressed Genes
DLBCL	Diffuse Large B-cell Lymphoma

DMEM	Dulbecco´S Modified Eagle Medium
DMSO	Dimethyl Sulfoxide
DNA	2'-Desoxyribonucleosid-5'-Triphosphat
DZ	Dark Zone
EDTA	Ethylenediaminetetraacetic Acid
ELISA	Enzyme-Linked Immunosorbent Assay
ER	Estradiol
ERK	Extracellular-Signal Regulated Kinase
et al.	Et Alii
FACS	Flourescence Activating Cell Sorting
FCS	Fetal Calf Serum
FDC	Follicular Dendritic Cells
FELASA	Federation Of European Laboratory Animal Science Associations
FITC	Fluorescein Isothiocyanate
FL	Follicular Lymphoma
FL-HSPC	Fetal Liver Hematopoietic Stem/Progenitor Cell
FL, fl	Follicular Lymphoma, Fetal Liver, Floxed
Flt3L	Fms-Like Tyrosine Kinase 3 Ligand
FOB	Follicular B-Cells
FSC	Forward Scatter
Fwd	Forward
GC	Germinal Center
GCB	Germinal Center B-cells
gDNA	Genomic Dna
GEM	Genetically Engineered Mouse
GFP	Green Fluorescent Protein
H&E	Hematoxylin And Eosin
HBSS	Hank'S Balanced Salt Solution
HCK	Hematopoietic Cell Kinase
Hoxb8	Homeobox B8
hr	Hour
HRP	Horseradish Peroxidase
HSC	Hematopoietic Stem Cells
HSPC	Hematopoietic Stem And Progenitor Cells
hu	Human
IFN	Interferon
Ig	Immunoglobulin
IgA	Immunoglobulin A
IgD	Immunoglobulin D
IgG	Immunoglobulin G
IgH	Ig Heavy Chain
Ighg1	Immunoglobulin Heavy Constant Gamma 1

IgL	Ig Light Chain
IgM	Immunoglobulin M
IgM MGUS	IgM-Secreting Monoclonal Gammopathy Of Undetermined Significance
IHC	Immunohistochemistry
IL	Interleukin
IL-1R	Interleukin 4 Receptor
IRAK	IL-1 Receptor-Associated Kinase
IRES	Internal Ribosomal Entry Site
IRF4	Interferon Regulatory Factor 4
ITAM	Immunonotyrosine-Based Activation Motif
J	Joining
JAK	Janus Kinase
JH	Janus Homology Domain
JNK	C-Jun N-Terminal Kinase
kb	Kilobases, 1000 Base Pairs
kDa	Kilodalton
Ki67	Kiel 67
L	Ladder
Lin	Lineage, Linear
LN	Lymph Node
LO	Lymphoid Organs
lo	Low
log	Logarithmic
loxP	Locus Of X Over In Pi, Recognition Sequence Of Cre
LP	Lymphoplasmacytic Cells
LPC	Lymphoplasmacytic Cells
LPL/WM	Lymphoplasmacytic lymphoma/Waldenström macroglobulinemia
LPS	Lipopolysaccharide
LSK	Lin-Sca1+C-Kit
Lymph	Lymphocytes
LZ	Light Zone
M-19	Myd88L252P; Cd19-Cre
M-Aid	Myd88L252P; Aidcre
mA	Milli Ampère
MAPK	Mitogen-Activated Protein Kinase
MCL	Mantle Cell Lymphoma
MHC-II	Major Histocompatibility Complex Class II
MIG	Mscv-Ires-Gfp
min	Minute
ml	Milliliter
mRNA	Messenger Rna

MSCV	Murine Stem Cell Virus
MTOR	Mechanistic Target Of Rapamycin
mut	Mutation
MYC	Myelocytomatosis Oncogene
MYD88	Myeloid Differentiation Primary Response 88
MZ	Marginal Zone
MZB	Marginal Zone B-Cells
MZL	Marginal Zone Lymphoma
n	Number
NF-κB	Nuclear Factor-Kappa B
NHL	Non-Hodgkin's lymphoma
NK	Natural Killer
ns	Not Significant
o/n	Overnight
OS	Overall Survival
PAMPs	Pathogen-Associated Molecular Patterns
PB	Plasmablast
PBS	Phosphate Buffered Saline
PC	Plasma Cell
PCA	Principal Component Analysis
PCR	Polymerase Chain Reaction
Pen/Strep	Penicillin/Streptomycin
PI	Propidium Iodide
PI3K	Phosphatidylinositol 3-Kinase
PIP	Phosphatidylinositol-4,5-Bisphosphate
pol	Polymerase
PRDM1	Pr Domain Containing 1
Pre	Precursor
Pro	Progenitor
PVDF	Polyvinylidene Fluoride
qRT-PCR	Quantitative Real Time Pcr
RAG1/2	Recombinase Activating Gene ½
rev	Reverse
RNA	Ribonucleic Acid
RNASeq	Rna-Sequencing
rpm	Rounds Per Minute
RPMI	Roswell Park Memorial Institute Medium
RT	Reverse Transcriptase, Room Temperature
S1PR1	Sphingosine-1-Phosphate Receptor 1
SDF-1	Stromal Cell-Derived Factor-1
SDS-PAGE	Sodium Dodecyl Sulfate Polyacrylamide Gel Electrophoresis
sec	Second

SEM	Standard Error Of The Mean
SHM	Somatic Hypermutation
SPF	Specific-Pathogen-Free
SPL	Spleen
SSC	Side Scatter
SYK	Spleen Tyrosine Kinase
T1	Transitional 1
T2	Transitional 2
TCR	T Cell Receptor
TD	T-Cell-Dependent
TEMED	N, N, N', N'-Tetramethylendiamine
Tfh	T Follicular Helper
TIR	Toll/Interleukin Receptor
TLR4	Toll-Like Receptor 4
TNF	Tumor Necrosis Factor
TP53	Tumor Protein 53 (Human)
TRAF-6	Tumor Necrosis Factor Receptor-Associated Factor 6
Tris	2-Amino-2-(Hydroxymethyl) Propane-1,3-Diol
Tween 20	Poly (Oxyethylen)N-Sorbitan-Monolaurate
Tyr	Tyrosine
U	Unit
UV	Ultraviolet
V	Volt, Variable
Vol	Volume
WBC	White Blood Cell
WM	Waldenström macroglobulinemia
WT	Wildtype
YFP	Yellow Fluorescent Protein

1. INTRODUCTION

1.1. The immune system

The immune system is composed of a wide variety of cells that have evolved to identify and eliminate a wide range of microbes, as well as to maintain an unresponsive state to coexist with a wide range of self-antigens. The two functional divisions of the immune system are the innate immune system and adaptive immunological responses, the latter of which involves humoral and cell-mediated responses. The immune system employs a variety of defenses to fend against microbial invasion. These processes cooperate, and the fully functional immune response incorporates components from numerous effector systems to specifically target the invading pathogen. Tissue injury can be acute or persistent if different effector systems are not properly regulated. It will be possible to produce more effective vaccinations, better immunomodulatory therapies, and prevent unintended tissue damage by understanding the connections among the various immune effector pathways.

The first line of defense that acts immediately to fend off an infectious attack is the inmate immunity system. Due to the absence of memory, the inmate immunity fails to distinguish between the infectious agents and has no benefit in efficacy despite repeated exposure. When infection or disease first manifests, the innate immune system is one to react. In all multicellular creatures, the innate immune response is present in some form. It is composed of a series of highly specialized cells – natural killer cells, myeloid cells as well as marginal zone B-cells, and B1 cells, which control the infection until adaptive immunity develops and attacks the remaining pathogens (Flajnik, 2002; Litman et al., 1999). Three types of defense mechanisms make up the innate immune system: physical barriers, cellular components, and humoral responses (Chaplin, 2010; Riera Romo et al., 2016). Pattern-recognition receptors (PRRs), whose specificity is genetically determined and highly conserved, allow cells of the innate immune system to selectively recognize pathogen-derived antigens (Kyewski et al., 2002). The Toll-like receptors (TLR) family includes these receptors, which can detect pathogen-associated molecular patterns (PAMPs) that are only expressed in the cells of

microbes and are not present in host cells (Aderem, 2000). The type I transmembrane proteins TLR possess an intracellular domain like the cytoplasmic domain of the interleukin-1 receptor (IL-1R) that may utilize a similar molecular signaling pathway. IL-1 activation facilitates several transcriptional factors, including nuclear factor kappa B (NF-κB) and c-jun/AP-1 which are responsible for triggering several co-stimulators, pro-inflammatory cytokines, and chemokines (Burns et al., 2003; O'Neill & Bowie, 2007)

In contrast to the innate immune system, the adaptive immune system displays high specificity for its target antigens. Adaptive responses mostly depend on the antigen-specific receptors expressed on the cell surface of B- and T-lymphocytes. The adaptive immune response's antigen-specific receptors, in contrast to the innate immune system's germ-line-encoded recognition molecules, are encoded by genes that are put together by somatic rearrangement of germ-line gene elements to form intact T-cell receptor (TCR) and immunoglobulin (B-cell antigen receptor; Ig) genes. Although the innate immune system acts as the initial line of defense for the host and the adaptive immune system emerges within a few days once antigen-specific T- and B-cells have undergone clonal expansion, the two immune systems are frequently seen as opposing, distinct parts of the host response.

1.2. B-lymphocytes

Both B- and T-cells are genetically programmed to encode for a surface receptor and are responsible for the recognition of a particular antigen. B-cells are lymphocytes that are specialized in the production of antibodies. Moreover, B-cells also work as antigen-presenting cells which activate T-cells and facilitate the production of cytokines that modulate immune response (Allman & Pillai, 2008).

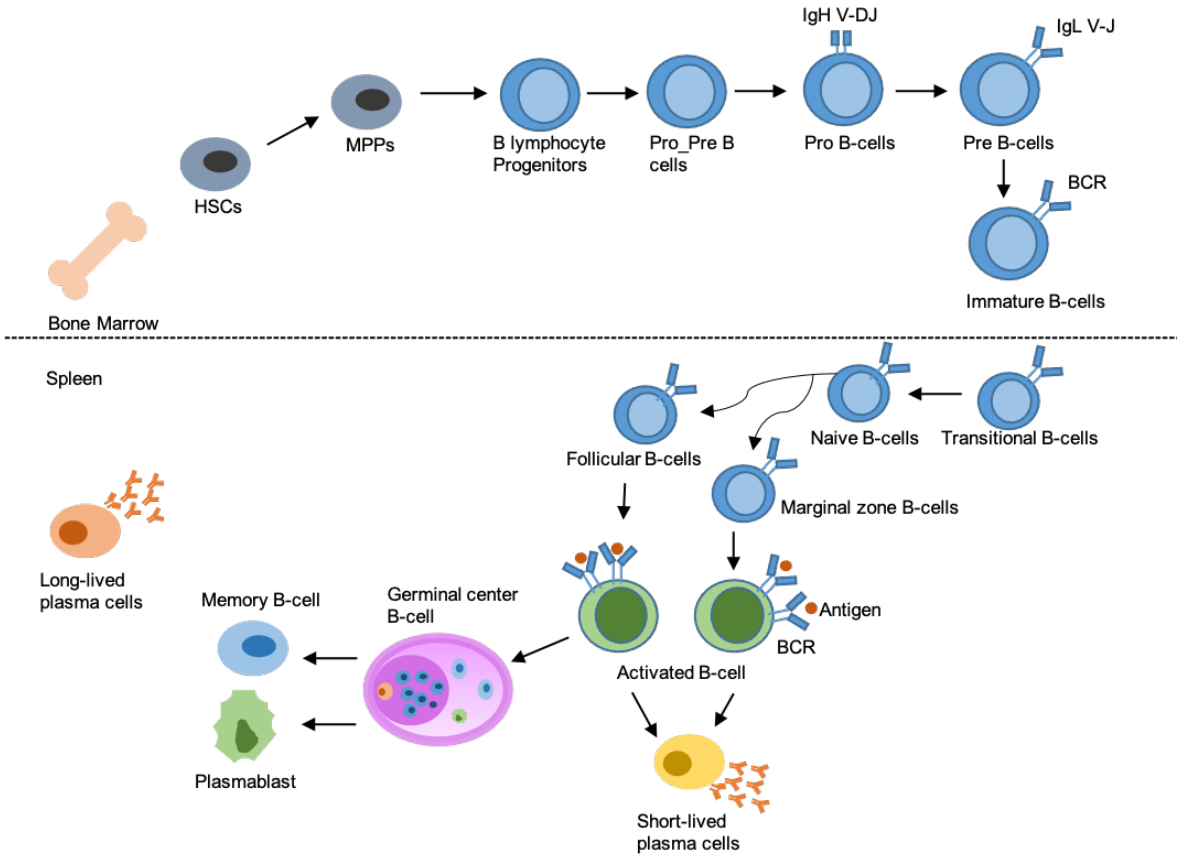

Figure 1. A graphical illustration depicting the different developmental stages in B-cell development. Early B-cell development in the bone marrow depends on the recombination of gene segments VDJ to produce functional BCR. Immature B-cells migrate to the spleen and differentiate into transitional cells. Mature B-cells differentiate in the spleen to form Follicular and Marginal Zone B-cells. Following exposure to antigen, a marginally small percentage of activated B-cells differentiate into short-lived plasma cells, while the majority take part in germinal center reaction in the spleen and differentiate into plasmablasts, memory B-cells, or antibody-secreting plasma cells which have the potential to migrate back to bone marrow. Adapted from (Edwards & Cambridge, 2006; Samitas et al., 2010).

1.2.1. Early B-cell development

B-cells develop from hematopoietic stem cells (HSCs) in the bone marrow, following very tight regulation HSCs give rise to multipotent progenitor cells which further differentiate into a common lymphoid progenitor giving rise to the Pro-B-cell stage (Hardy & Hayakawa, 2001; Melchers, 2015) (Fig. 1). The passage from the pro-B-cell stage to the large and later small pre-B-cells, culminating in the immature B-cell stage, makes up the early B-cell differentiation in the bone marrow. Pro-B-cells are identified by the expression of the c-kit and the IL-7 receptor alpha (IL-7R), which are essential for cell survival and proliferation. The expression

of c-kit and IL-7 receptor alpha is downregulated whereas that of IL-2 receptor alpha (IL-2R or CD25) is upregulated when cells develop into pre-B-cells. When the immunoglobulin heavy-chain (IgH) and light-chain (IgL) loci are efficiently rearranged to create a functioning non-self-reactive BCR, survival signals are produced that are closely linked to the progression through these stages. (Hardy & Hayakawa, 2001; Melchers, 2015). The immunoglobulin genes undergo two additional mechanisms that increase their diversity as they mature in the germinal center (GC). The first one results in point mutations in the already rearranged genes and is known as somatic hypermutation (SHM). The second is known as class switch recombination (CSR), which transforms immunoglobulin class immunoglobulin M (IgM) into immunoglobulin G (IgG), immunoglobulin D (IgD), or immunoglobulin A (IgA). Several transcription factors control the development of B lymphocytes, which is accompanied by several alterations in the immunophenotype of the cells. The first step in the maturation process is the differentiation of B-cell progenitors from hematopoietic stem cells into naive mature B lymphocytes in the bone marrow, which is followed by maturation into memory/effector cells in the secondary lymphoid organs, bone marrow, and spleen (Perez-Andres et al., 2010). Immunoglobulin heavy chain (Igh) DH-JH recombination is initiated by the Recombinase activating gene ½ (RAG1/2) recombinases, which results in the loss of the ability to differentiate into non-lymphoid lineages (Igarashi et al., 2002).

Numerous transcription factors that control the growth of cells are expressed and repressed in conjunction with the specification of the B-cell lineage. According to Busslinger M (2004), the multi-lineage potential of early lymphoid progenitors and common lymphoid progenitors (CLPs) is still present, and the B-cell lineage is still flexible up until progenitor B-cells (pro-B) express the B220 and CD19 cell surface proteins (Rumfelt et al., 2006).

1.2.2. VDJ/clonality

V(D)J recombination, which is primarily facilitated by RAG1/2 recombinase, is the term used to describe the ordered lineage-specific rearrangement of genes where after diversity (D) and

the joining (J) genes undergo lineage-specific recombination event (D-J) initiated in CLP, followed by the sequential recombination of the variable (V) gene (V-DJ). All Rearrangement is mediated by recombination signal sequence and RAG1/2 is responsible for the double-stranded breaks at these sites which initiates recombination (Oettinger et al., 1990). The dsDNA cleaved by the RAG1/2 is then shielded by a pair of hairpin loops; the Artemis which is a DNA-dependent protein kinase complex that facilitates the opening of the hairpin for repair (Ma et al., 2013). A blunt-end results from cleavage that occurs at the apex of the hairpins. In contrast, cleavage may occur several base pairs away from the apex, producing single-stranded overhangs. Palindromic DNA sequences that weren't present in the germline are produced because of filling these overhangs. The repairs majorly took place with the assistance of RAG1/2 recombinases, non-homologous end joining repair equipment, and terminal deoxynucleotidyl transferase. (Agrawal & Schatz, 1997; Schatz & Ji, 2011).

The pre-BCR, which includes the signal-transducing elements Ig-α and Ig-β (CD79-a and CD79-b), is transported to the cell surface after successful VHDJH recombination where the resultant heavy chain is conjugated to a substitute Ig light chain (IgL). For persistent differentiation into pre-B-cells, pre-BCR signaling is essential (Karasuyama et al., 1994; Pillai S & Baltimore D, 1987). The early B-cell stage is defined by efficient light chain rearrangement at either the Ig kappa or lambda light chain locus, which results in a complete BCR and an IgM molecule that is expressed on the cell surface. Immature B-cells depart from the bone marrow (BM) as transitional B-cells to the spleen where they complete their maturation.

1.2.3. Transitional B-cells

Immature B-cells move from the bone marrow to the spleen, whereas like in the BM, their development is a multistage process governed by several transcriptional factors and checkpoints (Allman et al., 2001; Loder et al., 1999). Based on differences in cell-surface marker expression, sensitivity to BCR signaling and T-cell assistance, and defined anatomical placement in the spleen, the passage of immature to mature B-cells can be separated into

three "transitional" stages: T1, T2, and T3. They are all transient cells that lack the functionality of mature B lymphocytes due to being nonresponsive toward antigen stimulation, making them all functionally incompetent (Chung et al., 2003; Hardy et al., 2007; Niiro & Clark, 2002).

T1 cells are the transitional B-cells that are the least developed and are identified by membrane-bound IgM, whereas T2 cells are late-developing cells and are identified by the expression of membrane-bound IgD as well as the surface markers CD21 and CD23. The mature naive B-cells are formed from the differentiation of these subgroups of transitional B-cells. In addition to this, there is a subset of the intermediate T3 developmental stage that has lower IgM levels and is similar to the T2 subset. It has been hypothesized that the cells in the T3 subgroup belong to self-reactive clones that have developed into anergic cells (Allman & Pillai, 2008; Chung et al., 2003; Matthias & Rolink, 2005). During T1 development, antigen-independent BCR signaling activates proximal phosphatidylinositol 3-kinase (PI3K) and AKT signaling pathways to boost B-cell survival and rescue B-cells from apoptosis. These signals are necessary for a successful transition from T1 to T2 B-cells. Additionally, to advance to the T2 stage, distal BCR signaling must be activated, which causes canonical NF-kB activation (Gerondakis & Siebenlist, 2010; Kurosaki et al., 2010).

1.2.4. Mature B-cells

Late transitional 2 (T2) B-cells differentiate into follicular B-cells (FOB) and marginal zone B-cells (MZB) (Fig. 1). FOB-cells are characterized by intermediate expression of CD21 and high expression of CD23, as well as high membrane-bound IgD expression with reduced IgM expression. Contrary to that, MZB-cells are characterized by high CD21 expression, negative expression of CD23, and high membrane-bound IgM along with reduced IgD expression. The fate of late immature B-cell differentiating into FOB or MZB is dependent upon the BCR signaling pathway, BAFF along with Notch 2 and cytokine-dependent signaling pathways influence the cellular fate of MZB-cells (Allman & Pillai, 2008; Casola et al., 2004; Niiro & Clark, 2002). FOB-cells participate in the T-cell-dependent immune response, as they have the ability

of antigen presentation and participate activate T-cells. Activated follicular B-cells could develop into short lives plasma cells early in a T-cell-dependent response. However, these short-lived plasma cells cannot migrate to distant locations. Meanwhile, activated germinal center B-cells may differentiate to form plasmablasts and may obtain the ability to migrate to the bone marrow where they may be sustained as long-lived plasma cells, this phenomenon is facilitated with help of the interaction of APRIL and/or BAFF, which are produced by stromal cells and interact with BCMA, a receptor of the BAFF-R family. Follicular B-cells are not only located in follicles in traditional secondary lymphoid organs but also in the bone marrow, where they gather in distinct groups near vascular sinusoids (Cariappa et al., 2005, 2007a; O'Connor et al., 2004).

On the other hand, MZB cells are thought to be innate-like cells that, in the absence of BCR ligation, can be stimulated to develop into short-lived plasma cells. MZB-cells may also be implicated in T-dependent B-cell responses, immunological responses to lipid antigens, and the transfer of antigens in immune complexes into splenic follicles (Allman & Pillai, 2008). MZB-cells are pre-activated B-cells that can self-renew and express high quantities of the co-stimulatory molecules CD80 and CD86 as well as the major histocompatibility complex class II (MHC-II) (Attanavanich & Kearney, 2004; Song & Cerny, 2003). Additionally, they have the capacity to carry antigens and immune complexes, can operate as antigen-presenting cells as they move between the marginal zone and the follicle, and exhibit high levels of MHC-II, CD80, and CD86 needed for the immunological synapse (Cinamon et al., 2008; Pillai & Cariappa, 2009). NF-κB signals have a crucial role in both the differentiating of FOB- and MZB-cells as well as the regulation of their development. However, the importance of NF-κB signals for MZB-cell development cannot be overstated (Pohl et al., 2002).

1.2.5. Germinal center B-cells

Upon antigen encounter, the naïve B-cells may follow three different fates. They can first escape the follicle and develop into short-lived extrafollicular plasmablasts that produce poor

affinity antigen-specific antibodies. Secondly, they may migrate to the T-cell zone and differentiate into memory B-cells (Takemori et al., 2014). Thirdly, they migrate to the follicular niche where with the help of follicular helper T-cells (Tfh) they form germinal center B-cells (GCB) and further mature into either antibody-secreting plasma cells or high-affinity memory B-cells (Klein & Dalla-Favera, 2008; Takemori et al., 2014; Zhang et al., 2016; Zotos & Tarlinton, 2012). Germinal center B-cells are characterized by the high expression of death receptor FAS (CD95) and GL7 monoclonal antibody. Additionally, they are also negatively selected through the downregulation of CD38.

The germinal center comprises two distinct zones, namely the dark zone (DZ) and the light zone (LZ) (Allen et al., 2007; Victora & Nussenzweig, 2012). A dense network of B-cells with increased proliferative activity makes up the DZ. The LZ, on the other hand, has a reduced density of B-cells and is home to follicular dendritic cells (FDCs), which bind immunocomplexes that carry antigens, as well as T follicular helper cells (Maclennan, 1994). The chemokine CXCL12 and its receptor CXCR4 are necessary for the development of the DZ and the LZ, whereas the chemokine CXCL13 and its receptor CXCR5 are necessary for the correct polarization of the DZ and LZ (Klein & Dalla-Favera, 2008). GC B-cells migrate back and forth between the DZ and LZ in a proportion of about 30%, where they undergo further mutation and growth. A B-cell's ability to deliver antigen appears to determine whether it will return to the DZ or instead differentiate into a memory B-cell or plasma cell (Hauser et al., 2007). Centroblasts, which are highly proliferating B-cells in the DZ, undergo somatic hypermutation to somatically mature their BCR by reducing their BCR expression. While in the LZ, cells cease proliferation, downregulate the expression of CXCR4, and migrate to the high CXCL13 gradient of LZ with help of CXCR5 expression (Klein & Dalla-Favera, 2008). Going further the chosen centrocyte in the LZ upregulates its CXCR4 expression and migrates to DZ for enhancing its BCR affinity. Cell in the DZ goes through a series of SHM for antibody affinity maturation process which is initiated by Activated induces deaminase enzyme (AID). In this process, the immunoglobulin variable region undergoes single nucleotide swaps throughout, changing C: G base pairs into U: G base pairs that must be repaired by the cell's

DNA-repair machinery. Therefore, changes in the immunoglobulin variable region acquired during GC passage can be used to identify GC-experienced B-cells. The B-cells go through a further procedure known as class switch recombination, where they switch their immunoglobulin heavy chain mu (IgM) and delta (IgD) constant regions for a different class, in an AID-dependent mechanism, after having been positively selected for high-affinity antibodies in the LZ (Klein & Dalla-Favera, 2008; Zhang et al., 2016).

The transcriptional repressor B-cell lymphoma 6 (BCL6) and the transcription factor Interferon regulatory factor 4 (IRF4) control the establishment and functioning of the GC reaction (B H Ye et al., 1997; de Silva et al., 2012; Ochiai et al., 2013; Willis et al., 2014). In the LZ, CD40 signaling prevents cells from going into apoptosis and encourages the production of the transcription factor IRF4 under the control of NF-κB. High amounts of IRF4 suppress Bcl6, promote AID expression for CSR, and activate the transcription factor B lymphocyte-induced maturation protein 1 (Blimp1) which is necessary for commitment towards PC fate (Klein & Dalla-Favera, 2008; Nutt et al., 2015; Zotos & Tarlinton, 2012) other transcription factors that play a major role are IL-4 which is crucial for DZ proliferation, following SHM, and differentiation into memory B-cells as well as IL-21, which is involved in early plasma cell formation and generation of antibody-secreting PC (Nojima et al., 2011; Zotos & Tarlinton, 2012)

1.2.6. Antibody secreting cells (plasmablasts and plasma cells) and memory B-cells

Following their exit from the follicle, the B-cells undergo differentiation into memory B-cells and long-lived plasma cells (Fig. 1). During the B-cell's development into plasma cells, there is a strict transcriptional regulation at the germinal center stage. The B-cell transcriptional pathway is driven by Pax5, Bcl6, and Bach2, whereas Blimp1 and Xbp1 regulate plasma cell development. Research so far has been focused on the factors that regulate the commitment of activated B-cells to the ASC fate. However, the transitional steps between short lives plasmablasts, cyclic plasma cells, and long-lived plasma cells still need to be deciphered (Nutt

et al., 2015). Long-lived PCs can produce high-affinity antibodies of several isotype classes and express the surface marker Syndecan-1 (CD138) (Aref et al., 2003). Based on the expression of Blimp1, plasmablasts and plasma cells may be separated prospectively, with plasmablasts showing a noticeably lower level of Blimp1expression than plasma cells. Whether plasma cells are a direct byproduct of GC B-cells or if they undergo a plasmablasts-like stage is still a matter of debate. Following primary immunization, analysis of the circulating antigen-specific cells in the blood of mice reveals that the ASCs, which are thought to be the precursors of the long-lived bone marrow plasma cells, express intermediate amounts of Blimp1and resemble plasmablasts. These cells upregulate Blimp1expression to levels that are indicative of plasma cells once they have reached the bone marrow (Blink et al., 2005; Kabashima et al., 2006). According to an analysis of the chemokine sensitivity of plasmablasts, only a portion of plasmablasts respond to bone marrow tropic factors. This finding suggests that only these responsive cells are the precursors of plasma cells, with the majority of the cells making up a distinct, transient entity. Furthermore, after a recall challenge, ASCs in the blood show the proliferation marker Ki67, which is consistent with them becoming plasmablasts (Odendahl et al., 2005). Most plasma cells are found in the bone marrow in healthy individuals, although long-lived plasma cells can also be found in non-lymphoid organs and other lymphoid organs throughout the body in disease conditions. The fact that plasma cells experience fast cell death when removed from the bone marrow microenvironment suggests that the lifetime of these cells is not intrinsic (Chu et al., 2012). Although the process of homing and retention of these long-lived plasma cells in bone marrow is poorly understood, it is known that activation of sphingosine-1-phosphate receptor 1 (S1PR1) is crucial for the efficient escape of ASCs from the secondary lymphoid organs whereas the CXCL12 and CXCR4 are important for the recruitment and retention of ASCs to the bone marrow site (Kabashima et al., 2006).

In general, the germinal center is considered to be the only site of memory B-cell generation. However, recent research has shown that memory B-cells also develop in response to a T-cell-dependent (TD) antigen before the GC reaction begins and independently of it. The two

classes of memory B-cells develop over the same period and achieve functional maturation across the distinct but heavily related transcriptional program. The production of GC-dependent memory B-cells requires T follicular helper cell assistance, whereas the generation of GC-independent memory cells do not, even though both forms of memory B-cell development require the assistance of conventional T-cells. These results lead to the conclusion that B-cell memory is produced through two cellular differentiation pathways that are fundamentally different from one another (Takemori et al., 2014; Tangye & Tarlinton, 2009). Memory B-cells are long-lived quiescent B-cells with a different phenotype from other types of B-cells, such as the capacity to elicit a more rapid and robust response upon re-exposure to an antigen compared to naive B-cells that have never encountered an antigen before. Memory B-cells typically undergo CSR and display antibodies of other isotypes, whereas naive B-cells only express IgM and IgD on the surface. Thus, antigen-binding cells expressing class-switched immunoglobulin in conjunction with high levels of CD38 and low expression of PNA surface molecules can be identified as mouse memory B-cells (Ridderstad & Tarlinton, 1998; Takahashi et al., 2001). Although there is no specific biomarker known for memory B-cells, CD80, CD86, PD-L1, PD-L2, MHC class II, and CD73 have been shown to be expressed in memory B-cells in the spleen (Good-Jacobson et al., 2010; Takahashi et al., 2001) as opposed to Germinal center B-cells and näive B-cells (Anderson et al., 2007).

1.3. T-lymphocytes

T-cells, which are characterized by the presence of a unique receptor on their cell surface, called the T-cell receptors are the second important cell type that makes up adaptive immunity. While the antigen-independent maturation of the B-cells mainly occurs in the bone marrow before migration into the secondary lymphoid organs like the spleen, the development and maturation of T-cells initiates with hematopoietic stem cells in the fetal liver and follows in the bone marrow where HSC differentiates into multipotent progenitors. Only a small subset of these multipotent progenitor cells migrates and undergo maturation phases in the thymus

starting with early thymic progenitors to forming fully functional T-cells (Cesar Nunez et al., 1996)(Cariappa et al., 2007; Kruisbeek, 1999; Yang et al., 2010). Unlike BCR which is able to recognize antigens directly, TCR only recognizes short peptides of protein antigen presented by the major histocompatibility complexes on the surface of the antigen-presenting cells (Eter et al., 2000). Before maturation, T-cells that express the distinctive surface molecule cluster of differentiation 3 (CD3) engage in positive and negative selection through interactions with MHC-I and MHC-II complexes in the thymus. The matured T-cells are composed of two subsets: CD4+ helper T-cells and CD8+ cytotoxic T-cells defined by surface markers CD4 and CD8, respectively (Eter et al., 2000). The matured T-cells exit the thymus and enter the bloodstream in a naive condition, where they remain dormant until they come into contact with any nearby antigens. The TCR complex includes CD4 and CD8 molecules. While CD8 helps TCR recognize antigens presented by MHCI molecules, CD4 helps TCR recognize antigens presented by MHC-II. When CD8+ T-cells mature into cytotoxic T lymphocytes (CTLs) in secondary lymphoid organs, they are able to cause the cytolysis/apoptosis of infected and transformed cells via the FASL (CD95) route. Additionally, in order to carry out their cytotoxic function, CTLs generate cytokines including IFN-γ and tumor necrosis factor (TNF) which play important roles in the defense against viral infections and controlling the proliferation of tumoral cells (Barry & Bleackley, 2002; Cox et al., 2013). Naive CD4+ T-cells differentiate into effector T-cell lineages with carrying double function of producing cytokines and stimulating B-cells to generate Abs. These include T helper cells type 1 (Th1), Th2, Th17, and T follicular helper cells, as well as regulatory T-cells (Treg) (Dutton et al., 1998; Sprent & Surh, 2002). The majority of effector T-cells do not survive after the primary responses, but a small percentage survive and develop into long-lived memory cells. Recently, T follicular regulatory (Tfr) cells were identified as a distinct subpopulation of T helper cells. Tfr cells share characteristics of both Treg and Tfh cells and act as a key suppressor of ongoing GC reactions (Fonseca et al., 2019)

1.4. TLR/MyD88 signaling pathway

Toll-like receptors are a family of type I transmembrane receptors that play a crucial role in the innate immune response (Li et al., 2013). They are abundantly expressed on several immune response-related cells, such as macrophages, dendritic cells, T-cells, B-cells, and epithelial cells (Fernández-Paredes et al., 2017). TLRs are divided into groups based on their localization, intracellular or extracellular. TLR1, TLR2, TLR4, TLR5, TLR6, and TLR11 are normally expressed on cell surfaces; whereas TLR3, TLR7, TLR8, and TLR9 are found intracellularly (Zheng et al., 2020). Genetic analysis of the physiological function of TLR revealed essential roles for TLR in pathogen recognition. Each TLR recognizes a specific component of a pathogen, hence demonstrating that the mammalian immune system detects pathogen invasion via the recognition of microbial components, with each TLR recognizing a specific component of a pathogen (Takeda et al., 2003). TLR1, TLR2, TLR5, and TLR6 recognize microbial membrane components, such as lipoproteins, and flagellin; TLR9 recognizes unmethylated CpG motifs; TLR3 is implicated in the recognition of viral dsRNA; and TLR4 recognizes lipopolysaccharide (LPS). TLR4 requires several membrane-linked molecules such as CD14 and MD-2 to recognize LPS (Tobias et al., 1988; Shimazu et al., 1999; Li et al., 2013; Fernández-Paredes et al., 2017; Zheng et al., 2020; Takeda et al., 2003; Tobias et al., 1988; Shimazu et al., 1999)

The activation of TLR signaling pathways originates from the cytoplasmic Toll/interleukin-1 (TIR) (Gray et al., 2006) domains. The role of the TIR domain was revealed in the C3H/HeJ mouse strain, which had a point mutation that resulted in an amino acid change in the form of substitution of histidine from proline at position 712 (Poltorak et al., 1998) (Akira Sanjo et al., 1999). In the signaling pathway downstream of the TIR domain, is the TIR domain-containing adaptor MyD88, which plays a crucial role, and it is also essential for signaling via IL-1 and IL-18 receptors (Kawai et al., 1999).

Recent evidence shows that TLR signaling pathways consist of at least a MyD88-dependent pathway that is conserved to all TLRs, and a MyD88-independent pathway that is specific to

the TLR3- and TLR4 signaling pathways (Akira, 2001). MyD88 possesses the TIR domain in the C-terminal portion and a death domain in the N-terminal portion. When TLR recognizes PAMPs or danger-associated molecular patterns (DAMPs), MyD88 interacts with the IL-1 receptor families. Upon stimulation, MyD88 recruits IL-1 receptor-associated kinase (IRAK) to TLR through the interaction of the death domains of both molecules to form the MyD88-IRAK-4 complex, which recruits IRAK-1 and IRAK-2, resulting in the activation of IRAKs by phosphorylation. IRAKs interact with tumor necrosis factor receptor-associated factor 6 (TRAF6) inducing activation of TAK-1 and TAB2/3 following subsequent activation of IkB and mitogen-activated protein kinase (MAPK) leading to the activation of two distinct signaling pathways, and finally to the activation of c-Jun N-terminal kinase (JNK) and NF-κB (Lin et al., 2010; Zheng et al., 2020). MyD88 knockout mice have been widely used to study TLR signaling pathways. MyD88 deficient mice were reported to show no response to the TLR4 ligand LPS and were insusceptible to inflammatory mediators, B-cell proliferation, or endotoxin shock (Kawai et al., 1999).

1.5. BCR signaling pathway

In both normal and pathological circumstances, the B-cell receptor (BCR) plays a critical role in signaling that promotes B-cell survival, development, and antibody production. Diverse B-cell subpopulations and developmental phases exhibit different BCR signaling characteristics, which can be divided into tonic and, chronic active. The beginning of B-cell activation and differentiation into antibody-secreting cells depends on antigen-driven priming signaling. Tonic BCR signaling must be constant for B-cells to survive and develop, however, chronic active BCR signaling promotes the unabated growth of B-cell lymphoma cells. Although the precise molecular mechanism underpinning various BCR signaling patterns has remained a mystery in immunology, the development and emergence of cutting-edge technology including next-generation sequencing have substantially increased our understanding in this area recently (Kwak et al., 2019; Liu et al., 2020; Rickert, 2013). Many common B-cell malignancies, such

as diffuse large B-cell lymphoma (DLBCL), Burkitt lymphoma, chronic lymphocytic leukemia (CLL), follicular lymphoma (FL), marginal zone B-cell lymphoma, Waldenstrom's macroglobulinemia (WM), and mantle cell lymphoma (MCL) have the B-cell receptor pathway identified as a potential therapeutic target (Efremov et al., 2020).

While the majority of BCR-expressing malignancies are assumed to be prone to malignant transformation, the BCR may act as a tumor suppressor in BCR-negative B-cell malignancies (Bräuninger et al., 2001; Sander et al., 2012). According to the expression of several surface markers, developing B-cell receptors can be divided into different stages. The variety of B-cell receptor specificities is produced by VDJ recombination of gene segments during early B-cell development, a process that carries the possibility of developing BCRs that recognize and destroy self-structures. Numerous studies have shown that the pre-B-cell receptor (pre-BCR), which signifies a crucial stage in the formation of B-cells, also functions as a surrogate for the autoreactive receptor. After further rearrangement and maturation, κ or λ light chains, together with the μ heavy chain form the BCR on mature B-cells (Herzog & Jumaa, 2012). Although it is only transiently expressed, the pre-BCR marks an important checkpoint in B-cell development (Herzog et al., 2009). Despite having similar signaling complexes and using the same signal transduction pathway, the main difference between BCR and Pre BCR is how the signaling is initiated and although the pre-BCR and the BCR both have ligand-independent signaling, mature B-cells are normally triggered by the BCR being engaged by an antigen, such as in germinal centers. Despite having comparable structural characteristics, pre-BCR and BCR signaling outcomes can differ and may be influenced by cellular organization, the expression of downstream mediators (such as transcription factors), and chromatin structure (Buchner & Müschen, 2014; Herzog et al., 2009; Rickert, 2013).

One of the main steps following the stimulation of BCR by antigen engagement is the activation of the SRC family protein tyrosine kinase LYN and the spleen tyrosine kinase (SYK). SYK binds to phospho-tyrosine residues within the CD79 immunonotyrosine-based activation motif (ITAM) domain and is activated (Flaswinkel & Reth1, 1994; Sanchez et al., 1993). The autophosphorylation of SYK due to its binding to ITAM facilitates kinase activity subsequently

leading to SYK-mediated phosphorylation of the neighboring BCR and Pre BCR complexes which in turn leads to a positive feedback loop, making SYK a central player in the activation of the pathways which regulate proliferation and differentiation of Pre-B-cells. This was depicted in SYK deficient mice which demonstrated developmental block at the Pre-B-cell stage and failed to undergo clonal expansion (Cheng AM et al., 1995; Fu È Tterer et al., 1998; Gallwitz et al., 2002; Rowley RB et al., 1995). Activated SYK then phosphorylates downstream adaptor molecules like BLNK and BCAP. Phosphorylated BLNK act as a scaffold for membrane-associated kinases PLCγ2 (PLCG2) and bruton's tyrosine kinase (BTK) and facilitates their activation (Satpathy et al., 2015). A series of pathway activation is followed including phosphorylation of membrane phospholipid phosphatidylinositol-4,5-bisphosphate (PIP2) and its conversion to phosphatidylinositol-3,4,5-triphosphate (PIP3) which is triggered by activated PI3Kδ. PIP3 is responsible for recruiting several downstream signaling molecules (Efremov et al., 2020). This catalytic activation of downstream targets induces the formation of a CARD11–BCL10–MALT1 (CBM) signaling complex that activates the transcription factor NF-κB (Antony et al., 2004; Blonska & Lin, 2009) along with MYC and NFAT.

1.6. CXCR4/CXCL12 signaling pathway

Chemokines are small (8–12 kDa) cytokines that control cell chemotaxis and arrest by interacting with specific cell surface receptors. Chemokines are well known to actively participate in hematopoiesis, mitogenicity, embryogenesis, as well as innate and adaptive immunity (Blanchet et al., 2012; Gerber et al., 2009; Mukaida et al., 2014; Ono et al., 2003). They are divided into four subfamilies based on how the different cysteine residues are arranged at the amino terminus (CC, CXC, CX3C, and C) (Nomiyama et al., 2013; Zlotnik et al., 2011). G-protein-coupled receptors (GPCR) and other receptors are bound and activated by chemokines, which chemotactically direct immune cells to specific sites (Gerber et al., 2009; Zlotnik et al., 2011). The homeostatic CXC chemokine stromal cell-derived factor-1 (SDF-1), commonly known as CXCL12, has seven distinct isoforms (Bachelerie et al., 2014).

Human organs such as the bone marrow, lymph nodes, lungs, liver, endothelial, and stromal cells all exhibit high levels of CXCL12 expression (Barrera et al., 2001; Guo et al., 2016; Sugiyama et al., 2006)). The main contributors to tumor development have been identified as CXCL12 and its receptor, CXCR4. In addition to CXCR4, CXCR7 has also been discovered to have a strong affinity for CXCL12 (Naumann et al., 2010). By interacting with its ligand CXCL12, CXCR4 has a biological effect on cells. CXCL12/CXCR4 axis leads to activation of the downstream protein kinase B AKT/MAPK and extracellular-signal regulated kinase (ERK) signaling cascade associated changes like gene expression, actin polymerization, facilitation of tumor cell growth, cell skeleton reorganization, and dissemination and cell migration (Décaillot et al., 2011; Saba et al., 2017; Sun et al., 2002). Moreover, progenitor cells that have CXCR4 expressed throughout embryonic development can migrate from their place of origin to the location where they would eventually differentiate into organs and tissues. The lethal phenotype of CXCR4/CXCL12-deficient animals supports its crucial role in embryonic development as well as indicates its function not being limited to the hematopoietic system (Nagasawa Takashi et al., 1996)

In tumor cells, CXCR4 can be stimulated in a variety of ways. First, CXCR4 signaling can be increased by hypoxia (Romain et al., 2014). Second, the expression of CXCR4 can be positively regulated by the Wnt signaling pathway (Yu et al., 2014). Third, CXCR4 expression can also be induced by NF-kB. The NF-kB subunits p50 and p65 attach to the CXCR4 promoter, where there is an NF-kB binding site, activating CXCR4 transcriptionally and promoting tumor invasion (Esencay et al., 2010; Helbig et al., 2003; Maroni et al., 2007). One of the major biological effects modulated by the CXCL12/CXCR4 axis is to regulate angiogenesis (Cai et al., 2014; Liang et al., 2007), promote tumor cell survival, progression, and metastasis (Bartolomé et al., 2009; Choi et al., 2014; Wang et al., 2014), and induce epithelial-mesenchymal transition (Onoue T et al., 2006). The CXCL12 axis also indirectly influences anti-apoptotic effects in cancer cells. As previously reported, the CXCL12/CXCR4 axis activates ERK and AKT, which subsequently leads to NF- κB accumulation, suppressing apoptotic signaling and promoting transcriptional activation (Ganju et al., 1998). CXCR4 is

overexpressed in more than 20 different cancer types including Multiple myeloma, chronic lymphocytic leukemia, Hodgkin lymphoma, non-Hodgkin lymphoma, and other lymphoproliferative diseases. Moreover in vivo studies have demonstrated CXCR4 involvement in the tumor microenvironment and promoting chemoresistance. As a result, CXCR4 is a biomarker of great importance for the therapeutic target for cancer but also CXCR4 antagonists are also useful for preventing CXCR4-dependent tumor-stroma interactions, which can reduce tumor growth and metastasis and increase the sensitivity of tumor cells to anticancer therapies.

1.7. Crosstalk between TLR-BCR-CXCR4/CXCl12 pathway

B-cells identify antigens through their B-cell receptor. The BCR constitutes the membrane-bound form of Ig in association with the Igα/Igβ (CD79a/CD79b) signaling subunits (Becker et al., 2017). Mature B-cells co-express BCR, as well as both IgM and IgD (Chen & Cerutti, 2011; Geisberger et al., 2006). IgM and IgD-BCR isotypes functionally differ from one another in the manner of antigen binding, the formation of isolated nanoclusters, and their interaction with co-receptors such as CD19 and CXCR4 on the plasma membrane even though they share identical antigen specificity (Maity et al., 2018).

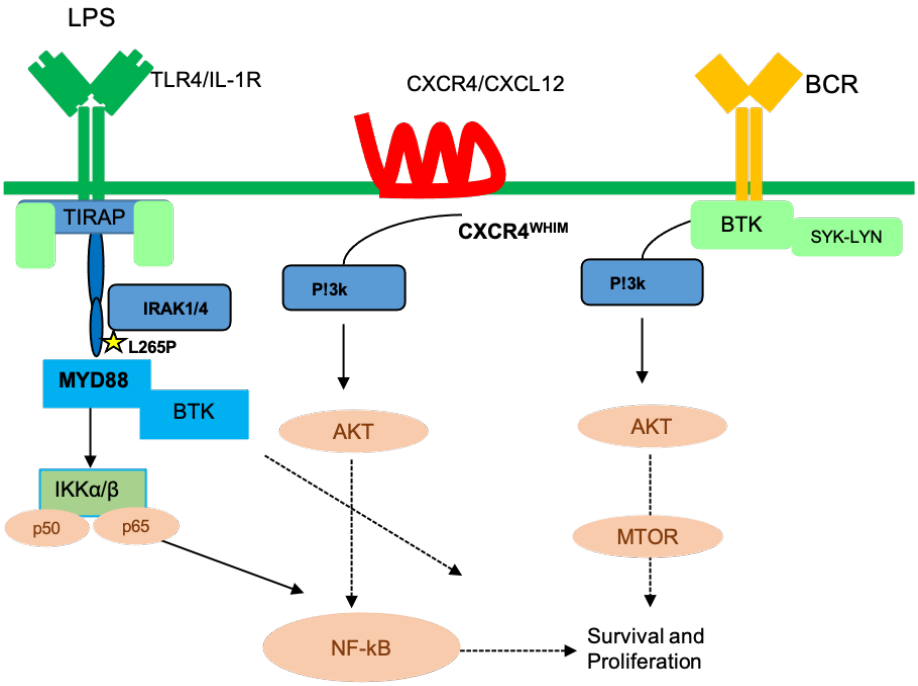

Figure 2. A simplified illustration depicts TLR-BCR-CXCR4/CXCL12 pathways crosstalk. Graphical illustration of the interaction and existing regulatory network linking BCR and TLR to CXCR4 signaling. Adapted from (Cojoc et al., 2013; Hunter et al., 2017; Profitós-Pelejà et al., 2022).

BCR and TLR signaling are involved in the formation and activation of B-cells via BTK, which is a signaling protein. BTK is a critical kinase in BCR signaling and is known to interact with several components of the TLR signaling pathway (Laurens P. Kil et al., 2012). A high level of BTK expression in the B-cells increases their receptivity to TLR stimulation indicating that BTK supports the synergistic activation of BCR and TLR interaction (Rip et al., 2019). Another study demonstrated how leukemic B-cell growth and survival are influenced by interactions between the chemokine receptor CXCR4 and the BCR of various immunoglobulin isotypes (Maity et al., 2018; ten Hacken et al., 2019). BCR activation and its interaction with TLR and CXCR4 signaling pathways encompass a sequence of molecular events including the activation of major downstream effectors like SYK, activation of PI3K/AKT and ERK pathways as well as the mobilization of intracellular calcium, along with integrating signals via other receptors like TLR7 and TNF (Dal Porto et al., 2004; Jellusova et al., 2013; Maity et al., 2015; Otipoby et al., 2015; Schweighoffer et al., 2013) (Fig. 2).

1.8. CXCR4/CXCL12 axis in B-cell malignancies

CXCR4 overexpression is known in more than 10 cancer types including ovarian, prostate cancer, oesophageal cancer, pancreatic cancer, melanoma, neuroblastoma, and renal cell carcinoma (Cooper et al., 2002; Geminder et al., 2001; Hall & Korach, 2003; Kaifi et al., 2005; Kim et al., 2008; Zagzag et al., 2005). Many preclinical models have revealed that cancer cell metastasis is mediated via pathways activated by CXCL12 binding to CXCR4 which plays a major role in tumor growth and progression. For example, the lung, bone marrow, lymph nodes, and, liver, have the highest level of CXCL12 mRNA expression and are the most common organs for the homing of the circulating malignant cells (Mu È ller et al., 2001). CXCR4/CXCL12 is known to play a major role in tumor cell microenvironment interactions, major pre-clinical mouse models of acute lymphocytic leukemia (ALL), multiple myeloma (MM), non-Hodgkin (NH) B-cell and T-cell lymphoma and chronic lymphocytic leukemia have demonstrated that CXCR4 positive cancer cells are recruited to mesenchymal stroma niches rich in CXCL12, mimicking the homing of the healthy stem cells to the bone marrow (Burger & Peled, 2009; Konopleva & Jordan, 2011). In a mouse model of acute promyelocytic leukemia (APL), it has been shown that cancer cells that have been homed in the bone marrow remain in a microenvironment that protects them from chemotherapy in a CXCR4-dependent manner (Nervi B et al., 2009). The survival of tumor cells in the stroma niche via the CXCL12 pathway is thought to be mediated by several mechanisms. One of these is the activation of PI3K/AKT kinases and MAPK/extracellular signal-regulated kinases, which at least partially confers the protective function of stromal cells (Zeng et al., 2009). According to several preclinical studies, CXCR4/CXCL12 signaling events in the bone marrow niche may, either directly or indirectly, lead to chemotherapy resistance in solid tumors and hematological malignancies (Frassanito et al., 2001; Gilbert & Hemann, 2010). CXCR4 inhibitors have been since investigated as chemosensitizing drugs in the field of leukemia treatment as the CXCL12-CXCR4 interaction was shown to be essential for attracting cancer cells to the bone marrow niche (Dillmann et al., 2009; Hassan et al., 2011). In the BALB/c mouse model intravenously implanted with

human acute myeloid leukemia (AML) cells, treatment with the CXCR4 antagonist AMD3465 resulted in the mobilization of AML cells from the bone marrow. This resulted in increased cytarabine's ability to induce apoptosis in these susceptible AML cells. In a murine APL model, stroma-derived CXCL12 protected leukemic cells against anthracycline and cytarabine treatment. Treatment with the CXCR4 inhibitor AMD3100 in this model led to the mobilization of APL cells from the bone marrow microenvironment and enhanced cancer cell death from chemotherapy (Nervi B et al., 2009). The expression of CXCR4 and CXCL12 on tumor cells as well as cells surrounding the tumor is crucial for the interaction of cancer cells with their microenvironment. CXCR4 antagonists have the potential to be effective treatments for making cancer cells more susceptible to chemotherapy. It is necessary to conduct more research to determine whether preventing solid tumor cells from interacting with the microenvironment will improve the effectiveness of conventional therapies.

1.9. *MYD88* role in lymphoid malignancies

Somatic *MYD88* mutations have been found in many B-cell malignancies, including lymphoplasmacytic lymphoma/Waldenström macroglobulinemia (LPL/WM), activated B-cell-like diffuse large B-cell lymphoma (ABC-DLBCL), and marginal zone lymphoma (MZL) (St´ et al., 2013; Treon SP et al., 2012a; Treon SP et al., 2012). These mutations are also seen in a considerable proportion of IgM-secreting monoclonal gammopathy of undetermined significance (IgM MGUS), where they are currently identified in between 60% and 80% of cases (Jiménez et al., 2013; Nakamura et al., 2019; Treon et al., 2012; Treon SP et al., 2012; Varettoni et al., 2013; Xu et al., 2013a) indicating that *MYD88* mutations are associated with an early genetic event in the development of LPL/WM. Lastly, Diffuse large B-cell lymphoma, which can be divided into two primary molecular subgroups based on the cell of origin, is where the recurrent *MYD88* L265P mutation was initially identified. In contrast to the activated B-cell-like subtype, which expresses genes triggered by NF-B during the *in vitro* activation of peripheral blood cells, the germinal center B-cell-like subtype has gene expression patterns that mimic those of nonmalignant B-cells that have entered the germinal center. Patients with

ABC-DLBCL showed a poor prognosis as compared to those with GCB-DLBCL. *MYD88* mutations were first discovered by Staudt and colleagues in ABC-DLBCL biopsies, with L265P being the most common mutation, occurring in roughly 29% of patients (Alizadeh et al., 2000; V. N. Ngo et al., 2011). Although there are other distinct *MYD88* mutations, the L265P missense substitution is the most common. L265P accounts for the majority (about 75%–80%) of the *MYD88* alterations described in ABC-DLBCL and CLL, and it is the only *MYD88* variant observed in LPL/WM, IgM-secreting MGUS, and MZL. The L265P mutation and nearly all other *MYD88* mutations found in B-cell tumors congregate in the TIR domain's evolutionary conserved beta-beta loop, which leads to structural change in MYD88, allowing homodimerization and hence recruitment of IRAK1 and IRAK4. In B-cell malignancies, mutated *MYD88* consistently results in unregulated assembly of the MYD88/IRAK complex that leads to the recruitment of TRAF6, phosphorylation of TAK1, and, eventually, an increase in NF-κB activity (Ngo VN et al., 2011; Ansell SM et al., 2014). Studies conducted using selective small molecule inhibitors for IRAK1-IRAK4 induced cell death in ABC-DLBCL cell lines but not in GCB-DLBCL or myeloma cell lines, indicating ABC-DLBCL requires IRAK1-IRAK4 to induce signal through *MYD88* L265P to promote cancer cell survival (V. N. Ngo et al., 2011) A crucial node in BCR signaling cascades, BTK mediates the signal from BCR to downstream pathways like NF-κB, PI3K/AKT, and NFAT (Young & Staudt, 2013). In WM cells with *MYD88* L265P, *MYD88* preferentially complexes to phosphorylated BTK (pBTK), while no complexing is seen in lymphoma cells with WT *MYD88* (G. Yang et al., 2013). In comparison to lymphoma cells with WT *MYD88*, WM cells with *MYD88* L265P had a higher level of pBTK. Importantly, WM cell apoptosis was caused by the inhibition of either BTK or IRAK1/4. These findings identify BTK as a downstream target of *MYD88* L265P and offer a cutting-edge method for treating WM and other cancers that express *MYD88* L265P (G. Yang et al., 2013).

In conclusion, patients with IgM MGUS, WM, ABC-DLBCL, and other NHL frequently have the somatic mutation *MYD88* L265P. With the identification of this somatic mutant, we now have

various potentials to enhance lymphoma diagnosis and care. By further analyzing *MYD88* L265P at the molecular and cellular levels in murine models, it will be possible to develop new approaches for treating lymphoid malignancies and gain insight into the underlying processes driving its oncogenic action.

1.10. Waldenström macroglobulinemia

Waldenström macroglobulinemia is a rare and indolent type of lymphoproliferative disorder characterized by pleomorphic B-cells and high concentrations of monoclonal serum IgM (Owen et al., 2003). WM patients develop excessive lymphoplasmacytic cells (LPCs) in the BM, spleen, and lymph nodes, along with a high level of IgM production that can result in symptoms including cryoglobulinemia, hyperviscosity, and autoimmune-related problems (Treon, 2009). The U.S. has an estimated incidence of 1000–1500 new cases per year (Grimont et al., 2021). The median age at diagnosis is approximately 70 years. WM is twice as common in males with 3.4 million/year cases recorded. Encouragingly, the 5-year survival has improved to 78% among those diagnosed between 2000 and 2010 in comparison to 67% among those diagnosed earlier (Castillo, Bibas, et al., 2015; Castillo, Olszewski, et al., 2015; Groves et al., 2000). There are a series of advances in the diagnosis and management of WM in recent years, and along with an increasing number of genomic-driven treatments, it is expected that the therapeutic advancements will translate into efficient and more durable responses, as well as lower toxicity rates (Castillo et al., 2019). However, despite improvements in therapy regiment, WM remains incurable. The majority of WM treatment options have been based on therapies researched for other diseases, with more recent developments made possible by next-generation sequencing. WM LPC was found to have recurrent somatic mutations in *MYD88*, *CXCR4*, *CD79*, and *ARID1A* using NGS (Hunter et al., 2017; Treon, Xu, Luisa Guerrera, et al., 2020). Whole-genome sequencing identified a recurrent somatic mutation in *MYD88*(L265P) carrying a point mutation that switches leucine to proline at amino acid position 265 in 91% of patients with WM. This mutation was later confirmed by Sanger sequencing as well as allele-specific polymerase chain reaction (AS-

PCR) assays. AS-PCR assays detected *MYD88* L265P in 93% of WM patients and 54% of IgM MGUS patients. Numerous IgM MGUS patients carrying this mutation suggested that *MYD88* L265P represents an early oncogenic event in the development of WM (Xu et al., 2013b).

Patients with wildtype *MYD88* present a more aggressive disease and are associated with a severely poor prognosis. Moreover, they exhibit somatic mutations that are found in diffuse large B-cell lymphoma (Hunter et al., 2018; Treon et al., 2018). Somatic mutation(s) involving the C terminal domain of the G-protein coupled chemokine receptor, CXCR4, is present in up to 40% of patients with WM (Hunter et al., 2014b). *CXCR4* mutations are essentially unique to WM with few cases reported for marginal zone lymphoma and activated B-cell subtype of DLBCL. Frequently the *CXCR4* mutation associated with WM is the germline mutation in *CXCR4* encountered in patients with WHIM syndrome, an autosomal dominant disorder with Warts, Hypogammaglobulinemia, Infections, Myelokatheksis (Hernandez et al., 2003). CXCR4 activation by its ligand CXCL12 is known to activate AKT as well as MAPK signaling, facilitating cell proliferation and BM homing of WM cells (H. T. Ngo et al., 2008). Both the *MYD88* and *CXCR4* genes produce proteins that are important in cellular signaling. The MYD88 protein transmits signals that support cell viability by preventing cells from apoptosis. The CXCR4 protein activates internal signaling pathways that assist in controlling cell proliferation, which is the process of dividing and growing new cells. The variation of these genes result in the creation of proteins that are hyperactive. This hyperactive protein-mediated excessive signaling promotes the survival and proliferation of aberrant cells that ought to die, which perhaps helps explain why lymphoplasmacytic cells accumulate in Waldenström macroglobulinemia (Cao et al., 2015; Hunter et al., 2014b). Another recurring mutation associated is a somatic mutation in ARID1A, seen in 17% of the WM patients, including frameshift and nonsense variants. Patients with *ARID1A* and *MYD88* L265P mutations had poorer hemoglobin and platelet counts as well as more severe bone marrow disease involvement. On chromosome 6q.1,12, *ARID1A* and its frequently deleted counterpart *ARID1B* are located. Both act as chromatin remodeling genes, which affects how genes are

regulated. Although it is yet unclear how the mechanism work, ARID1A can alter TP53 and is thought to work as an epigenetic tumor suppressor. Furthermore, 8% to 12% of WM patients express CD79A and CD79B. Both can combine to produce heterodimers and are parts of the B-cell receptor pathway. For BCR to express on the cell surface and for BCR-induced signaling to occur, the CD79A/B heterodimer must bind with the immunoglobulin heavy chain. SYK and BTK are activated by mutations in the ITAM of CD79A and CD79B, which have been observed in ABC DLBCL (Guerrera et al., 2018; Hunter et al., 2017; Treon et al., 2019).

The identification of recurrent somatic mutations in *MYD88*, *CXCR4*, *CD79B*, and *ARID1A* in WM provides crucial new insights into the pathophysiology, prognosis, and development of WM therapeutics, with later mutation ones including inhibitors of BTK, IRAK, and hematopoietic cell kinase (HCK) as well as substances that focus on important pro-survival signals in the MYD88 pathways. The BTK inhibitors ibrutinib, zanubrutinib, and acalabrutinib have demonstrated impressive activity in WM, and ibrutinib is currently licensed for the treatment of symptomatic WM in the US, Europe, and other countries (Dimopoulos et al., 2018). Additionally, selective inhibitors are being developed for IRAK and HCK that are in pre-clinical and/or early clinical stages. With clinical trial evaluating the effects of the CXCR4 inhibitor ulocuplomab with ibrutinib in CXCR4 mutant WM patients marked a promising step forward (Hunter et al., 2014a; Treon, Xu, Guerrera, et al., 2020). Based on preclinical studies that suggest the possibility of synergistic interactions with ibrutinib, it is also plausible to target CD79B signaling with SYK inhibitors, which may be suitable for patients with CD79B mutations. Therefore, genomic discoveries provide the basis for the creation of targeted drugs and the possibility of WM treatment via personalized medicine (Munshi et al., 2020)

1.11. Aim of the study

Waldenström macroglobulinemia is a B-cell lymphoproliferative disorder that is characterized by the presence of a high concentration of monoclonal IgM paraprotein in blood serum. This neoplasm is typically associated with invasion and proliferation of lymphoma cells in the bone marrow.

This study aimed to develop an autochthonous mouse model of Waldenström macroglobulinemia which are genetically modified to possess genomic abnormalities that perfectly match or biologically correspond to those identified in the corresponding human disease. This model will allow to better understand the mechanisms of tumor development and progression in humans, as well as to provide an accurate tool for evaluating the biological effects of targeted therapies.

The study further aims to decipher the pathogenesis of a combined conditional Myd88 mutation and gain-of-function CXCR4 mutation in B-cells, which are known to contribute to the development and progression of WM. We focus on the phenotypic characterization of the development of lymphoplasmacytic lymphoma and its ability to accurately mimic the corresponding human WM disease. Through this mouse model, we hope to gain valuable insights into the biology of WM and identify potential targeted therapeutic agents. The results of this study may ultimately help to improve the diagnosis, treatment, and management of WM in human patients.

2. MATERIALS AND METHODS

2. 1. Materials

2. 1. 1. Equipment and consumables

Table 1: Equipment

Instrument	Company
Agilent Bioanalyzer 2100	Agilent technologies
Camera	Carl Zeiss (Suzhou) Co., Ltd
Cell incubator (Heraeus Hera cell 240)	Heraeus
ChemoStar PLUS Imager	Intas Science Imaging Instruments GmbH
Countess II FL Automated Cell Counter	Invitrogen by Life Technologies
Cytoflex S	Beckman Coulter
Dissecting instruments	Fine Science Tools
Dissecting Board	Simport
Electrophoresis chamber	Bio-Rad Laboratories GmbH
Eppendorf Centrifuge 5417R	Eppendorf AG
Eppendorf Mastercycler PCR device	Eppendorf AG
Eppendorf Minispin Plus Centrifuge	Eppendorf AG
Epifluorescence microscope	Carl Zeiss Microscopy GmbH
FACSAria™ III cell sorter	BD Biosciences
Fridges and lab freezers	Liebherr-Hausgeräte GmbH
GelDoc System Universal Hood II	Bio-Rad Laboratories GmbH
Glassware Duran®	Labware SCHOTT AG
Liquid nitrogen tank Biosafe® MDβ	Cryotherm GmbH & Co. KG
Magnetic Stirrer MS 3000	neoLab Migge GmbH
MACS MultiStand	Miltenyi Biotec
Microplate reader - Luminometer	Berthold Technologies
Microwave Oven	Commercial
Multi-Channel Pipettes Research Plus®	Eppendorf AG
Multi-Channel Pipette (electronic)	Brand GmbH & Co KG
Multi-step pipette	Eppendorf AG
NanoDrop 2000c	Thermo Fisher Scientific
Neubauer hemocytometer	Paul Marienfeld GmbH & Co. KG
pH-meter HI2020 edge R	Hanna instruments
Pipet boy	Integra Biosciences Ag from INTEGRA Holding AG
Pipettes Research Plus®	Eppendorf AG
Power Pac 200	Bio-Rad Laboratories GmbH
Power Pac P25T	Biometra GmbH
Pump tube (Sample pump) kits	Beckman Coulter
QuantiFluor® ONE dsDNA System	Promega Corporation
Quintix® Analytical balance	Sartorius Lab Instruments GmbH & Co.KG
Safety cabinet HERAsafe® HSP18	Heraeus
Scil Vet ABC Blood Counter	Scil animal care company GmbH

SDS-Gel electrophoresis chamber (Multigel Long)	Biometra GmbH
Spectophotometer CLARIOstar	BMG Labtech
StepOne Plus tm Real-time PCR System	Applied Biosystem
Vortex Genie 2	Bender&Hobein AG
Vortex	neoLab Migge GmbH
Water bath	Memmert GmbH + Co. KG
Wet-transfer device	Bio-Rad Laboratories GmbH

Table 2: Consumables

Consumable	Company
96-well cell culture plate (Corning™ Falcon™)	Nunc
48-well cell culture plate (Corning™ Falcon™)	Nunc
24-well plate Falcon (Corning™ Falcon™)	Nunc
12-well cell culture plate (Corning™ Falcon™)	Nunc
6-well plate Falcon (Corning™ Falcon™)	Nunc
BD Plastipak™ 1 ml Sub-Q insulin syringes	BD Biosciences
Blood lancets	Sarstedt AG & Co.
Cell culture flasks 25 cm², 75 cm², 175 cm²	Sarstedt AG & Co.
Cell culture dish 10 cm, 15 cm	Sarstedt AG & Co.
Cell strainers 70 µm	Sarstedt AG & Co.
Combitips advanced 5 ml	eppendorf
Conical tube 15 ml (Corning™ Falcon™)	Thermo Fisher Scientific
Conical tube 50 ml (Corning™ Falcon™)	Thermo Fisher Scientific
Multi-step tips, sterile, combitips advanced, 1.0 ml, 5 ml	Eppendorf AG
Countess Cell Counting Chamber Slides	Thermo Fisher Scientific
Cryovials 2 ml	Sarstedt AG & Co.
FACS tubes	Sarstedt AG & Co.
Filter tips sterile 200 µl, 100 µl, 20 µl Biosphere®	VWR International
Filter tips sterile 1250 µl	Greiner Bio-One GmbH
Filter 0.45 µm	neoLab Migge GmbH
Glass Pasteur pipette 150 mm	Brand GmbH & Co KG
MACS LS Columns	Miltenyi Biotech
Microvette 300	Sarstedt AG & Co.
Parafilm	Brand GmbH & Co KG
Pipette tips 1250 µL, non-sterile	Greiner Bio-One GmbH
Pipette tips 2-200, 20 µL, non-sterile	Sarstedt AG & Co.
PCR-strips Single Cap 8er-Soft-Strips 0.2 ml	Byozim Scientific GmbH
PCR plate 96-well	Eppendorf AG
Reaction tube 1.5 ml, 2 ml safe seal	Sarstedt AG & Co.
ROTILABO® Embedding cassettes, White	Carl Roth GmbH + Co. KG
ROTILABO® Embedding cassettes, Green	Carl Roth GmbH + Co. KG

ROTILABO® Embedding cassettes, Blue	Carl Roth GmbH + Co. KG
Serological pipette 5 ml, 10 ml, 25 ml	Sarstedt AG & Co.
Syringes 2 ml, 5 ml, 10 ml	BD Discardit™ II
Syringes 1 ml	B Braun
S-Monovette EDTA	Sarstedt AG & Co.
Sterican® Gr. 1, G 20 x 1 1/2"" / ø 0,90 x 40 mm, gelb	B Braun
Sterican® Gr. 17, G 24 x 1""/ ø 0,55 x 25 mm, lila	B Braun
Sterican® Gr. 12, G 22 x 1 1/4"" / ø 0,70 x 30 mm, schwarz	B Braun

2. 1. 2. Chemicals and reagents

Table 3: Chemicals

Reagent	Company
2-Mercaptoethanol, 50 mM	Sigma-Aldrich
Acetic acid	Carl Roth GmbH + Co. KG
ACK Lysis buffer	Thermo Fisher Scientific
Acrylamide-Bisacrylamide mixture (37.5:1)	Carl Roth GmbH + Co. KG
Adenosine triphosphate (ATP)	Sigma-Aldrich
Agarose	Byozim Scientific GmbH
Ammonium persulfate (APS)	Sigma-Aldrich
Annexin V binding buffer (10X)	BD Pharmigen Inc
Bio-Rad Protein Assay Dye Reagent Concentrate (5X)	Bio-Rad Laboratories GmbH
Bovine Serum Albumin (BSA)	Carl Roth GmbH + Co. KG
Bromophenol blue	Sigma-Aldrich
CytoFLEX Daily QC fluorospheres	Beckman Coulter
CytoFLEX Sheath Fluid	Beckman Coulter
DAPI (4',6-Diamidino-2-Phenylindole, Dihydrochloride)	Invitrogen by Life Technologies
Dimethylsulfoxid (DMSO)	Carl Roth GmbH + Co. KG
Dithiothreitol (DTT)	Sigma-Aldrich
Ethanol 70%	Carl Roth GmbH + Co. KG
Ethanol absolut	Nunc A/S, Roskilde, Denmark
Ethylenediaminetetraacetic acid (EDTA)	Carl Roth GmbH + Co. KG
Flowclean cleaning agent	Beckman Coulter
Formaldehyde solution 37%	Carl Roth GmbH + Co. KG
Glycerol	Sigma-Aldrich
Glycine	Carl Roth GmbH + Co. KG
Hank's Balanced Salt Solution, 10x (HBSS)	Thermo Fisher Scientific

4-(2-hydroxyethyl)-1-piperazineethanesulfonic acid (HEPES)	Thermo Fisher Scientific
Hydrogen chloride (HCl)	Merck KGaA
Isoflurane CP® [1 mg/ml]	CP-Pharma
Isopropanol	Carl Roth GmbH + Co. KG
Kit ECL Prime detection reagent	GE Healthcare
LB-Agar (Luria/Miller)	Carl Roth GmbH + Co. KG
LIVE/DEAD™ Fixable Violet Dead Cell Stain Kit, for 405 nm excitation	Invitrogen by Life Technologies
Magnesium chloride ($MgCl_2$)	Sigma-Aldrich
Methanol	Carl Roth GmbH + Co. KG
N, N, N ', N'-Tetramethylethylenediamine (TEMED)	Sigma-Aldrich
NP-40	Sigma-Aldrich
Osteosoft	Sigma-Aldrich
Phenol – chloroform – isoamyl alcohol mixture	Sigma-Aldrich
Polyethylene glycol 4000	Carl Roth GmbH + Co. KG
Ponceau Staining solution	VWR International
Potassium chloride (KCl)	Merck KGaA
Propidium iodide (PI)	Sigma-Aldrich
Restore™ PLUS Western Blot Stripping Buffer	Thermo Fisher Scientific
RNase*Zap*™-RNase Decontamination Wipes	Invitrogen by Thermo Fisher Scientific
Roti Histofix 4%	Carl Roth GmbH + Co. KG
Skim milk powder	Carl Roth GmbH + Co. KG
Sodium acetate anhydrous (NaOAc)	Merck KGaA
Sodium chloride (NaCl)	Carl Roth GmbH + Co. KG
Sodium deoxycholate detergent	Sigma-Aldrich
Sodium dodecyl sulfate (SDS pelletes)	Carl Roth GmbH + Co. KG
Sodium hydroxide (NaOH)	Carl Roth GmbH + Co. KG
Trichlormethan/Chloroform	Sigma-Aldrich
Tris (hydroxymethyl) aminomethane HCl (Tris HCl)	Carl Roth GmbH + Co. KG
Triton X-100 (t-Octylphenoxypolyethoxyethanol)	Sigma-Aldrich
Trypan Blue	Sigma-Aldrich
Tryptone	Sigma-Aldrich
Tween® 20 molecular biology grade	Serva Electrophoresis GmbH
Yeast extract	BD Biosciences

Table 4: Reagents

Reagent	**Company**
100 b DNA Ladder	New England Biolabs GmbH
1 kb Plus DNA Ladder	New England Biolabs GmbH

complete Mini, EDTA-free (Protease inhibitor cocktail tablets)	Roche Diagnostics GmbH
DNA Ladder 100 bp	New England Biolabs GmbH
dNTP mix, 10 mM	Rapidozym GmbH
Gel blotting paper (Whatman®)	Merck KGaA
Gel Loading Dye Purple (6X)	New England Biolabs GmbH
Immun-Blot® PVDF Membrane 0.2 µm	Bio-Rad Laboratories GmbH, Munich, Germany
Immun-Blot® PVDF Membrane 0.45 µm	Thermo Fisher Scientific
Lipofectamine™ 2000 Transfection Reagent	Invitrogen by Thermo Fisher Scientific
Midori Green Advance NonToxic DNA and RNA staining	Nippon Genetics Europe GmbH
Nuclease-Free Water (not DEPC-Treated)	Thermo Fisher Scientific
PageRuler™ Plus Prestained Protein Ladder, 10 to 250 kDa	Thermo Fisher Scientific
PHOSSTOP, 10 TABLETS	Roche Diagnostics GmbH
Poly-L-lysin solution	Sigma-Aldrich
Polybrene Infection / Transfection Reagent	Merck KGaA
Scil Vet abc Plus+ Reagent pack	Scil animal care company GmbH

2. 1. 3. Kits and enzymes

Table 5: Kits

Kit	Company
Agilent RNA 6000 Pico Kit	Agilent Technologies
CD19 Microbeads, Mouse	Miltenyi Biotec
HiSpeed Plasmid Maxi Kit	Qiagen
IgA mouse uncoated ELISA kit with plates	Invitrogen by Life Technologies
IgG(total) mouse uncoated ELISA kit with plates	Invitrogen by Life Technologies
IgM mouse uncoated ELISA kit with plates	Invitrogen by Life Technologies
NEBNext Ultra II Q5 Master Mix	New England Biolabs GmbH
Luna Universal Probe One-Step RT-qPCR kit	New England Biolabs GmbH
Pure Yield Plasmid Miniprep System	Promega Corporation
Qiagen DNeasy Blood and Tissue Kit	Qiagen
QIAshredder	Qiagen
RiboLock RNase inhibitor	Thermo Fisher Scientific
RNase-Free DNase Set	Qiagen
RNeasy Micro Kit	Qiagen
RNeasy Mini Kit	Qiagen
T4 DNA Ligase	Thermo Fisher Scientific
Taq 2X Master Mix	New England Biolabs GmbH
Terra PCR Direct Polymerase Mix	Takara Bio Inc.
VersaComp Antibody capture beads kit	Beckman coulter
Wizard SV Gel and PCR Clean-Up System	Promega Corporation

Table 6: Enzymes

Enzymes	Company
BsmBI	New England Biolabs GmbH
DNAase I	New England Biolabs GmbH
EcoRI	New England Biolabs GmbH
EmeraldAmp MAX HS PCR Master Mix	Takara
RNAse A	Sigma-Aldrich
Phusion High Fidelity DNA Polymerase	ThermoFisher Scientific
Proteinase K Solution (20 mg/mL)	Thermo Fisher Scientific
SapI	New England Biolabs GmbH
Taq 2X Master mix	New England Biolabs GmbH
XhoI	New England Biolabs GmbH

2. 1. 4. Cell culture

2. 1. 4. 1. Medium and reagents

Table 7: Medium, antibiotics, stimulants, and inhibitors

Medium/antibiotic/stimulants/inhibitors	Company
β-estradiol	Sigma-Aldrich
AMD3100 (CXCR4 antagonist)	Sigma-Aldrich
Ampicilin	Carl Roth GmbH + Co. KG
Antibiotic-Antimycotic (100X)	Thermo Fisher Scientific
Dulbecco's Modified Eagle Medium (DMEM), high glucose	Thermo Fisher Scientific
Dulbecco's phosphate-buffered saline (DPBS)	Gibco by Thermo Fisher Scientific
F(ab')2 goat anti-mouse IgM	eBioscience, Inc.
Fetal Bovine Serum (FBS)	Gibco by Thermo Fisher Scientific
FLT3 ligand mouse	Peprotech
IL-3 mouse	R & D systems
IL-4 mouse	Peprotech
IL-5 mouse	Miltenyi Biotec
IL-6 mouse	R & D systems
IL-7 mouse	R & D systems
Iscove's modified Dulbecco's medium (IMDM)	Gibco by Thermo Fisher Scientific
LPS	Sigma-Aldrich
Minimum essential medium (MEM) Alpha, 1X	Gibco by Thermo Fisher Scientific
Minimum essential medium non-essential amino acids (MEM NEAA), 100X	Gibco by Thermo Fisher Scientific
Opti-MEM, Reduced Serum Media, no phenol red	Thermo Fisher Scientific
Recombinant Mouse CXCL12 (SDF-1α) (carrier-free)	BioLegend

Recombinant mouse IL-7	R & D systems
Roswell Park Memorial Institute (RPMI) 1640 Medium	Thermo Fisher Scientific
SCF mouse	R & D systems
Trypsin-EDTA (0.5%), no phenol red, 10X	Gibco by Thermo Fisher Scientific

2. 1. 5. Buffer and solutions

Table 8: Buffer and solutions

Buffer/Solution	Composition
4% Formalin solution	40% Formalin solution (10%) 60% PBS
5X Loading buffer for SDS-PAGE (Laemmli) pH 6.8	0.35 M SDS 25 ml Glycerol 0.23 M Tris HCl 0.75 mM Bromophenol blue 2.5 ml 2-Mercaptoethanol to 50 ml of H_2O
10X PBS (Phosphate buffer saline) in ddH_2O (pH 7.4)	1.4 M NaCl 27 mM KCl 0.1 M Na_2HPO_4
50X TAE (Tris-Acetate-EDTA buffer) in ddH_2O	2 M Tris-HCl 0.95 M Acetic acid 50 mM EDTA pH 8.0
Agarose gel (1.5%)	1.5% Agarose 1X TAE buffer Boiled in microwave until dissolved
APS (10%) in ddH_2O	10% Ammoniumpersulfat
Blocking solution for WB	BSA 5% in TBS-T
DAPI solution for apoptosis assay in PBS	10 µg/ml DAPI
HF2 buffer in ddH_2O	10% HBSS, 10x 2% FCS (heat inactivated) 1% HEPES 1% Pen/Strep 0.22 µm sterile filtered
FACS buffer	PBS 0.5% BSA
Ligation buffer for 4C in ddH_2O	50 mM Tris HCl (pH 7.6) 10 mM $MgCl_2$ 1 mM ATP 1 mM DTT
Lysis buffer for 4C in ddH_2O	10 mM NaCl 250 mM Tris HCl (pH 8.0) 0.2% NP-40 1X Protease inhibitor
Propidium Iodide (PI) solution for cell cycle	0.2 µg/ml PI
RIPA buffer for protein isolation in ddH_2O	150 mM NaCl 1% NP-40 0.5% Sodium deoxycholate 0.1% SDS 50 mM Tris HCl (pH 8.0) 1 mM PMSF 2X Protease inhibitor

	2X Phosphatase inhibitor
SDS-PAGE 10X TBS (Tris-buffer saline) (pH 7.6)	0.2 M Tris-HCl 1.4 M NaCl
SDS-PAGE 1X TBS-T	1X TBS + Tween20 0.1%
SDS-PAGE 10X Running buffer in ddH_2O (pH 7.4)	35 mM SDS 0.25 M Tris HCl 2 M Glycine
SDS-PAGE 10X Transfer buffer	0.25 M Tris HCl 2 M Glycine
SDS-PAGE 1X Transfer buffer	10% transfer buffer 10 X 20% Methanol 100% 70% ddH_2O
SDS-PAGE Stacking gel buffer in ddH_2O	0.5 M Tris HCl pH 6.8
SDS-PAGE Resolving gel buffer in ddH_2O	1.5 M Tris HCl pH 8.8
SDS-PAGE Stacking gel (5%)	3 ml ddH_2O 1.3 ml stacking buffer 750 µl Acrylamide-bisacrylamide mixture 25 µl APS 10% 10 µl TEMED
SDS-PAGE Resolving gel (10%)	4.1 ml ddH_2O 2.6 ml resolving buffer 3.3 ml Acrylamide-bisacrylamide mixture 100 µl SDS 10% 50 µl APS 10% 15 µl TEMED
Stop solution in ddH_2O	2N H_2SO_4
Stripping buffer for WB	10% Methanol 10% Acetic acid 80% ddH_2O
Tail buffer in ddH_2O	1% SDS 0.1 M NaCl 0.1 M EDTA 0.05 M Tris (pH 8)
TE (Tris-EDTA) buffer	10 mM Tris HCl pH 8.0 1 mM EDTA
Wash buffer	1X PBS 0.05% Tween20

2. 1. 6. Antibodies

2. 1. 6. 1. Flow cytometry

Table 9: Extracellular Antibodies

Marker	Clone	Fluorescence	Company
CD3e	(145-2C11)	PerCP-Cyanine5.5	Invitrogen
CD93	AA4.1	PerCP-Cyanine5.5	Invitrogen
GL7	GL7	PerCP-Cyanine5.5	Biolegend
CD86	(B7-2)	PE-Cyanine5	Invitrogen
IgD	11-26c	eFluor 450	Invitrogen
CD19	eBio1D3 (1D3)	eFluor 450	Invitrogen
CD69	H1.2F3	eFluor 450	Invitrogen
CD95	Jo2	PE-Cy7	BD Biosciences
CD45R (B220)	RA3-6B2	PE-Cy7	Invitrogen
CD4	GK1.5	PE-Cy7	Invitrogen
CD23	B3B4	PE-Cy7	Invitrogen
CD8a	53-6.7	PE	BD Biosciences
CD80	16-10A1	PE	Invitrogen
CD138	Clone 281-2 (RUO)	PE	BD Biosciences
CD43	S7	PE	BD Biosciences
CD21/35	Clone 7G6 (RUO)	PE	BD Biosciences
B220/CD45R	RA3-6B2	APCcy7/APC-eFluor 780	Invitrogen
CD4	RM4-5	APCcy7/APC-eFluor 780	Invitrogen
MHCII	M5/114.15.2	APCcy7/APC-eFluor 780	Invitrogen
CD117 (c-Kit)	2B8	APCcy7/APC-eFluor 780	Invitrogen
CD38	90	APC	Invitrogen
IgM	II/41	APC	Invitrogen

Table 10: Intracellular Antibodies

Marker	Fluorescence	Species	Company
Phospho-AKT1	eFluor 450	Human, Mouse	Invitrogen
Phospho-ERK1/2	PE	Human, Mouse	Invitrogen
Mouse anti-Syk	PE	Mouse	BD BioScience
anti-STAT3 Phospho (Tyr705)	PE/Cyanine5	Human, Mouse	Biolegend
Phospho-STAT3	PE	Human, Mouse	Invitrogen
Phospho-AKT1	PE	Human, Mouse	BD BioScience
FC Block		Mouse	Invitrogen

2. 1. 6. 2. Immunoblots – primary

Table 11: Primary Antibodies

Target	Company	Dilution
Akt 9272	Cell Signaling	1:1000
Phospho-Akt (Ser473) 9271	Cell Signaling	1:1000
p44/42 MAPK (Erk1/2) 9102	Cell Signaling	1:1000
Phospho-p44/42 MAPK (Erk1/2) (Thr202/Tyr204) 9101	Cell Signaling	1:1000
β-Actin A1978	Sigma-Aldrich	1:10000

Table 12: Secondary Antibodies

Reactivity	Company	Dilution
Anti-rabbit HRP-linked	Sigma-Aldrich	1:5000
Anti-mouse HRP-linked	Sigma-Aldrich	1:5000

2. 1. 6. 3. Annexin V for apoptosis assay

Table 13: Annexin V Antibodies

Marker	Fluorescence	Name	Company
Annexin V	APC	APC Annexin V	Biolegend
Annexin V	Alexa Fluor® 647	Alexa Fluor® 647 Annexin V	Biolegend

2. 1. 7. Oligonucleotides

2. 1. 7. 1. Genotyping primers

Table 14: Genotyping primer

WHIM FP	CTTTAATCTCACTCAGCTCTGGCGAG
WHIM RP	ACACATTTATGGCTTCCCGGAGACC
MYD88 FP	GCCCTTCTGACATTCAATCC
MYD88 RP	ATGGCTCTACAAACTAACACTTCC
AIDCRE FP	CACTCGTTGCATCGACCGGTAATG
AIDCRE RP	GGACCCAACCCAGGAGGCAGATGT
CD19-Cre8	CCC AGA AAT GCC AGA TTA

CD19-19c	AAC CAG TCA ACA CCC TTC C
CD19d	CCAGACTAGATACAGACCAG

2. 1. 7. 2. qPCR primers

Table 15: qPCR primer

MYD88 (human)	GGTCTCCTCCACATCCTCCCTT
	AAAGTCCATCTCCTCCGCCAG
hGAPDH (human)	AGCTCAGGCCTCAAGACCTT
	AAGAAGATGCGGCTGACTGT

2. 1. 7. 3. Sequencing primers

pLXSN	CCCTTGAACCTCCTCGTTCGACC

2. 1. 7. 4. Mycoplasma test primers

Myco FP	GGGAGCAAACAGGATTAGATACCCT
Myco RP	TGCACCATCTGTCACTCTGTTAACCTC

2. 1. 7. 5. gblock sequence for MYD88^{L265P}

GCGCCGGAATTAGATCTctcgagATGCGACCCGACCGCGCTGAGGCTCCAGGACCGCCCGCCATG
GCTGCAGGAGGTCCCGGCGCGGGGTCTGCGGCCCCGGTCTCCTCCACATCCTCCCTTCCCCTG
GCTGCTCTCAACATGCGAGTGCGGCGCCGCCTGTCTCTGTTCTTGAACGTGCGGACACAGGTG
GCGGCCGACTGGACCGCGCTGGCGGAGGAGATGGACTTTGAGTACTTGGAGATCCGGCAACTG
GAGACACAAGCGGACCCCACTGGCAGGCTGCTGGACGCCTGGCAGGGACGCCCTGGCGCCTC
TGTAGGCCGACTGCTCGAGCTGCTTACCAAGCTGGGCCGCGACGACGTGCTGCTGGAGCTGGG
ACCCAGCATTGAGGAGGATTGCCAAAAGTATATCTTGAAGCAGCAGCAGGAGGAGGCTGAGAAG
CCTTTACAGGTGGCCGCTGTAGACAGCAGTGTCCCACGGACAGCAGAGCTGGCGGGCATCACC
ACACTTGATGACCCCCTGGGGCATATGCCTGAGCGTTTCGATGCCTTCATCTGCTATTGCCCCA
GCGACATCCAGTTTGTGCAGGAGATGATCCGGCAACTGGAACAGACAAACTATCGACTGAAGTT
GTGTGTGTCTGACCGCGATGTCCTGCCTGGCACCTGTGTCTGGTCTATTGCTAGTGAGCTCATC
GAAAAGAGGTGCCGCCGGATGGTGGTGGTTGTCTCTGATGATTACCTGCAGAGCAAGGAATGTG
ACTTCCAGACCAAATTTGCACTCAGCCTCTCTCCAGGTGCCCATCAGAAGCGACCGATCCCCAT
CAAGTACAAGGCAATGAAGAAAGAGTTCCCCAGCATCCTGAGGTTCATCACTGTCTGCGACTACA
CCAACCCCTGCACCAAATCTTGGTTCTGGACTCGCCTTGCCAAGGCCTTGTCCCTGCCCTGActcg
agGTTAACGAATTCCGCCC

Vector-specific linker sequence:

GCGCCGGAATTAGATCTctcgag

ctcgagGTTAACGAATTCCGCCC

2. 1. 8. Plasmids

MSCV-IRES-GFP (MIG)	Addgene
MSCV-Cre-YFP	Gift from Prof. Dr. Marc Schmidt-Supprian, Munich
MSCV-YFP	Gift from Prof. Dr. Marc Schmidt-Supprian, Munich
MSCV-ERHBD-HOXB8	Gift from Prof. Dr. Marc Schmidt-Supprian, Munich

2. 1. 9. Bacteria

DH5α	New England Biolabs GmbH

2. 1. 10. Mice

C57Bl6/J	Charles River Laboratories
$CXCR4^{+/1013}$	Prof. Karl Balabanian
$Myd88^{p.L252P}$	Prof. Christian Reinhardt
$B6.129P2\text{-}Aicda^{tm1(cre)Mnz}/J$	Charles River Laboratories
CD19Cre (B6.129P2(C)-Cd19tm1(cre)Cgn/J)	Charles River Laboratories

2. 1. 11. Cell lines

NIH 3T3	murine	DSMZ
Phoenix Eco	murine	DSMZ
$CXCR4^{+/1013}$ Hoxb8	murine	In-house
$MYD88^{p.L265P}$ Hoxb8	murine	In-house
Wildtype Hoxb8	murine	In-house
$CXCR4^{+/1013}$ $MYD88^{p.L265P}$ Hoxb8	murine	In-house
OP9	murine	Prof. Dr. Marc Schmidt-Supprian
Flt3-Ligand-producing B16 melanoma cell line	murine	Prof. Dr. Marc Schmidt-Supprian

2. 1. 12. Software and databases

Benchling	https://www.benchling.com
Image J	Fijite (CITE)
FlowJo v10	Tree Star Inc
GraphPad Prism 9	GraphPad Software Inc.
Incucyte S3 software	Sartorius Lab Instruments GbmH & Co.KG
Inkscape v0.92	Inkscape community
Mendeley	Elsevier
Microsoft Excel, Powerpoint, word	Microsoft Corporation
StepOne software v2.3	Thermo Fisher Scientific

2.2. Methods

2.2.1. Molecular biology techniques

2.2.1.1. Polymerase chain reaction (PCR)

The reaction for standard PCRs contained 50 - 100 ng of template DNA, 0.5 µM each of forward and reverse primers, 0.5 µl dNTPs (10mM each), 0.5 µl High-Fidelity DNA Polymerase and 2.5 µl of the 10 x reaction buffer in a final volume of 25 µl. The temperature for denaturation was set to 95 °C, annealing temperatures were between 45-68 °C depending on the primers, and elongation was carried out at 72 °C for 1-2 min depending on the length of the sequence. Typically, PCR reactions were performed within 30 - 35 cycles.

2.2.1.2. Agarose gel electrophoresis

In an agarose gel, DNA is separated in an electric field dependent on its size. Visualization is then realized by the addition of Midori green, a fluorescent agent. In this study, 1.5 % agarose gels were used. Therefore, agarose was dissolved in the appropriate volume of electrophoresis buffer (1X TAE), boiled, supplemented with Midori green, and cooled down in a gel chamber. DNA samples were then loaded into gel pockets together with 6X loading dye and with a marker (DNA ladder) before electrophoresis. Midori green stained DNA visualized under UV-light UV light.

2.2.1.3. Digestion of plasmid DNA with restriction enzymes

For cloning purposes, 0.5 - 1 µg plasmid DNA was digested using 5 units of appropriate restriction enzyme in the respective buffer for 1 h at 37 °C. To dephosphorylate digested plasmids, 10 units of calf intestinal alkaline phosphatase (CIP) were added and incubated for 1 h at 37 °C followed by 20 min incubation at 80 °C for inactivation. The restricted plasmid was run in a 1% agarose gel at 90 V for 90 min and purified with Wizard SV Gel and PCR Clean-Up System according to the manufacturer's recommendations. The final concentration was determined by absorbance in a nanodrop spectrophotometer.

2.2.1.4. Oligo annealing and ligation

The gblocks gene fragments were centrifuged for 3-5 seconds at a minimum of 300 x g to ensure the material was in the bottom of the tube. The final concentration of 10ng/µl was reached by adding TE buffer and vortexed briefly. Incubation was carried out at 50°C for 20 min and briefly vortex. For ligation, gblock and digested plasmid were mixed at a molar ratio of 1:2 and 1:4 with 100 ng of the digested and dephosphorylated vector. For the ligation, DNA was mixed with the 10x NEB 2 buffer and 3U/µl T4 Polymerase along with 10x BSA in a total volume of 15 µl for 2.5 min at RT and put directly on ice for 10 min to stop the reaction.

2.2.1.5. Transformation of competent bacteria

For transformation, 2 µl of the ligation reaction was added to 50 µl chemically competent DH5α bacteria. Bacteria were then incubated on ice for 30 min. Next, heat shock was performed at 42 °C for 45 sec followed by 2 min incubation on ice. Subsequently, bacteria were plated on LB agar plates containing 100 µg/µl ampicillin and incubated at 37 °C overnight. Next, bacterial plates were analyzed by colony PCR to determine the success of the cloning protocol.

2.2.1.6. Colony PCR

To determine whether the colonies have the vector of interest, colony PCR was performed using Taq 2X master mix. Colonies were picked and replated in a new LB agar plate with

antibiotics using a tip, the residual colony was resuspended in 50 µl of TE buffer + 0.1% triton X in 1.5 ml tubes. The tubes were heat inactivated at 99 °C for 5 min and centrifuged at 13000 rpm for 10 min. 2 µl of the boiled bacteria was used as a template for the colony PCR. pLXSN sequencing primer was used as forward primer and MYD88 (human) qPCR primer was used as reverse primer. A band of 400 bp was expected for successful cloning.

2.2.1.7. Plasmid purification

The colony with the successful vector integration was inoculated in 5 ml of LB liquid media supplemented with 100 µg/µl ampicillin. The bacteria were incubated overnight at 37 °C with continuous shaking at 200 – 250 rpm. The plasmid was purified with Pure yield plasmid miniprep following the manufacturer's instruction. The DNA concentration was measured using nanodrop an appropriate amount of plasmid was sequenced.

2.2.1.8. RNA extraction from eukaryotic cells

Cell lysates were first homogenized using a QIAshredder (Qiagen). Next, total RNA was extracted using the RNeasy Mini Kit Plus (Qiagen) according to the manufacturer's in-instructions. The final RNA concentration was measured by spectrophotometry with a NanoDrop (ThermoFisher Scientific) and a 260/280 ratio was obtained.

2.2.1.9. Quantitative real-time PCR (qRT-PCR)

qRT-PCR analysis was performed on a StepOne Plus tm Real-time PCR System according to the manufacturer's instructions. For data analysis, Ct values were compared to a control sample and normalized to the expression of human GAPDH

COMPONENTS	20 µl REACTION
Luna universal probe one step reaction mix (2X)	10 µl
Luna warmstart RT Enzyme mix (20X)	1 µl
Forward Primer (10µM)	0,8 µl
Reverse Primer (10µM)	0,8 µl
Template RNA	1 µl
Nuclease free water	upto 20 µl

Primer sequences are listed in section 2. 1. 7.

Program:

CYCLE STEP	TEMPERATURE	TIME	CYCLES
Reverse Transcription	55°C*	10 minutes	1
Initial Denaturation	95°C	1 minute	1
Denaturation	95°C	10 seconds	40-45
Extension	60°C	30 seconds**(+plate read)	

2.2.2. Experimental animals

2.2.2.1. Breeding of mice

All mice were bred and maintained in a specific pathogen-free facility, and the animal experiments were conducted under an approved license number (T0313/18 and G0327/19) and protocol according to Federation of European Laboratory Animal Science Associations (FELASA) guidelines and with permission of the respective authority Landesamt für Gesundheit und Soziales, Berlin, Germany. Mice used in this study were heterozygous female and male animals and were bred on a C57BL/6 background.

CXCR4^{C1013G} (Balabanian et al., 2012) and mice carrying the conditional *Myd88*^{L252P} allele (Knittel et al., 2016) were crossed and B-cell-specific Cre expression was achieved with Cd19Cre mice (Rickert et al., 1997) and AidCre (Robbiani et al., 2008) mice. Offspring were screened by PCR using specific primers for the indicated transgene.

2.2.2.2. Genotyping

For the genotyping of mice, DNA was isolated from ear punches or embryonic tissue by digestion in tail buffer with 200 µg/ml Proteinase K at 55 °C in a thermal shaker. After at least 8 h or overnight lysis, the reaction was stopped by heat inactivation at 98 °C for 5 min. The supernatant containing DNA was collected after centrifugation for 10 min at full speed in a table centrifuge. 1 µl of the supernatant was used as a template for genotyping. Genotyping

of *CXCR4*^{C1013G} mice was performed as described (Balabanian et al., 2012). Genotyping of *Myd88*^{L252P}, *AID Cre,* and *CD19Cre* mice has been performed following standard protocols. Primers used for genotyping are depicted in Table 13.

2.2.2.3. Necropsy

Upon reaching the endpoints of the study, mice were sacrificed using cervical dislocation of the neck. Blood samples were collected into 1.2 ml heparinized tubes and blood cells were counted on a Scil Vet ABC. Tumor tissue, as well as SPL, LN, BM, pieces of liver, kidney, gut, and brain, were dissected from the surrounding tissues and divided for further analyses: one part was fixed in 4 % Formalin solution for 48 h for immunohistochemical (IHC) analyses, the other part was passed through 100 µm cell strainers, washed in HF2+ buffer and frozen viably for further analyses. Femurs and tibias were also isolated. While one tibia was fixed in 4 % Formalin solution for 48 h followed by storage in Osteosoft for two weeks for subsequent IHC analyses, the BM from the additional bones was flushed out using HF2+ buffer, homogenized, and passed through a falcon before being frozen viably. If samples immediately underwent flow cytometric analysis, ammonium chloride–potassium bicarbonate (ACK) lysis buffer was used to lyse erythrocytes before staining.

2.2.2.4. Isolation of genomic DNA and analysis of IgH rearrangements

Genomic DNA was isolated from tissue samples using the DNeasy Blood & Tissue Kit according to the manufacturer's instructions (Qiagen). IgH rearrangements were amplified by PCR from genomic DNA as follows: MsVHe-AH-forward (TCGAGTTTTTCAGCAAGATGAGGTGCAGCTGCAGGAGTCTGG) was combined with JH4e-New-AH- reverse (ATCTTCTAGAAAGATGTCCCTATCCCATCATCCAGGG) to amplify rearrangements involving JH1-4. All samples were amplified by PCR for 35 cycles with Phusion High Fidelity DNA Polymerase (2 U/µl) (Thermo Fisher Scientific) with the following conditions: 2 mM MgCl2; melt at 98 °C for 10′00″, anneal at 72 °C for 1′00″, extend at 72 °C

for 10′00″ and then visualized on a 1.5 % agarose gel. Genomic DNA from the Eμ-Myc spleen was used for monoclonal and oligoclonal controls.

2.2.3. Cell culture and cell-based assay

2.2.3.1. Cell culture methods

The cells were incubated at 37°C in a humid atmosphere with 5% CO_2 and were regularly re-tested for authenticity and mycoplasma with polymerase chain reaction (PCR)

2.2.3.2. Culture of adherent cell lines

Phoenix Eco cells were cultured in DMEM with 10% FCS.

2.2.3.3. Culture of murine splenocytes

CD19 enriched splenocytes were cultured using RPMI (with 10% FCS, 1% P/S, 50μM β-mercaptoethanol, 1mM sodium pyruvate , and Minimum essential medium non-essential amino acids (MEM NEAA) 1X (Gibco) and stimulated with 20 ng/mL IL-4 (Peprotech) and 5 ng/mL IL-5 (Miltenyi).

2.2.3.4. Generation and culture of Hoxb8 cell lines

The Flt3 Ligand (Flt3L)-producing B16 melanoma cell line was cultured in high-glucose DMEM supplemented with 10% FBS and 1% Anti-Anti. Cells were seeded in T75 flasks and passaged every 3–4 days. To passage, cells were washed in 10 mL of PBS twice and incubated with 1 mL of 1×Trypsin for 5 min at 37°C. Cells were collected and centrifuged at 400 RCF for five minutes to pellet followed by inactivating trypsin with 15 mL of high-glucose DMEM. The supernatant was collected, filtered by 0.45 μM filters, and stored at −20 ◦C. The pellet was resuspended in high-glucose DMEM/10% FBS/1% Anti-Anti. Cells were replated at a low density in 10 mL of high-glucose DMEM for culturing. The OP9 cell line was cultured in Alpha Minimum Essential Medium, 20% FBS, and 1% Anti-Anti.

To generate Hoxb8 cell lines including Wildtype Hoxb8, *CXCR4*$^{+/1013}$ Hoxb8, *Myd88*^{L252P} Hoxb8, and *CXCR4*$^{+/1013}$ *Myd88*^{L252P} Hoxb8, we employed an immortalization protocol based

on Hoxb8 transcription factor expression (Redecke et al., 2013). This protocol involved retroviral transduction of mouse bone marrow cells with an estrogen-regulated Hoxb8 construct, allowing for the conditional immortalization of early hematopoietic progenitor cells, referred to as Hoxb8-FL cells. The bone marrow cells were obtained from 10–14 week old femurs, suspended in BBMM (IMDM, 30% FBS, 0.20% Mercapto Ethanol, 0.50% Anti-Anti, 1% Glutamine, 0.50% BSA), pelleted by centrifugation at 450 RCF for 5 min, resuspended in 5 mL ACK lysing buffer at room temperature for 5 min, pelleted again and resuspended in BBMM. A total of 4×10^6 bone marrow cells were pre-stimulated for 24 h in 2.5 mL BBMM, supplemented with rm-IL-3 (2 ng/µL), rm-SCF (10 ng/µL), IL-6 (10 ng/µL) in a 12-well plate. After removing 2 mL supernatant, cells were transduced with 1 mL ER-Hoxb8 retrovirus-containing supernatant by spinoculation (1000 RCF, 90 min, 32°C) in a medium containing 8 µg/mL polybrene and incubated at 37°C. After 24 h, all the cells were centrifuged at 300 RCF, washed with PBS, and resuspended in a 2.5 mL progenitor outgrowth medium for the generation of Hoxb8–FL cells (Redecke et al., 2013). In the following 3 weeks, progenitor outgrowth medium (RPMI1640, 10% FBS, 0.10% Mercapto Ethanol, 1% Anti-Anti, 1 µM β-estradiol, 5% FLT3L supernatant) was changed every 2–3 days and serially passaged to new wells and even flasks after stable expansion. The cell density was always kept between 1×10^5 and 1×10^6 cells/mL medium.

2.2.3.5. Transfection of eukaryotic cells

For the generation of ecotropic retroviral particles, PhoenixEco cells were seeded at a density of 4 x 10^6 cells in 5 ml PhoenixEco media in a 10 cm cell culture dish. For each approach, 30 µl of Lipofectamine 2000 was mixed with 1500 µl Opti-MEM® I Reduced Serum Media and 10 µg plasmid DNA. The mixture was incubated for 30 min at RT. After the removal of media from PhoenixEco cells, 3.5 ml fresh PhoenixEco medium was added to the culture dish along with 1500 µl transfection mix per dish. After 6-hour incubation, the media was replaced by fresh PhoenixEco medium. The supernatant containing viral particles was collected after 24-, 36-, and 48-hour post-transfection and filtered through a 0.45 µm What-man® Filter Unit.

2.2.3.6. Retroviral transduction

Suspension cells were transduced with the virus supernatant collected. 2 x 10^6 cells were seeded in 1 ml of progenitor outgrowth medium in a 6-well plate. 3 ml of virus supernatant in the presence of 1 µg/ml polybrene was added to the indicated cell line. Suspension cells were transduced using spin-transduction at 1,500 RPM for 1 h at 32 °C.

2.2.3.7. Differentiation of immortalized Hoxb8-FL cells

To differentiate ER-Hoxb8 progenitors to B-cells, OP9 cells were collected in 50 mL tubes for irradiation at 15Gy in Mibi (Clinac 2100 CD, Varian, Palo Alto, CA, USA) and then seeded at a petri-dish to >80% confluence in the OP9 medium. Following day, 1 × 10^6 Hoxb8–FL cells were co-cultured on irradiated OP9 cells that were seeded on a petri-dish and maintained in B-cell differentiation medium (RPMI1640, 10% FBS, 0.10% Mercapto Ethanol, 1% Anti-Anti, 1 µM β-estradiol, 5 ng/mL FLT3L, 25 ng/mL SCF, 7 ng/mL IL-7). Every 2–3 days, cells were passaged onto fresh OP9 cells for 2 weeks. B-cell differentiation has been determined by fluorescence-activated cell scanning (FACS) analysis using antibodies against CD19 and B220.

2.2.3.8. Freezing and thawing of cells

For long-term storage, cells were pelleted and re-suspended in a freezing medium (FCS supplemented with 10% DMSO) and transferred into cryotubes. The maximum concentration was 1 x 10^8 cells/ml. Tubes were then transferred to a – 80 °C freezer in a freezing container for at least 24 h. The cells were then transferred to liquid nitrogen for long-term storage. For re-culturing, cells were rapidly thawed at 37 °C, and DMSO was washed out with the respective culture medium. After each thawing cycle, the cell lines were re-tested for mycoplasma.

2.2.3.9. Mycoplasma test

All cultured cell lines were tested for presence/absence of contaminating Mycoplasma spp. 2 ml of the medium from the culturing cells were centrifuged for 2 min at 250 g and the supernatant was transferred to a fresh 2 ml tube. The tubes were centrifuged for 10 min at 20.000 g, the supernatant was discarded, and the pellet was resuspended in 50 ul of PBS. Next, they were boiled at 95°C for 3 min and this mixture was used as a PCR template. The PCR was done as described below with the primers listed in section 2.1.7.4. The template was mixed with 6X loading buffer, run in a 1.5% agarose gel and if the PCR was positive (270 bp), the cells had a Mycoplasma spp. contamination.

COMPONENTS	20 µl REACTION
2X Taq ready mix	10 µl
Forward Primer (10µM)	1 µl
Reverse Primer (10µM)	1 µl
Template	1 µl
Nuclease free water	upto 20 µl

Program:

CYCLE STEP	TEMPERATURE	TIME
Initial Denaturation	98°C*	5 minutes
X 35 cycles	94°C	1 sec
	60°C	1 sec
	72°C	1 sec
Extension	72°C	10 min
Hold	12°C	

2.2.3.10. *In vitro* functional assay

CD19 enriched splenocytes were cultured using RPMI (with 10% FCS, 1% P/S, 50µM β-mercaptoethanol, 1mM sodium pyruvate , and Minimum essential medium non-essential amino acids (MEM NEAA) 1X (Gibco) and stimulated with 20 ng/mL IL-4 (Peprotech) and 5 ng/mL IL-5 (Miltenyi). Splenocytes were supplemented with 1µg/mL LPS (Sigma) and/or 50 nM Cxcl12 (BioLegend) and/or 1µM AMD3100 (Sigma-Aldrich, Saint Louis, MI). For

plasmablast differentiation samples were then stained with fluorophore-coupled primary antibodies (Table 9) and assessed by flow cytometry.

2.2.3.11. Proliferation assay

Trypan blue negative cells were counted in all four 4x4 squares to determine the number of cells in a given volume. To finally calculate the number of cells, the following equation was used: $\boldsymbol{number\ of\ cells\ per\ ml} = (\boldsymbol{cell\ count}/2)\ \mathrm{x}\ 10^4$. Cells were thoroughly mixed and a 10µl sample was taken from each cell suspension for counting. 10µl of trypan blue was added and mixed with the sample. Viable (=brightly shimmering, Trypan Blue negative) cells were then counted under a microscope using a Neubauer hemocytometer. Counting was always performed at least in triplicates.

2.2.4. Immunological methods

2.2.4.1. Flow cytometry

Single-cell suspension was processed from BM and Spleen in PBS containing 0.5% BSA. Red blood cells were lysed using ACK lysis buffer. Cell suspensions were resuspended at 4°C in PBS. For extracellular staining, cells were incubated with fluorescently labeled antibodies (Tables 9 and 10) in FACS buffer for 30 min on ice in the dark. Unbound antibodies were removed by subsequent washing with FACS buffer. Viability distinction was realized by resuspending the cell pellet with LIVE/DEAD™ Fixable Violet Dead Cell Stain according to the manufacturer's protocol. Labeled cells were run on Cytoflex S (Beckman Coulter, BREA, USA) and data were analyzed with FlowJo™ Version 10.6.0 software.

Cellular stages of B-cell development and differentiation by flow cytometry panel were developed to define various B-cell differentiation in Bone marrow and secondary lymphoid organs. This panel was based on the previous study design conducted for B-cell subsets differentiation (Alouche et al., 2021; Anderson et al., 2007; Balabanian et al., 2012; Biajoux et al., 2016; Patton et al., 2014; Perlot & Penninger, 2012; Tomayko et al., 2010). An initial basic

gating strategy was used to identify B-cells and to exclude dead and doublets collected during the acquisition. Specific subsets in bone marrow were identified by further sequential gating based on the surface expression of various markers (Fig. 3A).

For the spleen, the heterogeneous population of cells with the unique functional property was identified with help of an extensive gating strategy for B-cell differentiation (Fig. 3B-D). Sequentially designed gating followed the B-cell development through various stages of transition and maturation identifying memory B-cells, transitional B-cells, plasmablasts, and plasma. cells.

A

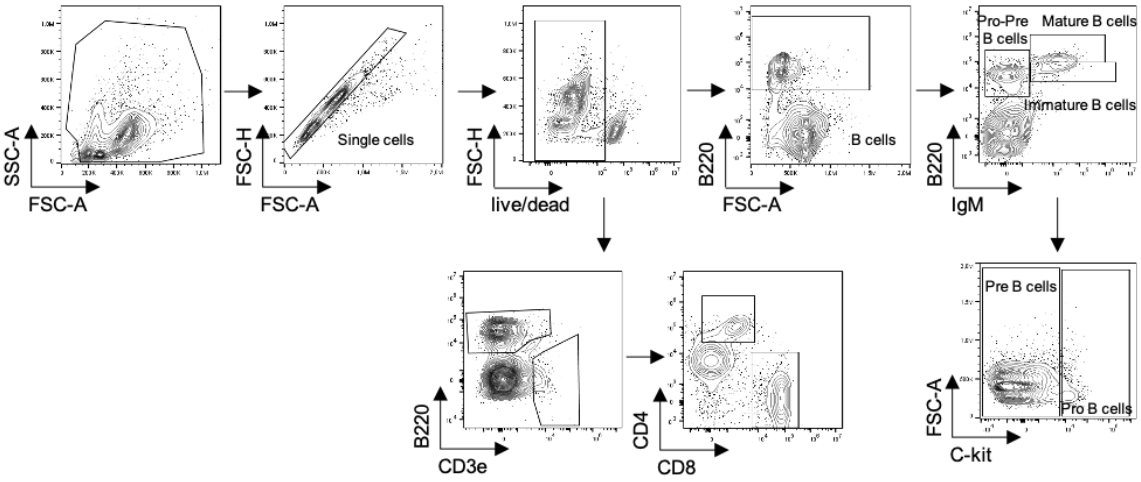

B

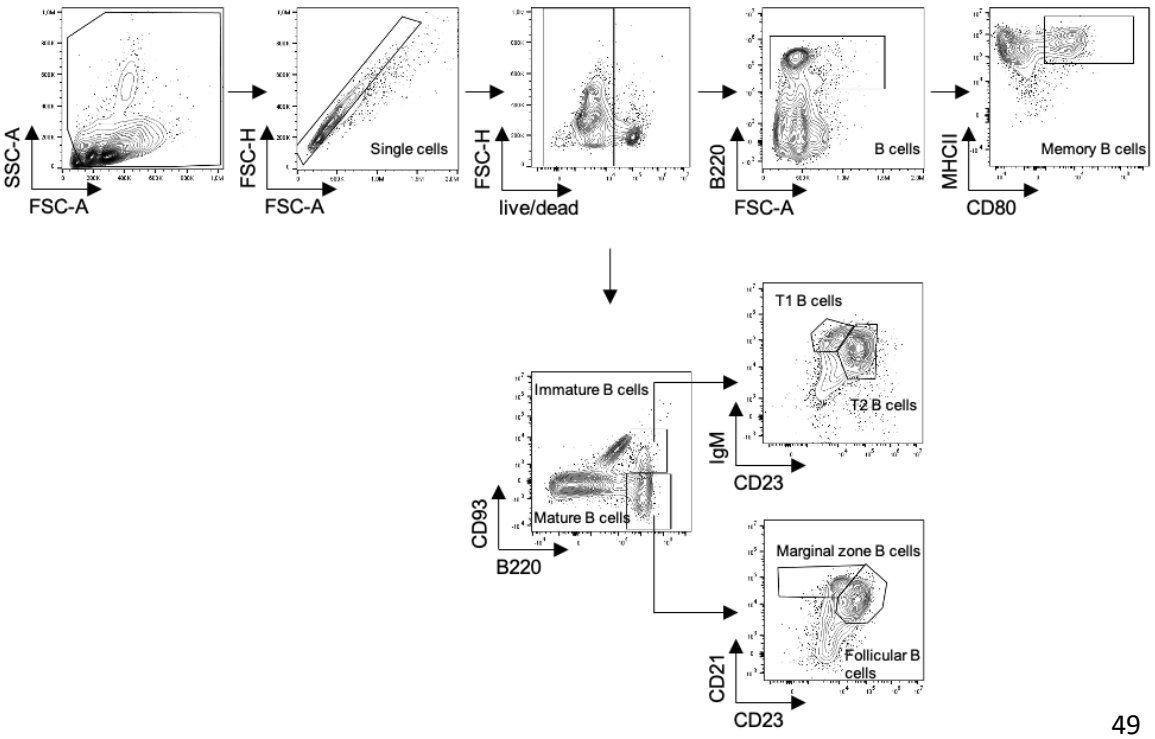

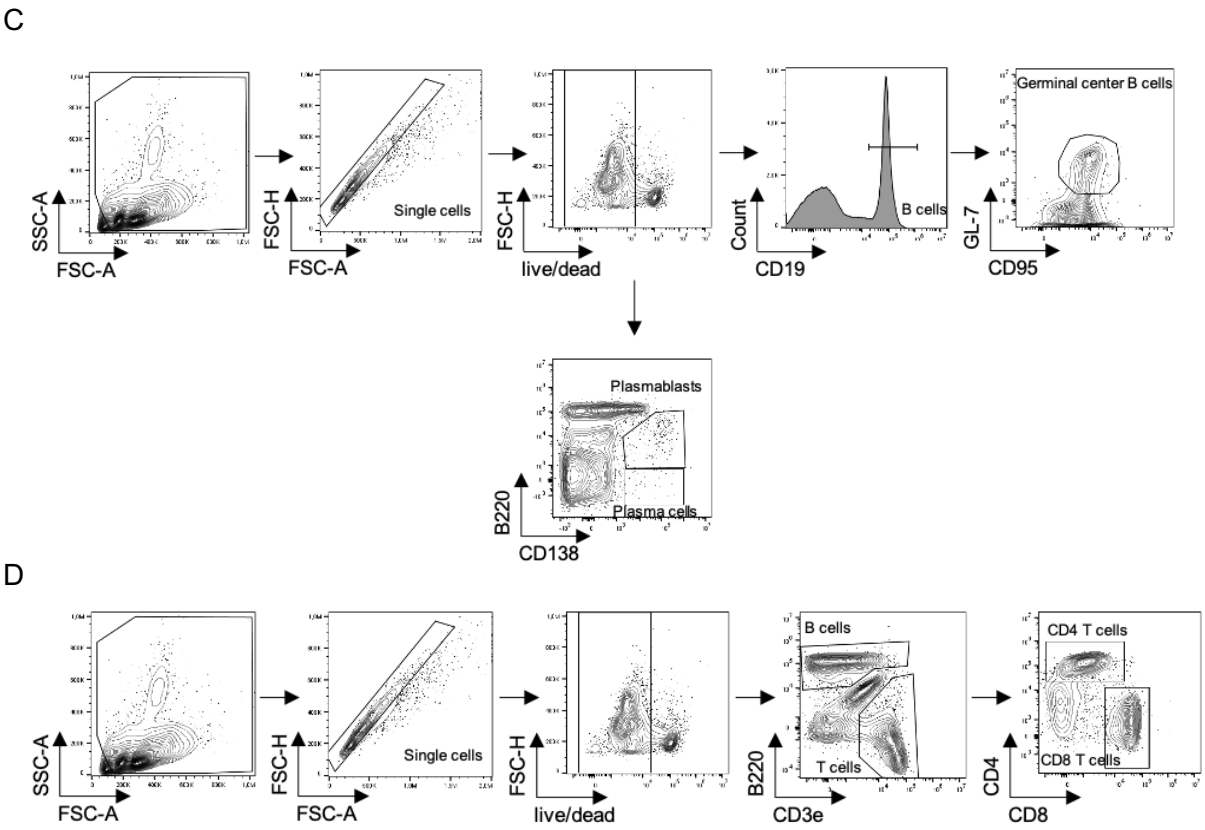

Figure 3. Illustration of the gating strategy used to quantify different B-cell developmental stages in the bone marrow and in the spleen. First, debris and red blood cells (RBC) are excluded by their cell size and granularity (FSC/SSC) followed by doublet exclusion. Aqua blue was used to eliminate dead cells. **A** Pro/Pre and immature B-cells were defined by gating B220 against IgM, further differentiation between Pro/Pre cells was done with the help of the c-kit. T cells were differentiated from B-cells by gating CD3e against B220 and further for CD4 and CD8. **B** FACS panel distinguishing B-cell ($B220^+$), memory B-cells ($B220^+$ $CD80^+$ $MHCII^+$), immature ($B220^+CD93^+$) and mature B cells ($B220^+CD93^-$), T1 (IgM^+CD23^-), T2 (IgM^+CD23^+) transitional B-cells, and follicular B cells ($B220^+CD21^+CD23^+$) and marginal zone B-cells ($CD21^{hi}CD23^{lo}$) in the spleen. **C** $CD19^+$ B cell population defined GC B-cells via GL7 and CD95 staining. Plasma cells and plasmablasts population were defined via B220 and CD138 staining **D** T cells were differentiated from B-cells by gating CD3e against B220 and further for CD4 and CD8

2.2.4.2. Collection of serum

Up to 300µl of whole blood from mice were collected in microvette tubes and allowed to clot for 20 min at RT. The clot was removed by subsequent centrifugation in a table centrifuge at 2.000 x g for 10 min at 4 °C. The supernatant was collected and stored at – 20 °C.

2.2.4.3. Enzyme-linked immuno assays and serum protein electrophoresis

Sera were harvested by cardiac puncture after euthanasia. Basal Ig concentrations of IgM, IgA, and IgGtotal were determined by ELISA (EBioscience, CA, USA). Optical densities were measured on a Microplate Reader (BioTek 800 TS). Statistical analysis was performed via Student's t-test on GraphPad Prism Version 9.0. (GraphPad Software, La Jolla, CA). Electrophoresis of mouse sera was performed on agarose gels employing a Hydrasis 2 Scan (Sebia, Fulda, Germany).

2.2.4.4. Magnetic cell separation

Murine B-cells were magnetically purified from BM, Spleen, and tumor material from young as well sick and aged-matched mice using CD19 MicroBeads according to the manufacturer's protocol. The efficiency of purification was assessed by flow cytometry.

2.2.4.5. Histology and immunohistochemistry

Mouse spleen, lymph nodes, and tumor tissues were fixed in 4% histofix solution for min. 48 h, bone marrow samples were fixed for 24 h in 4% histofix followed by min. 72 h in Osteosoft solution dehydrated under standard conditions and embedded in paraffin. Sections prepared with a rotary microtome were collected and subjected to histological and immunohistochemical analysis. Hematoxylin-Eosin (H.E.) staining was performed on deparaffinized sections with Eosin and Mayer's Haemalaun according to a standard protocol. Formalin-fixed murine samples were embedded in paraffin and were then sent to the Institute of Pathology in Tübingen, where the samples were cut into sections using a microtome and processed according to local standard protocols.

2.2.5. Protein biochemistry

2.2.5.1. Cell lysis

Single-cell suspension generated from the spleen was purified using CD19 MicroBeads. Cells were serum starved in RPMI for 2 hours, stimulated with 10 μg/ml F(ab')2 goat anti-mouse

IgM (Ebioscience) and 100 nM Cxcl12 (BioLegend), and lysed in 50 – 100 µl RIPA buffer (Table 8) containing phosphatase and protease inhibitors. The tubes were incubated in ice for 30 min, centrifuged for 10 min at 4 °C and the supernatant was transferred to a clean 1.5 ml tube. Protein concentration was determined using Bradford Protein assay following the manufacturer's protocol. 15 to 100 µg protein was mixed with 1 x SDS loading buffer and boiled at 95 °C for 5 min.

2.2.5.2. SDS-PAGE and immunoblotting

An equivalent amount of protein sample was resuspended in 6X Laemmli buffer in a final volume of 30µl. Gels were prepared as described in Table 8. Samples, 30µl of pre-stained molecular weight marker, and any empty well filled with 30µl to avoid differences in the run were loaded onto 10% SDS polyacrylamide gels and electrophoretically separated in 1X Running Buffer in an electrophoresis chamber at 100 V for 2.5 hours. Alternatively, proteins were transferred at 30 V overnight. The gel was blotted onto a 0.45 µm PVDF membrane. The membranes were previously activated with methanol for 5 min. The blot sandwich was placed in a transfer chamber submerged in 1X transfer buffer and a block of ice. The gel-to-membrane sandwich was left for blotting for 2 h at 100 V. After blotting, membranes were blocked with 5% BSA in TBS-T or 5% skim milk in TBS-T. Following blocking, membranes were washed 3 times for 10 minutes in TBS-T and incubated overnight with a primary antibody on a shaker at 4°C. Membranes were washed 3 times in TBS-T and incubated with the corresponding HRP-conjugated secondary antibody for 1 hour. After washing, ECL prime detection reagent was used on the membrane for 30 sec, and visualization was done by ChemoStar PLUS Imager. Protein quantification was performed using Image J software. Primary and secondary antibodies and their dilutions used in this study are listed in Tables 11 and 12.

2.2.5.3. Membrane stripping

To re-probe the PVDF membranes with more antibodies, the membranes were incubated with a stripping buffer for 10 min. Next, the membranes were washed 3 times for 10 min in TBS-T

on a shaker and blocked again followed by overnight incubation with the corresponding primary antibodies on a shaker at 4°C.

2.2.6. Transcriptome analysis

2.2.6.1. RNA isolation from tissue material for RNA-sequencing

Spleens and Bone Marrow were harvested and strained through a 70µm cell strainer. Erylysis was performed using ACK-Lysing Buffer (Thermofisher Scientific, Waltham, MA). Murine cells were magnetically purified using CD19 MicroBeads (Miltenyi Biotec, Bergisch Gladbach, Germany). Enrichment was controlled by Flow cytometry to ensure a purity of at least 90%. RNeasy Plus Mini Kit (Qiagen) was then used to isolate RNA according to the manufacturer's protocols. RNA quality was assessed with the Agilent RNA 6000 Pico Kit according to the manufacturer's instructions in the Agilent Bioanalyzer 2100. Only RNA with a RIN higher than 7 was considered for further analyses.

2.2.6.2. RNA-sequencing

Library preparation for bulk 3'-sequencing of poly(A)-RNA was done as described previously (Parekh et al., 2016). Briefly, the barcoded cDNA of each sample was generated with a Maxima RT polymerase (Thermo Fisher Scientific) using an oligo-dT primer containing barcodes, unique molecular identifiers (UMIs), and an adapter. 5' ends of the cDNAs were extended by a template switch oligo (TSO) and after pooling of all samples, full-length cDNA was amplified with primers binding to the TSO-site and the adapter. cDNA was fragmented with the Nextera XT kit (Illumina, San Diego, CA, USA), and 3'-end fragments were finally amplified using primers with Illumina P5 and P7 overhangs. In comparison to (Parekh et al., 2016), P5 and P7 sites were exchanged to allow sequencing of the cDNA in read1 and barcodes and UMIs in read2 to achieve better cluster recognition. The library was sequenced on a NextSeq 500 (Illumina) with 75 cycles for the cDNA in read1 and 16 cycles for the barcodes and UMIs in read2. Data were processed using the published Drop-seq pipeline (v1.0) to generate sample- and gene-wise UMI tables. Reference genome (GRCm38) was

used for alignment. Transcript and gene definitions were used according to the ENSEMBL annotation release 75. RNA-Seq data were aligned and quantified with STAR and mRNA reads were identified using an in-house analysis pipeline detecting exons in a shuffled order. Differential gene expression analysis was carried out with DEseq2, and volcano plots were generated using GraphPad Prism Version 9.0. (GraphPad Software, La Jolla, CA).

2.2.7. Statistical analyses

Statistical analyses were performed using GraphPad Prism Version 9.0. (GraphPad Software, La Jolla, CA). The error bars shown in the figures represent the standard deviation (SD) unless specified otherwise. The statistical tests in each experiment are indicated in the figure legends. A 2-tailed Student's t-test was used to compare quantitative data between 2 independent samples. When comparing 3 or more groups, a one-way ANOVA statistical test was used to compare group means followed by Tukey's multiple comparisons tests. Survival data were completed using a log-rank (Mantel-Cox) test. Results with a P value of less than 0.05 were considered significant (*$P < 0.05$, **$P < 0.01$, ***$P < 0.001$) and indicated in the figures.

3. RESULTS

3.1. Development of novel transgenic mouse models for the investigation of B cell lymphomagenesis

This study aimed to investigate the *in vivo* effects of combined MYD88^{L265P} and CXCR4^{C1013G} mutations in murine B-cells. To achieve this, two conditional mouse models were generated. The first model used the CD19-Cre allele to conditionally express the Myd88^{L252P} mutations in the pan B-cells, while the second model utilized the Aid-Cre allele to conditionally express the mutation in germinal center B-cells. The mutation was expressed upon Cre-mediated recombination from the endogenous mouse Myd88 locus. For the breeding of the transgenic model mice, heterozygous mice for the Cre, mutant Myd88, and CXCR4 alleles were used. This allowed for the selective expression of the mutations and the generation of mice with the desired genotypes. The purpose of these models was to better understand the biological effects of these mutations on B-cell development and function, as well as their role in the development of lymphoid malignancies. (Fig. 4A and B).

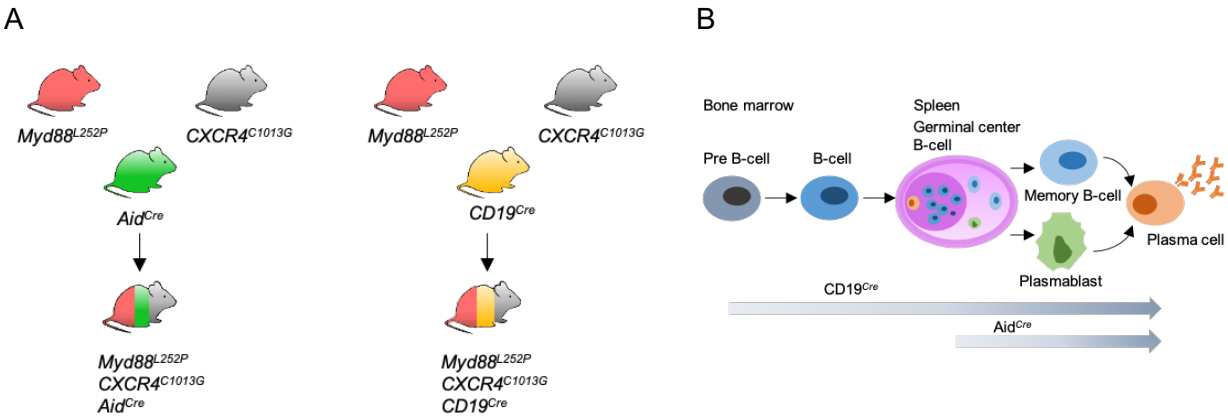

Figure 4. Schematic representation of breeding strategy for the generation of transgenic mouse model. (**A)** Schematic illustration of the breeding strategy to generate *CXCR4*^{C1013G}; *Myd88*^{L252P}; Aid$^{Cre/+}$ (CM-Aid) mice and *CXCR4*^{C1013G}; *Myd88*^{L252P}; *CD19*$^{Cre/+}$ (CM-19) mice. (**B)** B-cell–specific *Myd88*^{L252P} expression induced by Cre-mediated recombination under the control of the Aid promoter active in germinal center B-cells, and the CD19 promoter active throughout B-cell development.

3.2. Assessment of B-cell lymphomagenesis and disease progression in *Myd88^{L252P}* and *CXCR4^{C1013G}* transgenic mouse models

To determine whether the presence of *Myd88^{L252P}* and *CXCR4^{C1013G}* transgenes in mice is associated with the development of B-cell lymphomas or any significant pathological changes consistent with B-cell lymphoproliferation, we monitored the phenotype of transgenic animals for changes in weight, spleen size, and lymph node size. Between the groups of wildtype (WT), *CXCR4^{C1013G}* (C), *Myd88^{L252P};AidCre* (M-Aid), and *CXCR4^{C1013G};Myd88^{L252P};AidCre* (CM-Aid) mice, our results indicated that the presence of CXCR4^{C1013G} significantly accelerated Myd88-driven lymphomagenesis, as CM-Aid mice showed reduced overall survival with a median survival of 77 weeks compared to M-Aid and other controls (Fig. 5A). The physiological alterations observed in the CM-Aid mice consisted of splenomegaly and lymphadenopathy development, which occurred in 40% of the mice (Fig. 5B and C). Additionally, we assessed *CXCR4^{C1013G};Myd88^{L252P};CD19-Cre* (CM-19), *Myd88^{L252P};CD19-Cre* (M-19), and their respective controls for signs of disease development. CM-19 mice were observed to have a reduced overall survival with a median survival of 67 weeks compared to M-19 and other controls (Fig. 5D). Furthermore, the development of lymphadenopathy is more frequent in CM-19 mice compared to controls, indicating a more severe pathological phenotype (Fig. 5E and F). Overall, our findings suggest that the concurrent presence of *CXCR4^{C1013G}* and *Myd88^{L252P}* transgenes in mice is associated with more aggressive development of B-cell lymphomas and significant pathological alterations.

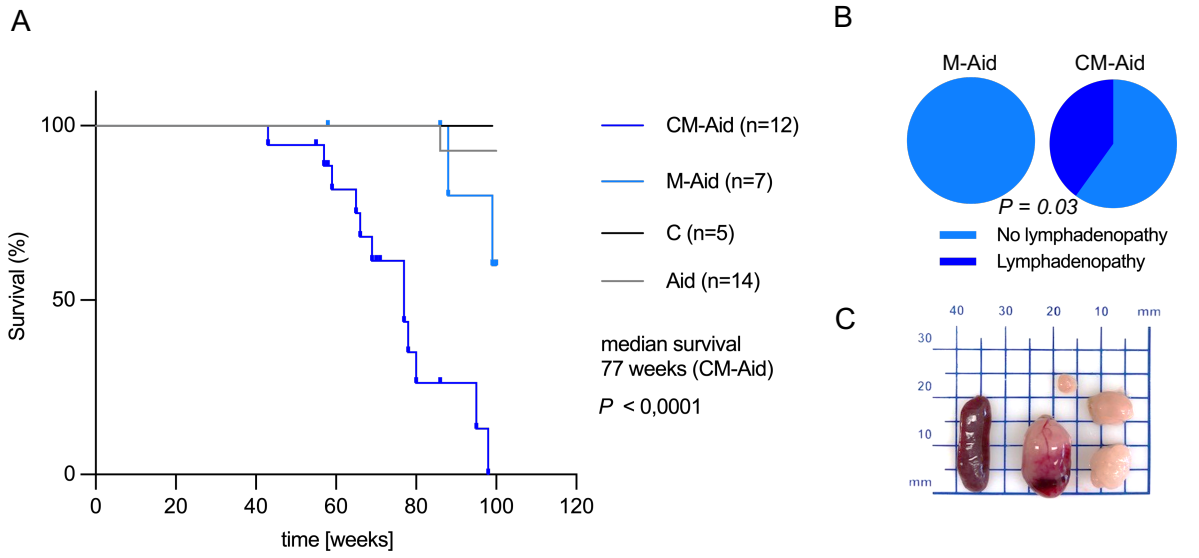

D

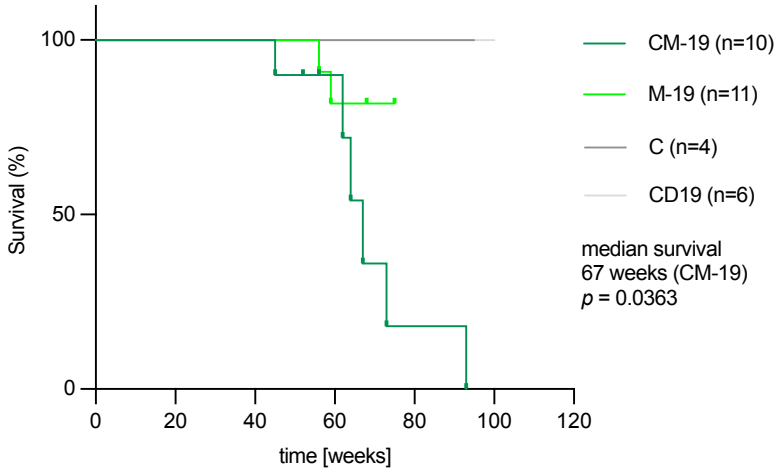

E

Genotype CM-19	Age (weeks)	Phenotype
1	45	weight loss
1	62	lymphadenopathy, splenomegaly
1	64	lymphadenopathy
1	67	lymphadenopathy, splenomegaly
1	100	lymphadenopathy

F

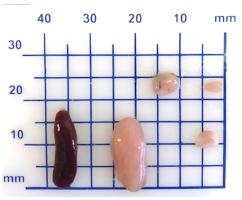

Figure 5. Co-expression of the B-cell lymphoma driver *Myd88^{L252P}* with activated *CXCR4^{C1013G}* promotes lymphomagenesis. A) Kaplan-Meier curve showing the overall survival of CM-Aid (n=12), M-Aid (n=7), C (n=5), and Aid (n=14). Median survival and P-value of log-rank Mantel-Cox test are displayed. **B** Pie chart representing the percentage of animals with lymphadenopathy in CM-Aid (n=13) and M-Aid (n=12). P value was calculated using Fisher's exact test. **C** Necropsy image of representative spleen and lymph node of CM-Aid mice. **D** Kaplan-Meier curve showing the overall survival of CM-19 (n=10), M-19 (n=11), C (n=4), and CD19 (n=6). The median survival and P-value of the log-rank Mantel-Cox of the test are displayed. **E** Tabular chart representing the characteristic phenotype of animals with lymphadenopathy in CM-19 mice (n=5). **F** Necropsy image of representative spleen and lymph node of CM-19 mice.

3.3. Phenotypic and histopathological characterization of *CXCR4^{C1013G}* and *Myd88^{L252P}* co-expressing mice reveals lymphoma with plasmacytic differentiation and non-GC Phenotype

The study further aimed to investigate the observed phenotype in the sick *CXCR4^{C1013G}* and *Myd88^{L252P}* co-expressing, CM-Aid and CM-19, mice and evaluate its impact on the morphology and cellularity of the tissues. To accomplish this, histopathological analysis was performed on the BM, spleen, and lymph nodes collected from the mice at the endpoint. The criteria of endpoint for sick animals were defined by the presence of lymphadenopathy, expanded belly due to splenomegaly, and reduced physical activity while the endpoint for the control animals was defined by their age (102 weeks). The samples were analyzed by H&E staining and additional immunohistochemistry staining was performed for B220, CD3, IRF4, BCL6, and CD138 markers. The histological examination of the disease-bearing CM-Aid and CM-19 mice invariably demonstrated enlarged lymph nodes with prominent infiltration of tumoral cells, reflecting the tumor morphology and immunophenotype detected in the spleen.

In the CM-Aid mice, five of eight mice showed complete loss of architecture with the expansion of the marginal zone, moderate loss of the T cell zone, expansion of the B cells, and a slight increase of the IRF4^{+} CD138^{+} plasma cells. The tumor cells presented with medium-sized cells with moderate cytoplasm, predominantly centroblast morphology, and were positive for B220 and IRF4. The spleen's morphology and immunophenotype pointed to a low-grade lymphoma with plasmacytic differentiation. Whereas, three out of eight mice presented characteristics of DLBCL with a non-GC phenotype (Fig. 6A). In the CM-19 mice, the spleen from three out of five mice showed abnormal architecture with an atypical expansion of the B cells. The tumor cells were positive for B220 and IRF4, pointing to a low-grade lymphoma with plasmacytic differentiation. In contrast, two out of five mice presented with loss of the spleen architecture with a prominent expansion of the white pulp. The tumoral cells were large-sized polymorphic cells with open chromatin, central nucleolus, B220 and IRF4 positive and BCL6 negative, pointing to a DLBCL of non-GC phenotype (Fig. 6A). The spleen of the wildtype (Fig. 6B) and Aid Cre (Figure not shown) control mice showed normal architecture with well-developed white and red pulp. The spleens of the *CXCR4*^{C1013G} mice showed disorganized architecture with reduced B and T cell populations. Two out of five M-Aid mice spleens respectively showed B220+ IRF4+ infiltrating cells pointing towards a low-grade B-cell lymphoma with plasmacytic differentiation and a morphological immunophenotype of a DLBCL with a non-GC phenotype (Fig. 6B).

To determine whether *CXCR4*^{C1013G} and *Myd88*^{L252P} expression indicate clonal B-cell expansion, we performed a PCR-based VD(J) rearrangement assay with DNA samples collected from tumors of CM-Aid and CM-19 mice. The different amplified PCR VDJ IgH rearrangements can be visualized by size separation via agarose gel electrophoresis: rearrangements into JH1 will produce an amplicon of 1.5 Kb size, while rearrangements into JH2, JH3, and JH4 will have a size of 1.2 Kb, 1 Kb, and 0.5 Kb respectively. PCR-based VDJ rearrangement assays revealed that the majority of CM-19 and CM-Aid lymphomas represented oligoclonal disease in affected lymph nodes (Fig. 6C).

These findings suggest that the *CXCR4*^{C1013G} and *Myd88*^{L252P} co-expression promotes oligoclonal tumor progression and contributes to the development of B-cell lymphoma with plasmacytic differentiation or DLBCL with a non-GC phenotype.

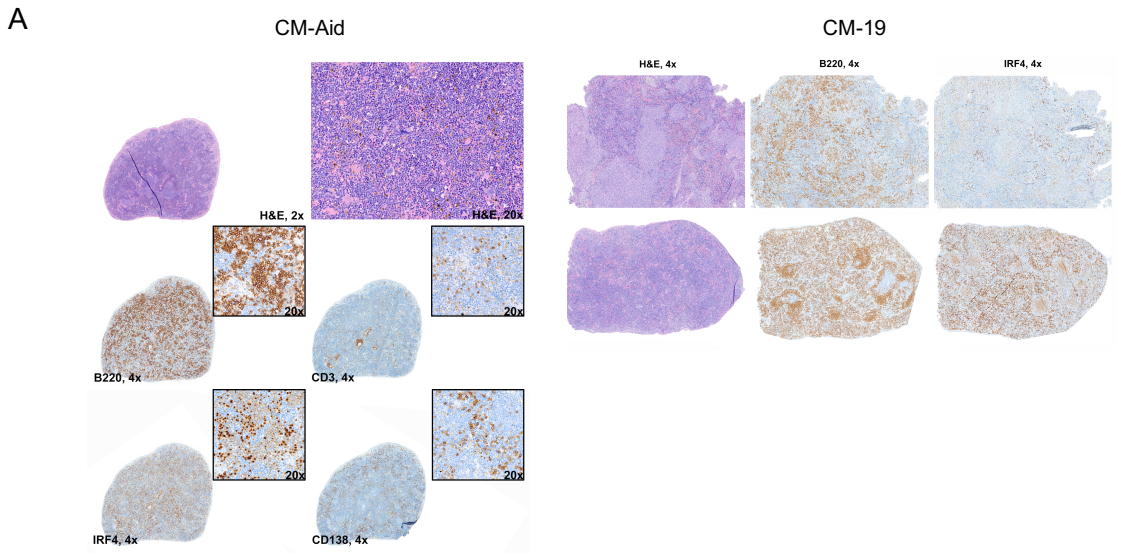

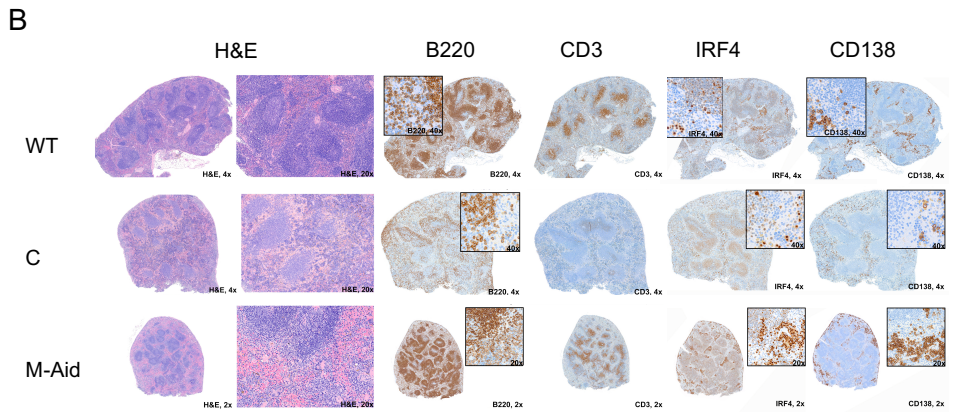

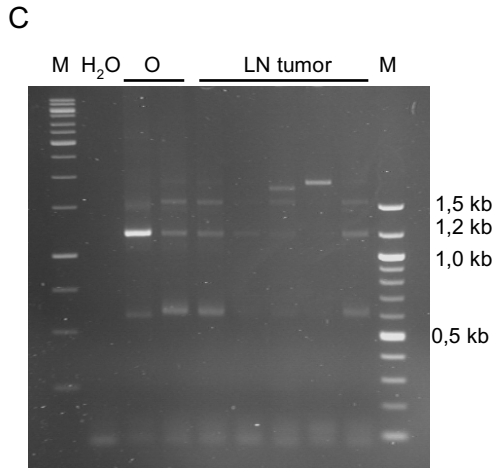

Figure 6. Histopathology and clonality analysis of tumor samples from CM-Aid and CM-19 mice. A Representative image from histopathology analysis of CM-Aid and CM-19 mice. **B** Representative image from histopathology analysis of the control mice. Histopathological analyses were performed by Prof. Dr. Leticia Quintanilla-Fend and Dr. Irene Gonzalez-Menendez. **C** Clonality analysis from isolated tumor DNA of CM-Aid and CM-19 mice. O: oligoclonal control, H_2O: negative control, M: marker, LN tumor: genomic DNA extracted from lymph node tumor of CM-Aid and CM-19 mice.

3.4. *CXCR4*^{C1013G} advances *Myd88*^{L252P}-induced lymphomagenesis with key features of human Waldenström macroglobulinemia

As the pathogenesis of Waldenström macroglobulinemia is characterized by IgM hypergammaglobulinemia, we assessed the serum IgM levels of the sick mice. Our results demonstrated that CM-Aid mice did not exhibit significantly elevated serum IgM levels compared to M-Aid mice as the presence of *Myd88*^{L252P} alone resulted in higher serum IgM (Fig. 7A). However, upon serum electrophoresis analysis, we observed clonal IgM peaks in 3 out of 5 CM-Aid mice, indicating the progression of a malignant clone, as compared to M-Aid mice (Fig. 7B). These findings suggest that CXCR4^{C1013G} advances Myd88^{L252P}-induced progression of a malignant clone, with elevated IgM levels mimicking that of human Waldenström macroglobulinemia.

To further investigate the effect of enhanced *CXCR4*^{C1013G} and *Myd88*^{L252P} signaling in B-cells on oligoclonal tumor progression and reduced survival, we performed extensive immunophenotyping in the sick and age-matched control mice. Bone marrow and spleen were collected from sick mice upon phenotypic representation of disease development, particularly lymphoma-related symptoms such as weight loss, lymph node enlargement, abdominal distension from splenomegaly, and mesenteric tumor formation. We found that in the bone marrow, CM-Aid mice did not exhibit a significant difference in B-cell count compared to the control genotypes (Fig. 7C). In contrast, there was a slight increase in CM-Aid spleen weight and splenic cell count compared to WT, C, and M-Aid mice (Fig. 7D). In the spleen of sick CM-Aid mice, we did not observe a significant increase in CD138^{+}B220^{lo} plasmablasts and MHCII^{+}CD80^{+} memory B-cells (Fig 7E). Moreover, red blood cell counts, platelet counts, and

hematocrit and hemoglobulin levels did not differ between the CM-Aid and control mice (Fig. 7F). While our observations made in the sick and aged mice did not reach statistical significance, they represent the late phases of lymphomagenesis and may not accurately reflect the initial onset of disease progression.

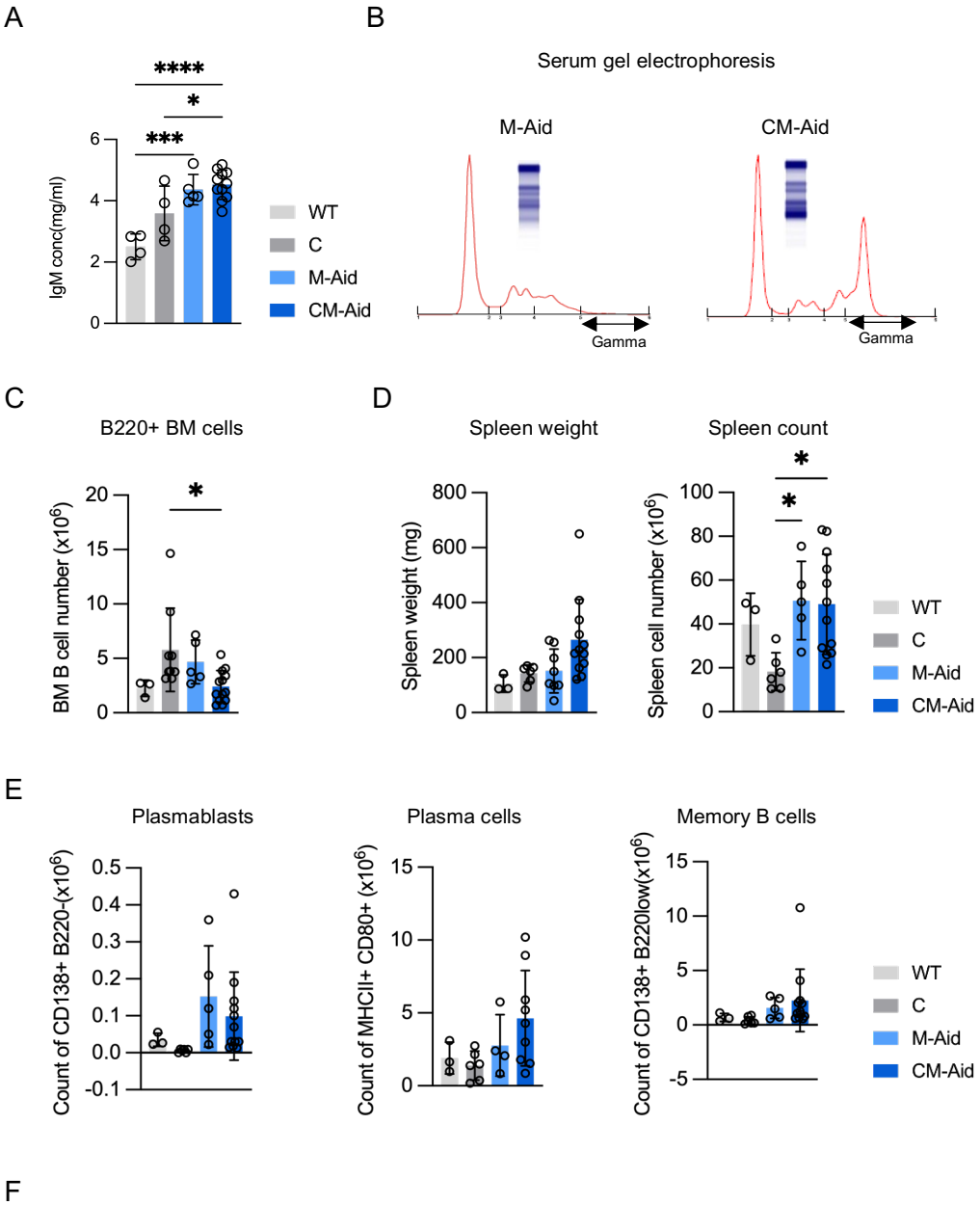

F

Blood characterization in WT, C, M-Aid, and CM-Aid mice

Blood Parameters	WT (n = 3)	C (n = 3)	M-Aid (n = 5)	CM-Aid (n = 7)
White blood cell (10^3 /mm^3)	7.40 ± 2.8	1.50 ± 1.08	4.50 ± 3.05	1.90 ± 0.56
Blood Lymphocyte (10^3 /mm^3)	3.80 ± 1.23	0.96 ± 0.6	3.34 ± 1.68	1.10 ± 0.35
Platelets (10^3 /mm^3)	235 ± 80	144 ± 52	818.6 ± 582.7	322.5 ± 342.1
Haemoglobin (g/dl)	12.8 ± 0.44	10.2 ± 1.3	12.90 ± 0.72	8.00 ± 4.96

Data are means ± SD.

Figure 7. Enhanced CXCR4 and Myd88 signaling cooperate to promote clonal progression in a mouse model of Waldenström macroglobulinemia. A Serum immunoglobulin levels for IgM in WT (n=4), C (n=4), M-Aid (n=5), and CM-Aid (n=11) mice. Control mice were at an experimental endpoint of 102 weeks. **B** Representative image of the serum gel electrophoresis histogram from M-Aid (n=5) and CM-Aid (n=7) mice. Serum electrophoresis analysis was performed by Dr. Markus Thaler. **C** Bone marrow B-cells cell count from 2 femur and 1 tibia of aged WT (n=4), C (n=4), M-Aid (n=5), and CM-Aid (n=7) mice. **D** Spleen weight and spleen count in aged WT (n=4), C (n=4), M-Aid (n=5), and CM-Aid (n=7) mice. **E** Flow cytometric analysis and respective quantification for $CD138^{+}B220^{lo}$ plasmablasts, $CD138^{+}B220^{-}$ plasma cells, and MHCII+CD80+ memory B-cells in aged WT (n=3), C (n=6), M-Aid (n=5), and CM-Aid (n=9) mice. **F** Blood characterization was calculated from the Scil animal counter for aged WT (n=3), C (n=3), M-Aid (n=5), and CM-Aid (n=7) mice. Statistical analyses were performed with one-way ANOVA with Tukey correction for multiple comparisons. *, $p \leq 0.05$; **, $p \leq 0.01$; ***, $p \leq 0.001$

3.5. *CXCR4*^{C1013G} and *Myd88*^{L252P} cooperatively promote the accumulation of $CD138^{+}B220^{lo}$ plasmablasts and $MHCII^{+}CD80^{+}$ memory B-cells without expansion of the splenic B-cell pool

To identify the early events that lead to the development of the disease and the effect of B-cell-specific expression of *Myd88*^{L252P} with *CXCR4*^{C1013G} on B-cell development and differentiation in a premalignant state, we analyzed mice at the age of 10 to 14 weeks. Bone marrow and secondary lymphoid organs of M-Aid, CM-Aid, M-19, CM-19, and their respective controls were examined. Gross pathological assessment upon necropsy did not reveal any internal lesions, and only showed a slight increase in spleen weight and total splenic B-cells for *Myd88*^{L252P}; *CXCR4*^{C1013G} transgenic mice and mice carrying *Myd88*^{L252P} mutation alone (Fig. 8A). Moreover, the B220+ B-cell population in the bone marrow and spleen showed no significant difference between the experimental and control animals (Fig. 8B). The overall architecture of the spleen across the genotypes remained similar indicating no significant lymphoproliferation. However, FACS-based analysis from the harvested bone marrow and spleen samples displayed a striking expansion of the $CD138^{+}B220^{lo}$ plasmablasts population in the CM-Aid and CM-19 transgenic mice. CM-19 mice displayed a significantly higher IgM^{+} plasmablast compared to CM-Aid mice, indicating that an early *Myd88*^{L252P} expression in B-cells along with *CXCR4*^{C1013G} activation drives the accumulation of IgM^{+} plasmacytic

differentiation (Fig. 8C). These IgM^{+} plasmablasts are derived from mature B-cells which do not pass-through germinal center reaction but are generated as an extra-follicular response. The early activation of *CXCR4*^{C1013G} and *Myd88*^{L252P} mutations in naïve B-cells leads to the rapid maturation of memory B-cells, represented by the expansion of MHCII+CD80+ B-cells (Fig. 8D). This expansion of memory B-cells, which is proposed as the main cell type for WM progression, is shown to be crucially dependent on the CD19-mediated co-expression of *CXCR4*^{C1013G} and *Myd88*^{L252P}. These findings provide important insights into the cellular origin of WM.

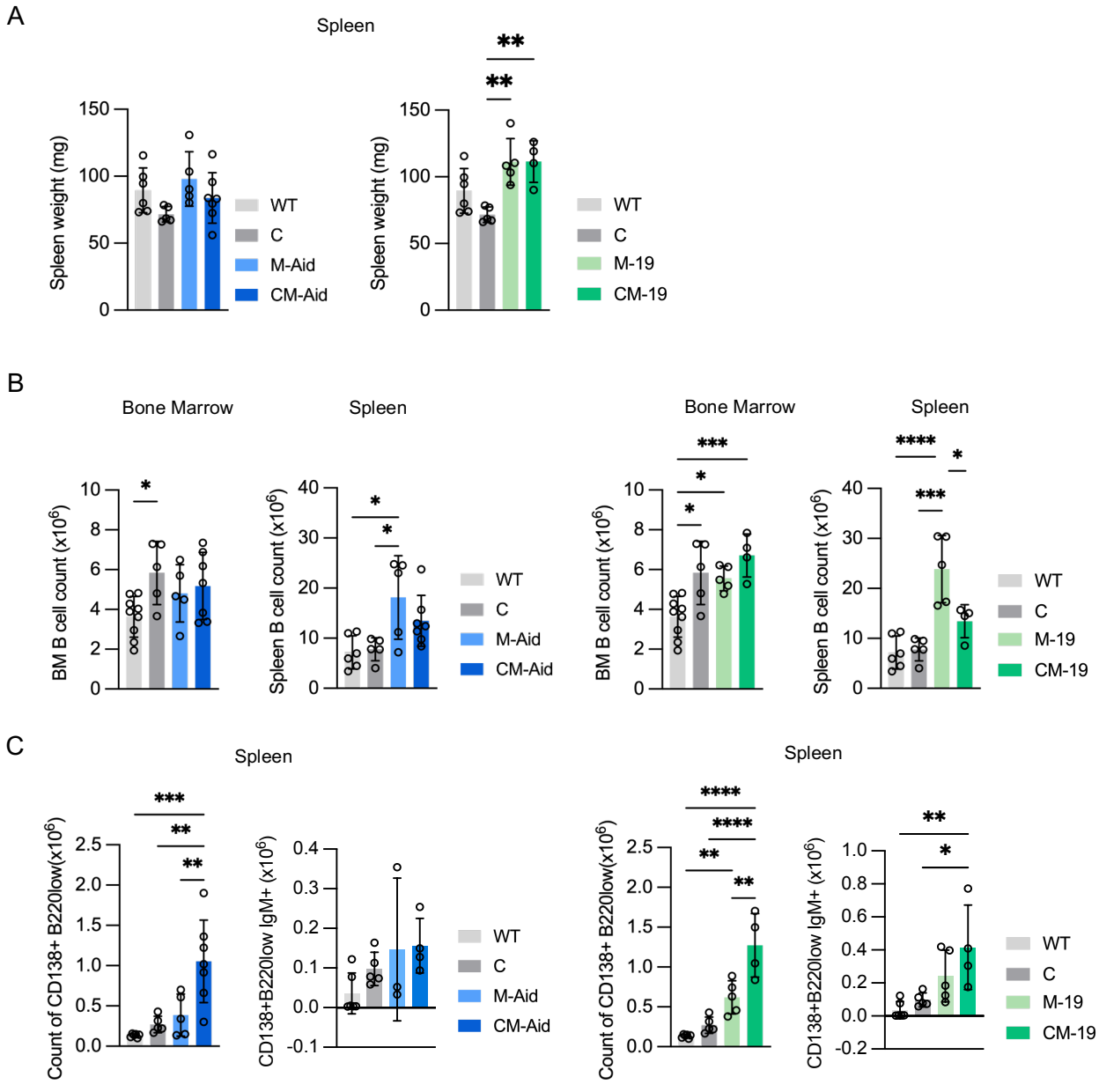

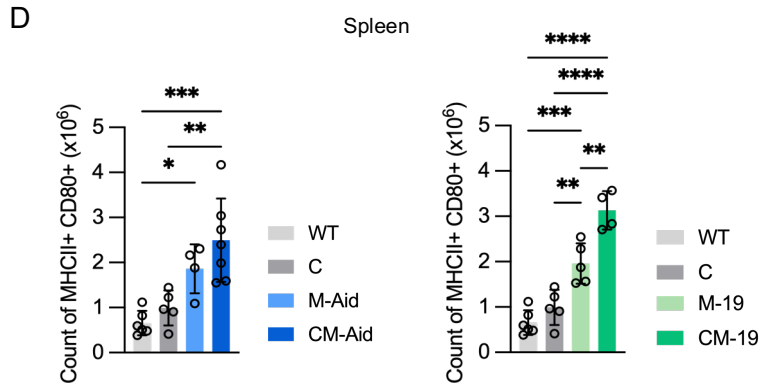

Figure 8. *CXCR4*^{C1013G} and *Myd88*^{L252P} promote the accumulation of IgM-positive CD138^{+}B220^{+} plasmablasts and MHCII^{+}CD80^{+} memory B-cells. A Spleen weight comparison of WT (n=6), C (n=5), M-Aid (n=5), CM-Aid (n=7), M-19 (n=5), and CM-19 (n=4) mice. **B** Flow cytometric analysis and quantification of B-cells in the bone marrow and spleen. WT (n=6), C (n=5), M-Aid (n=5), CM-Aid (n=7), M-19 (n=5), and CM-19 (n=4). **C** Flow cytometric analysis and quantification for IgM^{+}CD138^{+}B220^{lo} plasmablasts in 10 - 14-week-old WT (n=6), C (n=5), M-Aid (n=5), CM-Aid (n=7), M-19 (n=5) and CM-19 (n=4) mice in the spleen. **D** Flow cytometric analysis and quantification for MHCII^{+}CD80^{+} memory B-cells in the spleen of 10 - 14-week-old WT (n=6), C (n=5), M-Aid (n=4), CM-Aid (n=7), M-19 (n=5) and CM-19 (n=4) mice. Statistical analyses were performed with one-way ANOVA with Tukey correction for multiple comparisons. *, $p \leq 0.05$; **, $p \leq 0.01$; ***, $p \leq 0.001$.

3.6. *CXCR4*^{C1013G} and *Myd88*^{L252P} cooperatively promote the accumulation of plasmacytic cells and selectively increase serum IgM

To further explore the B-cell differentiation in the bone marrow and spleen, we examined the plasma B cell compartment using CD138 expression. Plasma cell populations did not differ between CM-Aid and M-Aid where *Myd88*^{L252P} activation took place upon germinal center formation (Fig. 9A). Remarkably, we observed significantly elevated levels of CD138^{+}B220^{-} plasma cells in the bone marrow compartment of CM-19 mice (Fig 9B). In line with this observation, the spleen also displayed a significant increase in plasma cells in CM-19 animals. When examined for the total count of plasma cells in the bone marrow and spleen of the two models in the study, CM-19 mice exhibited a significantly higher number compared to CM-Aid (Fig. 9C). This is potentially due to the larger pool of B-cells expressing *Myd88*^{L252P} mediated by CD19-linked Cre expression. Furthermore, the majority of these CD138^{+}B220^{-} plasma cells

in both organs expressed surface IgM (Fig. 9D). These results suggest that CD19-mediated co-expression of *CXCR4*^{C1013G} and *Myd88*^{L252P} cause an accumulation of IgM+ plasma cells in both bone marrow and spleen, potentially contributing to the rapid pathogenesis of lymphoproliferation with features of lymphoplasmacytic lymphoma.

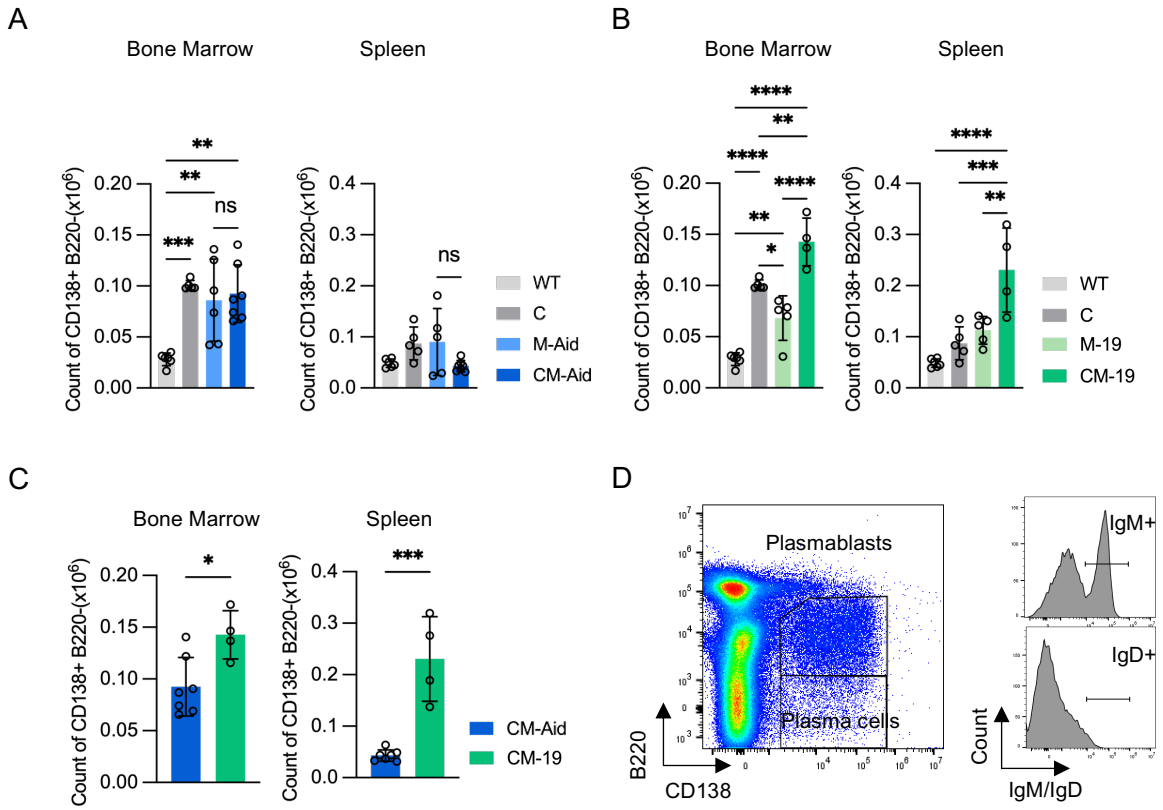

Figure 9. Early B-cell-specific expression *Myd88*^{L252P} with activated *CXCR4*^{C1013G} leads to increased IgM^{+} plasma cells. A Flow cytometric analysis and quantification of CD138^{+}B220^{-} Plasma cells in the bone marrow and spleen of 10 - 14 week old WT (n=6), C (n=5), M-Aid (n=5), and CM-Aid (n=7) mice. **B** Flow cytometric analysis and quantification of CD138^{+}B220^{-} Plasma cells in the bone marrow and spleen of 10 - 14 week old WT (n=6), C (n=5), M-19 (n=5) and CM-19 (n=4) mice. **C** Flow cytometric analysis comparing the quantification for CD138^{+}B220^{-} plasma cells in 10 - 14 week CM-Aid (n=7) and CM-19 (n=4) mice. **D** Flow cytometric gating of CD138^{+}B220^{-} plasma cells and histogram depicting IgM and IgD surface expression on gated CD138^{+}B220^{-} plasma cells. Statistical analyses were performed with one-way ANOVA with Tukey correction for multiple comparisons. *, $p \leq 0.05$; **, $p \leq 0.01$; ***, $p \leq 0.001$.

3.7. Pan-B-cell co-activation of *Myd88^{L252P}* and *CXCR4^{C1013G}* leads to IgM-hypergammaglobulinemia indicating deregulation of B-cell development

In this study, we investigated the expression of surface IgM in plasma cells of *Myd88^{L252P}*; *CXCR4^{C1013G}* transgenic mice, which is one of the major characteristics of human Waldenström macroglobulinemia. To assess the levels of immunoglobulin (Ig) titers in serum, we performed a serum enzyme-linked immunosorbent assay (ELISA) for IgM, IgA, and total IgG. Consistent with the increase in IgM-expressing plasma cells observed, CM-19 mice showed substantially increased serum IgM concentration compared to CM-Aid and control animals (Fig. 10A and B). However, there was no significant difference observed in the serum IgA and total IgG concentration across the models and genotypes. To further explore this finding, we performed serum protein electrophoresis on the sera collected from the experimental and control mice. We observed that young mice of 10-14 weeks had normal gamma globulin levels, with only a mild increase in CM-19 mice compared to controls (Fig.10C and D). These results demonstrate that the lymphoplasmacytic cell phenotype in WM is derived from the CD138^{+}B220^{-} plasma cells that have undergone somatic hypermutation, but not class switch recombination. Taken together, our results suggest that *Myd88^{L252P}* along with activated *CXCR4^{C1013G}* in an early B-cell developmental stage leads to the deregulation of B-cell development in the mature B-cells, potentially contributing to malignant transformation.

A

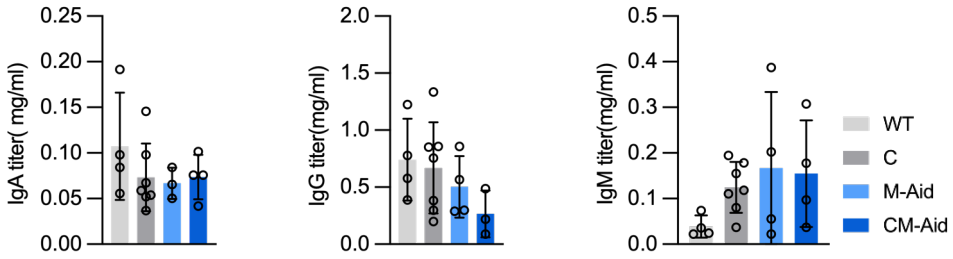

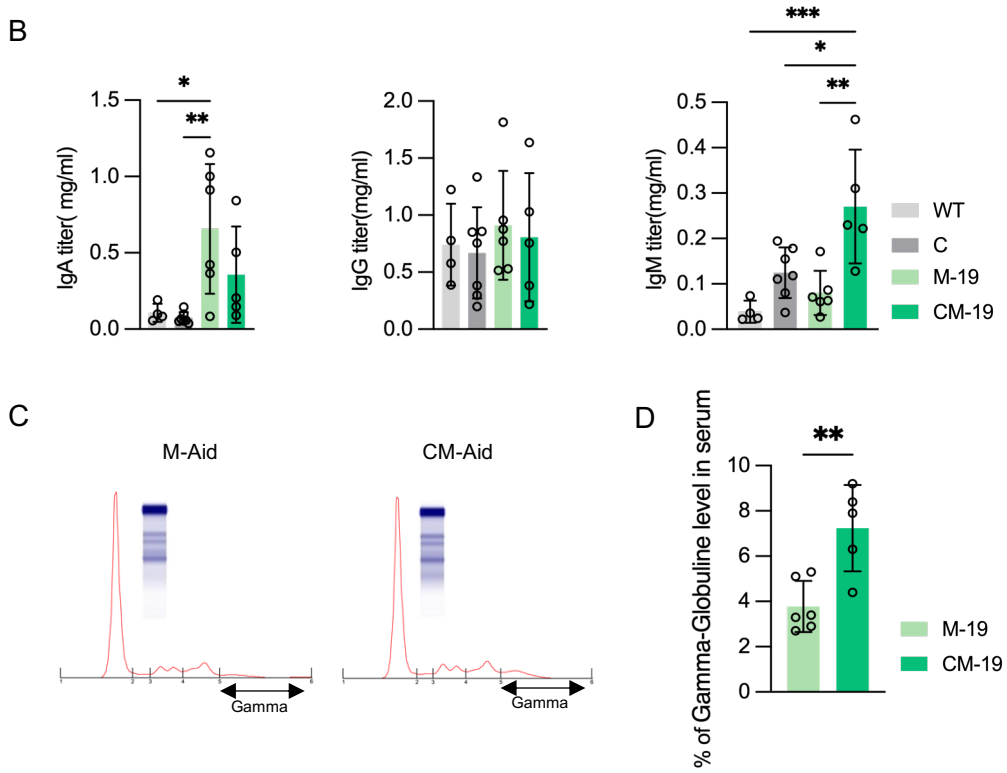

Figure 10. Early B-cell specific expression *Myd88*^{L252P} with activated *CXCR4*^{C1013G} leads to increased serum IgM level. A Serum immunoglobulin level for IgA, total IgG, and IgM in 10 - 14-week old WT (n=4), C (n=7), M-Aid (n=4), CM-Aid (n=4) mice. **B** Serum immunoglobulin level for IgA, total IgG, and IgM in 10 - 14 week old WT (n=4), C (n=7), M-19 (n=6), and CM-19 (n=5) mice. **C** Serum gel electrophoresis analysis in 10 - 14-week-old M-19 (n=7) and CM-19 (n=5) mice. Serum electrophoresis analysis were performed by Dr. Markus Thaler. **D** Quantification of the percentage of Gamma globulin level in the serum of 10 - 14-week-old M-19 (n=7) and CM-19 (n=5) mice. P value calculated using unpaired t-test. Statistical analyses were performed with one-way ANOVA with Tukey correction for multiple comparisons. *, $p \leq 0.05$; **, $p \leq 0.01$; ***, $p \leq 0.001$

3.8. Co-activation of *CXCR4*^{C1013G} and B-cell-specific *Myd88*^{L252P} induces germinal center expansion in the premalignant mice

To investigate the effects of *CXCR4*^{C1013G} and B-cell-specific *Myd88*^{L252P} gain-of-function mutations on the expansion of germinal center and other histological alterations in various tissues of mice, we performed histopathological analyses in 10-14 week-old mice. Histology samples for spleen, thymus, lymph node, lung, heart, intestine, kidney, liver, brain, and bone marrow from WT (n=4), C (n=4), M-Aid (n=5), CM-Aid (n=7), C19 (n= 4), M-19 (n=5) and CM-19 (n=3) mice were analyzed by H&E staining. Measurement of the spleen in all samples

revealed a significant increase in the size and number of the germinal centers detected in the CM-19 mice, suggesting that *CXCR4*^{C1013G} further accelerates the expansion of germinal centers in an early *Myd88*^{L252P} expressing model (Fig. 11A).

Immunohistochemistry analysis was performed in selected samples of all genotypes for B220, CD3, IRF4, CD138, and BCL6 to identify the progression towards a disease phenotype. The spleens of the *CXCR4*^{C1013G} animals showed reduced/atrophy of the T-cell population upon CD3 staining. The B220 and IRF4 staining revealed a mild to moderate expansion of the B-cell area in the white pulp along with the presence of weak IRF4 staining. Additionally, an increase in the CD138^{+} plasma cell population was detected slightly more compared to that in the WT animals. Furthermore, in the *CXCR4*^{C1013G} animals, only one mouse showed hyperplastic GCs (Fig 11B). The M-Aid mice spleens showed normal histology with proper white and red pulp as revealed by the B220 and CD3 IHC. A normal population of plasma cells was shown by the CD138 IHC and no IRF4 expression was detected in the B-cells. Finally, numerous GCs were revealed by the BCL6 IHC. The M-Aid spleens were found to be morphologically similar to the WT (Fig 11C). CM-Aid spleens showed mild expansion of the B-cell area on the white pulp as revealed by the B220 and IRF4 IHC. Additionally, a moderate to prominent increase in the CD138^{+} plasma cells was observed (Fig 11B).

A

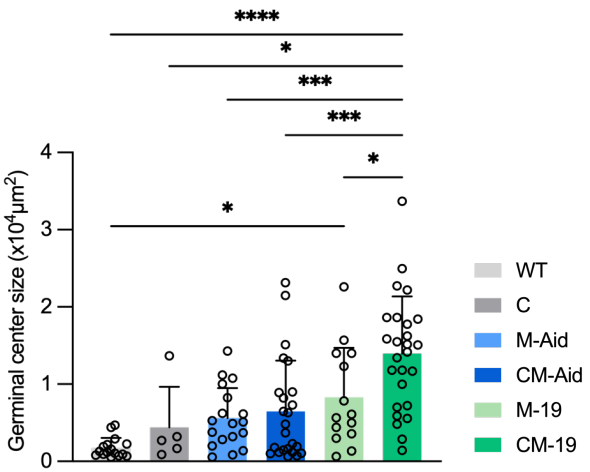

Name	N.GC	Size GC	Total area
WT	4	1760,3	7041
CD19	11	4547,6	50024
CD19	1,25	4423,4	5529
M-Aid	13,6	5762,4	78368
CM-Aid	11,4	8310,9	94744
M-19	15	10329,8	154947
CM-19	17	12033,5	204570

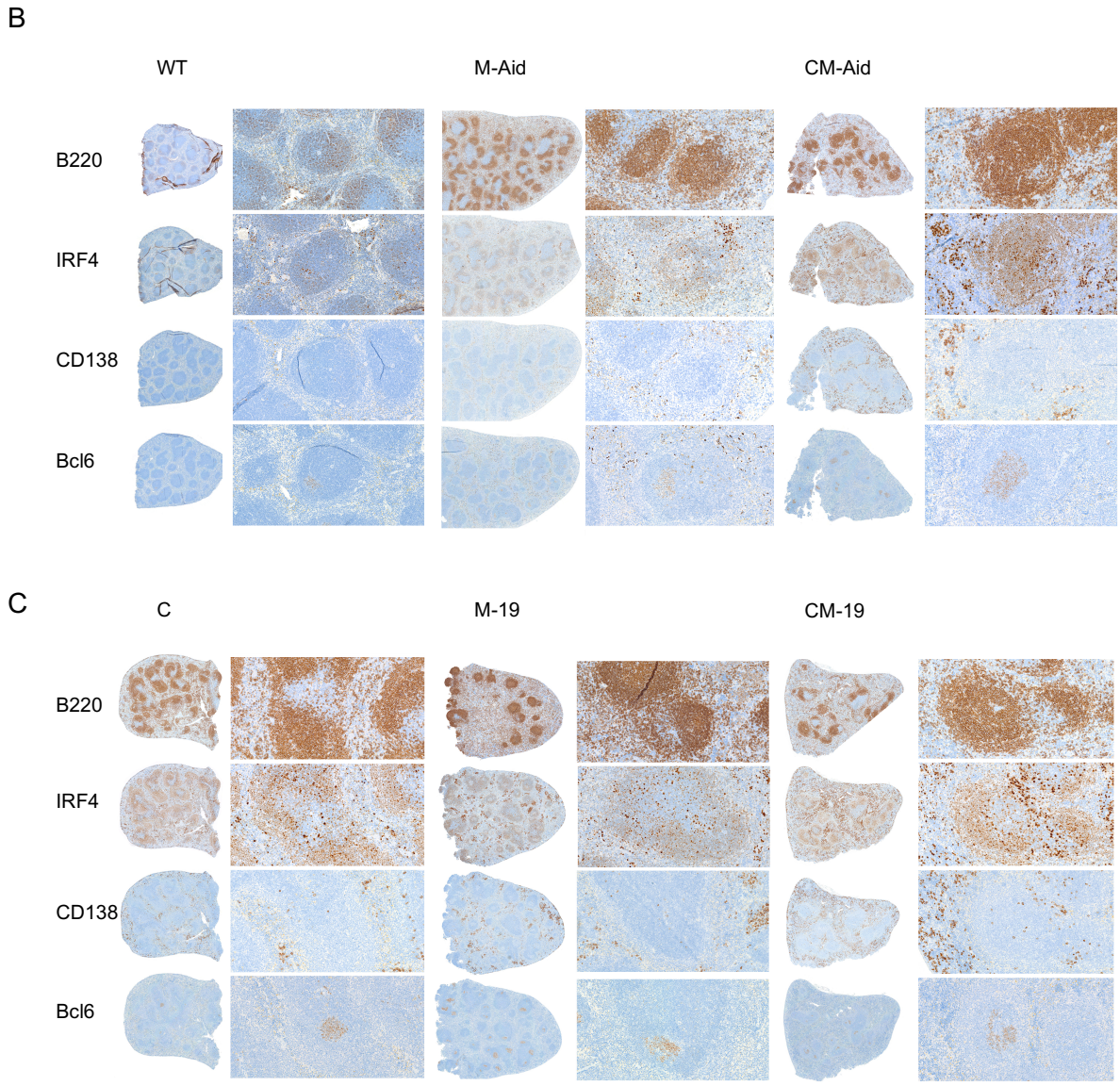

Figure 11. Enhanced *Myd88*^{L252P} and *CXCR4*^{C1013G} signaling in B-cells lead to increased germinal center size and number. A Enumerated germinal centers were measured for surface area in 10 - 14-week-old WT, C, M-Aid, CM-Aid, M-19, and CM-19 mice. Each point represents a single germinal center; germinal center number (N. GC) and size (size GC) measured in 10 - 14-week-old WT (n=4), C (n=4), M-Aid (n=5), CM-Aid (n=7), C19 (n= 4), M-19 (n=5), and CM-19 (n=3) mice. **B** IHC staining for B220, IRF4, CD138, and BCL6 of the splenic section in 10 - 14-week-old WT, M-Aid, and CM-Aid (n = 3 per genotype) mice. **(D)** IHC staining for B220, IRF4, CD138 and BCL6 of splenic section in 10 - 14-week-old C, M-19 and CM-19 (n = 3 per genotype) mice. Histopathological analyses were performed by Prof. Dr. Leticia Quintanilla-Fend and Dr. Irene Gonzalez-Menendez. Statistical analyses were performed with one-way ANOVA with Tukey correction for multiple comparisons. *, $p \leq 0.05$; **, $p \leq 0.01$; ***, $p \leq 0.001$.

The spleen of the WT animals showed normal architecture with well-developed white and red pulp evident from B220 and IRF4 IHC. A few small germinal centers (GCs) were identified in 2 of 4 animals. The other tissues analyzed showed normal histology including the lymph nodes

which appeared small and showed no histological alterations (Fig. 11C). The spleens from M-19 mice showed interfollicular expansion of the B220+ B-cells with weak expression of IRF4. A mild increase in the plasma cell population was revealed by the CD138 IHC. Additionally, a moderate increase in the number of GCs and a moderate increase in their size was detected with the BCL6 IHC (Fig 11C). Strikingly, although it is known that CXCR4^{C1013G} animals have improperly structured secondary lymphoid organs with reduced B-cell follicles (Balabanian et al., 2012), the collaboration of *CXCR4^{C1013G}* and B-cell-specific *Myd88^{L252P}* led to an increase in the number and size of germinal centers in CM-19 mice (Fig 11C). The spleens from CM-19 mice displayed mild B220^{+} B-cell expansion on the white pulp and expression of IRF4 on the B-cells. The increase in the CD138^{+} plasma cell population was moderate to prominent. CM-19 mice showed the largest and more numerous GCs as revealed by the BCL6 IHC staining as compared to the other genotypes (Fig 11C). Histological investigation of lymph nodes and thymus from CM-19 mice also showed an increased presence of plasma cells in the bone marrow which was not displayed in other genotypes. Our results provide novel insights into the interaction between *CXCR4^{C1013G}* and B-cell-specific *Myd88^{L252P}* and their effects on the expansion of germinal centers in various organs, highlighting the importance of *CXCR4^{C1013G}* in B-cell development and function.

3.9. Co-activation of *CXCR4^{C1013G}* and *Myd88^{L252P}* in B-cells leads to normal B-cell development in bone marrow

To address whether B-cell-specific expression of *Myd88^{L252P}* with activated CXCR4 influences B-cell development, we compared WT, C, M-Aid, M-19, CM-Aid, and CM-19 mice at the pre-malignant stage of 10-14 weeks old. B-cell development in bone marrow appeared unchanged (Fig. 12A), as indicated by the total count of bone marrow cells as well as progenitor, precursor, immature, and mature B-cell compartments (Fig 12B). The CXCL12/CXCR4 pair is thought to regulate the lymphoid trafficking of T-cells and orchestrate B-cell homing, maturation, and differentiation in secondary lymphoid organs (LOs) and bone marrow (Biajoux

et al., 2016). Hence, we further looked into the T-cell compartment of the bone marrow for the CM-Aid, CM-19 transgenic mice as well as the control primarily focusing on CD3 T-cells, CD4 helper T-cells, and CD8 cytotoxic T-cells. We observed a CXCR4-associated expanding population of CD3, CD4, and CD8 positive cells in mice carrying a gain-of-function mutation of *CXCR4*^{C1013G}, which was completely absent in the mice carrying only *Myd88*^{L252P} mutation (Fig. 12C). All together, our results indicate that B-cell-specific expression of *Myd88*^{L252P} with activated CXCR4 does not influence B-cell development, but CXCL12/CXCR4 axis regulates T-cell population and collaboration of *CXCR4*^{C1013G} and *Myd88*^{L252P} signaling affects the mature B-cell population.

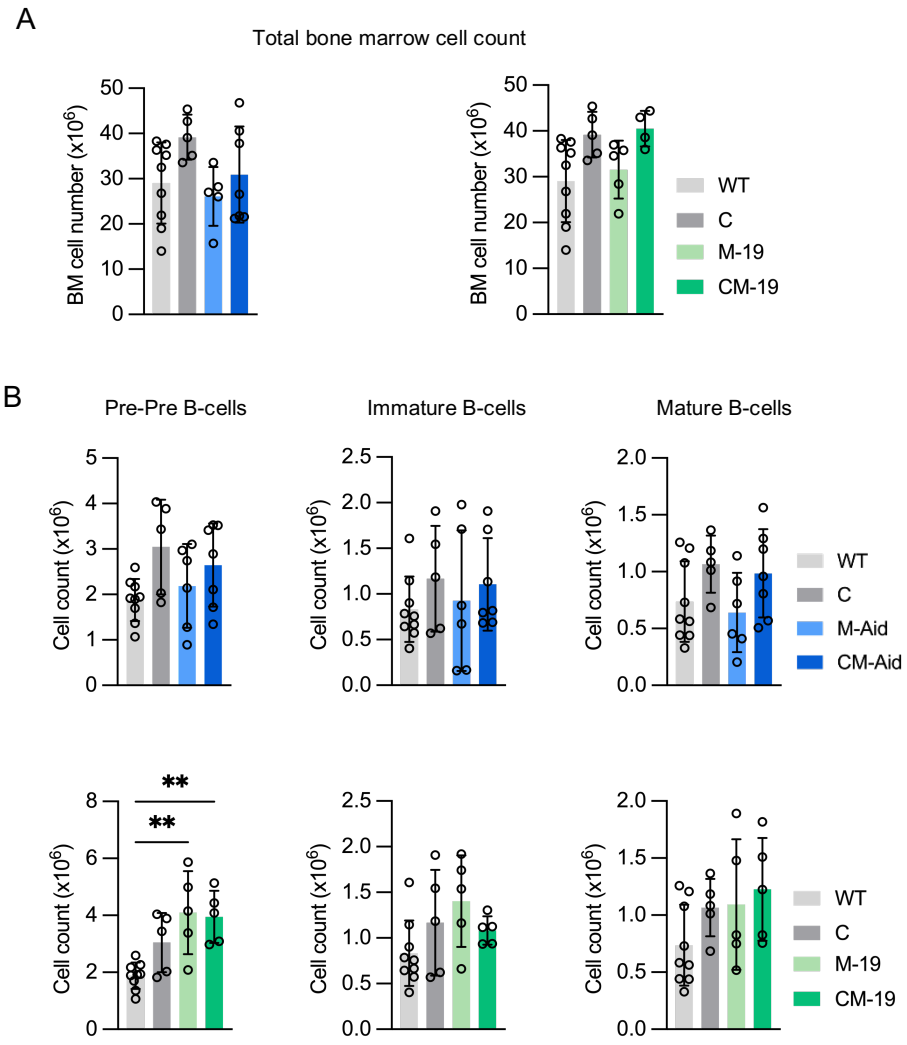

C

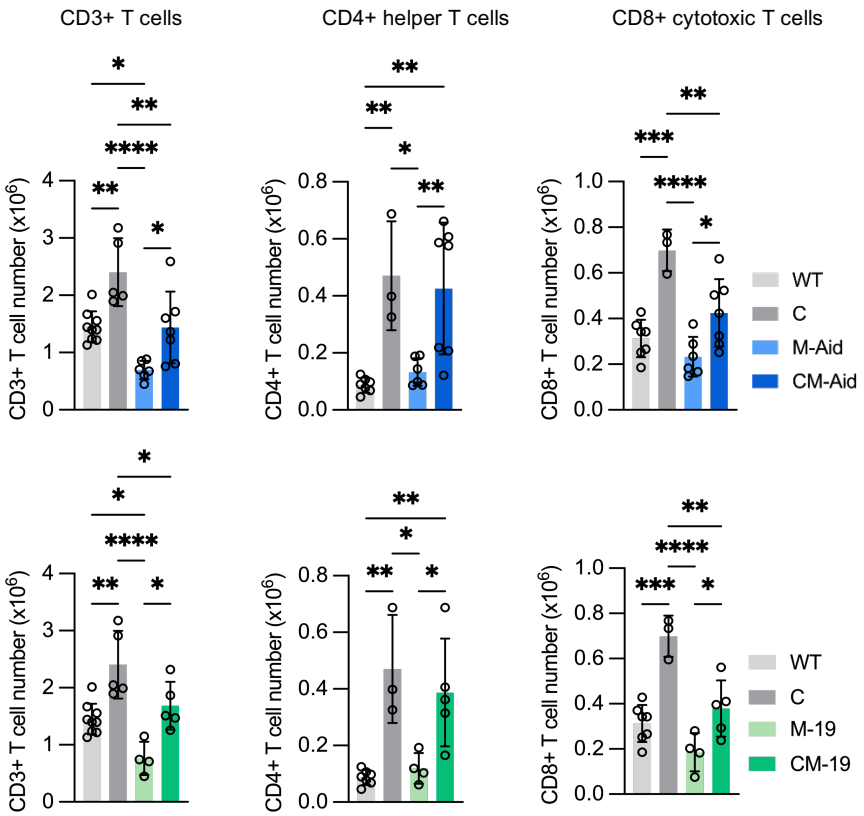

Figure 12. Collaboration of *Myd88*^{L252P} and *CXCR4*^{C1013G} signaling displays normal B-cell development. (A) Bone marrow cell count from 2 femurs and 1 tibia of 10 - 14-week-old WT (n=9), C (n=5), M-Aid (n=5), CM-Aid (n=7), M-19 (n=5), and CM-19 (n=5) mice **(B)** Pro-Pre, Immature and Mature B-cell population in 10 - 14-week-old WT, C, M-Aid, CM-Aid, M-19, and CM-19 mice. **(C)** CD3$^+$ total T-cells, CD4$^+$ helper T-cells, and CD8$^+$ cytotoxic T-cell population in 10 - 14-week-old WT, C, M-Aid, CM-Aid, M-19, and CM-19 mice. Statistical analyses were performed with one-way ANOVA with Tukey correction for multiple comparisons. *, $p \leq 0.05$; **, $p \leq 0.01$; ***, $p \leq 0.001$.

3.10. Co-activation of *CXCR4*^{C1013G} and *Myd88*^{L252P} affects B-cell developmental stages in the spleen

The *Myd88*^{L252P} mutation has been reported to induce lymphoplasmacytic-like lymphoma in mice, characterized by the expansion of early lymphoplasmacytic cells and plasma cells in the peripheral region followed by B-cell transformation (Ouk et al., 2021). To understand the mechanism underlying the aberrant expansion of differentiated B-cells in secondary lymphoid organs, we performed immunophenotyping on total splenic cell counts from experimental and control mice. While the spleen histology of the CM-19 mice depicted higher expression of CD138$^+$ plasma cells, the spleen architecture remained normal. The lymphoplasmacytic-like

phenotype observed in the spleen of CM-19 mice constituted a mixture of numerous $CD138^{+}B220^{lo}$ lymphoplasmacytic cells (LP cells) and plasma cells (Fig. 8C and 9B). To follow the progression of this phenotype, we focused on the transitional 1 B-cells ($CD93^{+}B220^{+}IgM^{+}CD23^{-}$), transitional 2 B-cells ($CD93^{+}B220^{+}IgM^{-}CD23^{+}$), follicular B-cells ($CD93^{-}B220^{+}CD21^{lo}CD23^{+}$), marginal center B-cells ($CD93^{-}B220^{+}CD21^{+}CD23^{-}$) and germinal center B-cells ($CD19^{+}CD95^{+}GL7^{+}$).

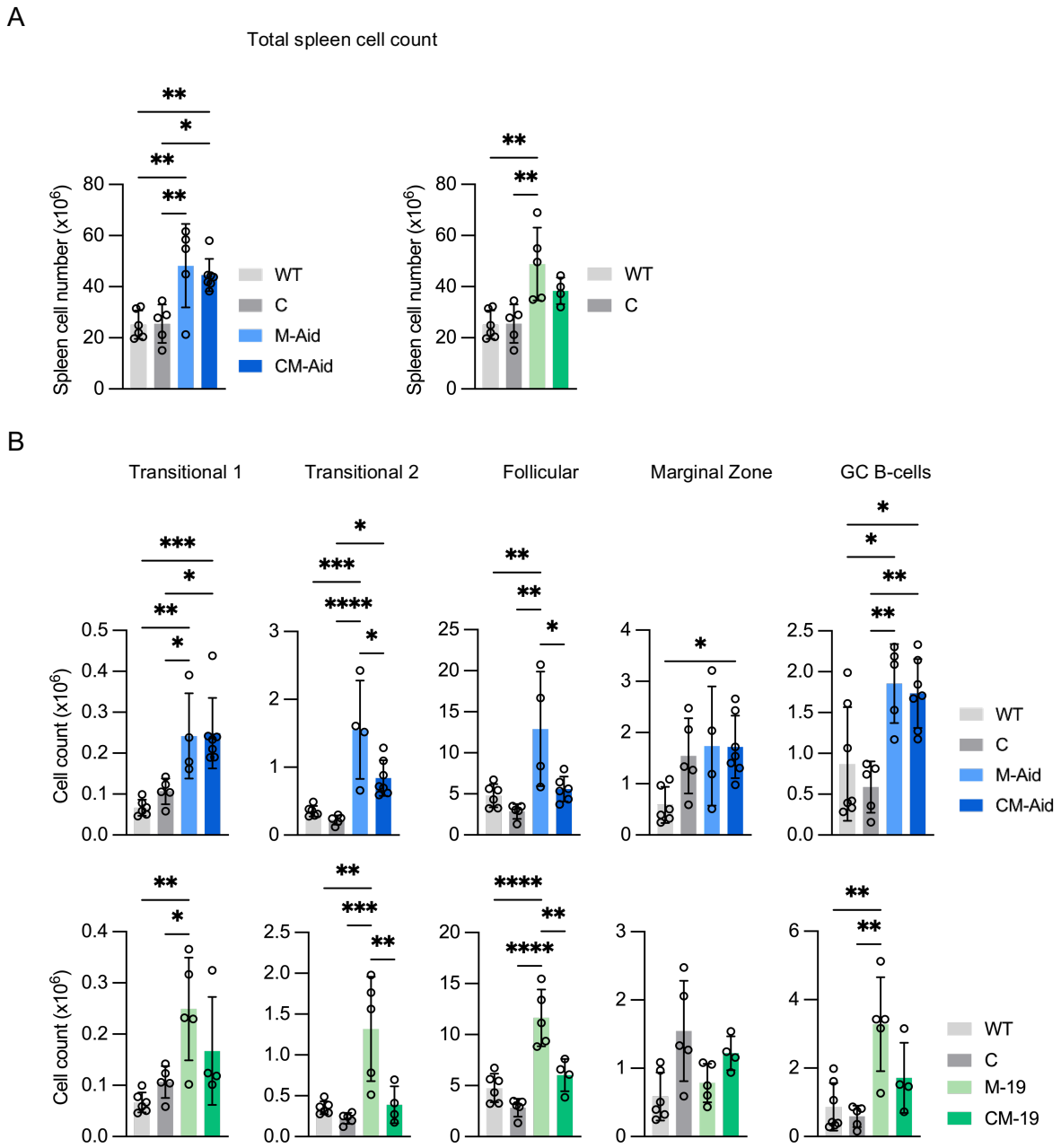

C

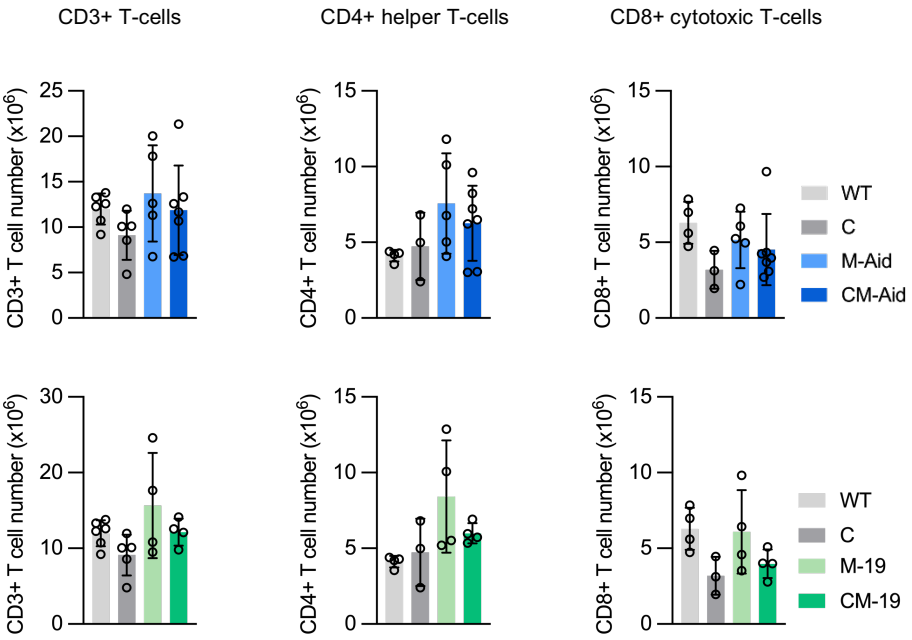

Figure 13. B-cell-specific *Myd88*^{L252P} expression is associated with aberrant B-cell differentiation in the spleen. A Total spleen count in 10-14 week old WT (n=6), C (n=4), M-Aid (n=5), CM-Aid (n=7), C19 (n= 4), M-19 (n=5) and CM-19 (n=3) mice. **B** Transitional 1 B-cells (CD93^{+}B220^{+}IgM^{+}CD23^{-}), Transitional 2 B-cells (CD93^{+}B220^{+}IgM^{-}CD23^{+}), Follicular B-cells (CD93^{-}B220^{+}CD21^{lo}CD23^{+}), Marginal center B-cells (CD93^{-}B220^{+}CD21^{+}CD23^{-}) and Germinal center B-cells (CD19^{+}CD95^{+}GL7^{+}) in 10 - 14 week old WT (n=6), C (n=4), M-Aid (n=5), CM-Aid (n=7), C19 (n= 4), M-19 (n=5) and CM-19 (n=3) mice. **C** CD3+ total T-cells, CD4+ helper T-cells, and CD8+ cytotoxic T-cell population in 10 - 14-week-old WT, C, M-Aid, CM-Aid, M-19, and CM-19 mice. Statistical analyses were performed with one-way ANOVA with Tukey correction for multiple comparisons. *, p ≤ 0.05; **, p ≤ 0.01; ***, p ≤ 0.001.

We observed an increased number of total splenic cells in the mice expressing *Myd88*^{L252P}mutation alone and the presence of *CXCR4*^{C1013G} did not further contribute to expanding the subset (Fig. 13A). The frequencies of CD93^{+}B220^{+}IgM^{+}CD23^{-} transitional 1 B-cells and CD93^{+}B220^{+}IgM^{-}CD23^{+} transitional 2 B-cells were not significantly altered for the transgenic CM-Aid and CM-19 mice, although a significant increase was observed in mice carrying the *Myd88*^{L252P} mutation only. Similarly, frequencies of CD21^{lo}CD23^{+} follicular B-cells were not significantly altered in mice carrying both *CXCR4*^{C1013G} and *Myd88*^{L252P} mutation (Fig 13B). On the contrary CD21^{+}CD23^{-} marginal center B-cells displayed no difference among the different genotypes. We only observed a slight increase in the CD19^{+}CD95^{+}GL7^{+} germinal center B-cells in M-Aid and M-19 mice as compared to the control genotypes (Fig 13B).

Although histological assessment of the spleen showed an increase in the number and size of germinal centers in CM-19 mice, flow cytometry-based analysis did not reveal an increase in the total cell number of germinal center B-cells. In addition, to investigate the impact of *CXCR4*^{C1013G} and *Myd88*^{L252P} co-expression on the T cell compartment, we also examined the spleen of the CM-Aid and CM-19 mice as well as the control mice with a primary focus on CD3 T-cells, CD4 helper T-cells, and CD8 cytotoxic T-cells. Upon quantification of the results, we observed no significant alterations in the T-cell compartment of the spleen among the genotypes (Fig. 13C).

The result suggests that the *Myd88*^{L252P} mutation alone is responsible for the expansion of differentiated B-cells in secondary lymphoid organs. However, the co-expression of *CXCR4*^{C1013G} and *Myd88*^{L252P} did not lead to any significant alterations in the B-cell subset or T-cell subset.

3.11. *CXCR4*^{C1013G}; *MYD88*^{L265P} collaboration enhances differentiation into a B cell lineage

Investigation of immune cell differentiation capacity and function is limited by the shortcomings of the suitable and scalable experimental model (Redecke et al., 2013). While animal models are essential for the study of biochemical and physiological processes of the occurrence and development of tumors, the mechanistic investigation of the tumor model transformation is often limited by the availability of the immune cells. To examine the differentiation processes of *CXCR4*^{C1013G}; *MYD88*^{L265P} B-cells, Hoxb8 progenitor model was utilized for the generation of scalable numbers. Hoxb8 progenitor lines for the genotypes *WT* and *CXCR4*^{C1013G} were generated from bone marrow cells by transduction with the conditional Hoxb8-ER fusion protein, as described before in (Redecke et al., 2013) (Fig. 14A). Cells were cultured in a medium containing estrogen to maintain the progenitor-like phenotype. Upon confirmation of genotype, WT Hoxb8, and *CXCR4*^{C1013G} Hoxb8 cells were introduced with *MYD88*^{L265P} via the transduction of MSCV-IRES-GFP(MIG) vector carrying human *MYD88*^{L265P} sequence or MIG-

vector control to generate *MYD88*^{L265P} Hoxb8 cells (Fig. 14B). The generated Hoxb8 cells were validated and confirmed by sequencing as well as quantitative real-time PCR to confirm the expression of hu- *Myd88*^{L265P} (Fig. 14C). WT Hoxb8 cell line grew exponentially in the condition media, whereas *CXCR4*^{C1013G}; *Myd88*^{L265P} Hoxb8 cells grew comparatively slower reflecting no growth benefits from the presence of activation mutation of *CXCR4*^{C1013G} and *Myd88*^{L265P} (Fig. 14D)

To test the potential of the cell lines to differentiate into B-cells *in vitro,* generated Hoxb8 cell lines were co-cultured on OP9 feeder cells in the presence of Flt3L. Every 2-3 days the cells were passaged onto the fresh OP9 cells and acquisition was performed using FACS to observe the progression. After 6 days, a large percentage of cells from the *CXCR4*^{C1013G}; *MYD88*^{L265P} cell line was double positive for the B-cell marker B220 and CD19 as compared to WT, *MYD88*^{L265P} and *CXCR4*^{C1013G} cell line (Fig. 14E). Altogether, we successfully established WT, *CXCR4*^{C1013G}, *MYD88*^{L265P,} and *CXCR4*^{C1013G}*; MYD88*^{L265P} Hoxb8 cell lines, which could be expanded and subsequently differentiated *in vitro.* The greater fraction of *CXCR4*^{C1013G}*; MYD88*^{L265P} cells progressing towards B-cell lineage indicated that *CXCR4*^{C1013G} and *MYD88*^{L265P} collaboration enhances differentiation into the B-cell lineage of multipotent progenitor cells.

A

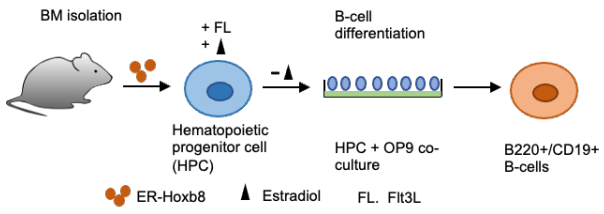

B

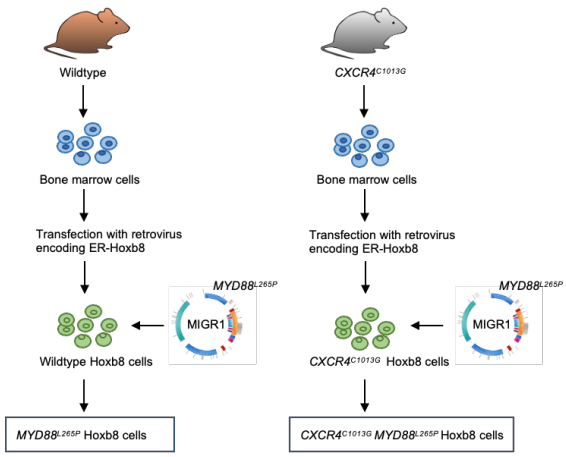

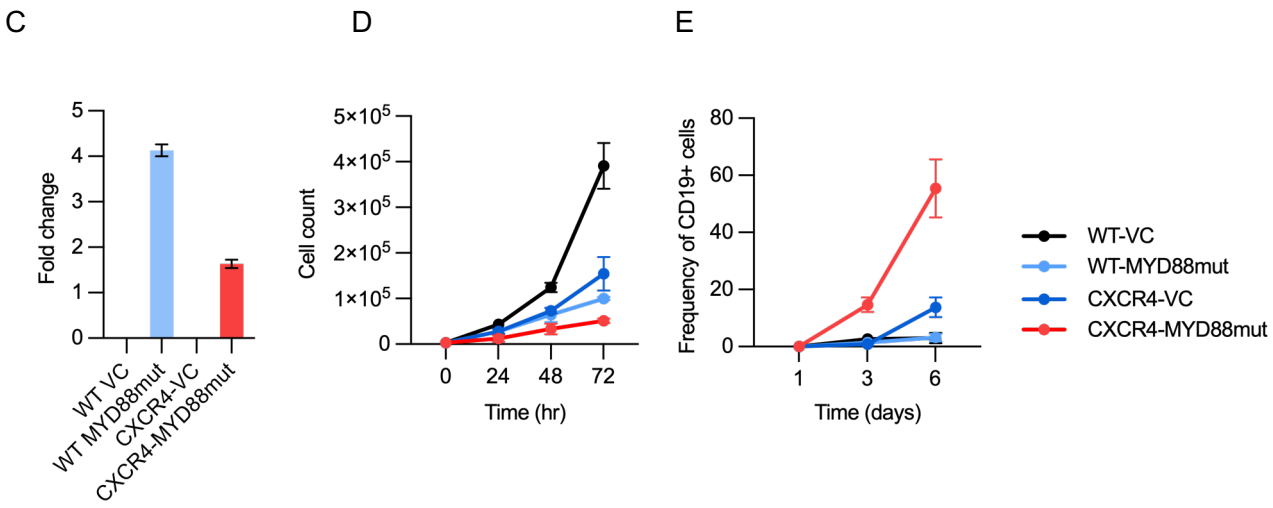

Figure 14. Generation of *CXCR4*^{C1013G} and *MYD88*^{L265P} Hoxb8 cell line to investigate B-cell differentiation potential *in vitro*. **A** Schematic representation of the workflow for generation and subsequent differentiation of Hoxb8 immortalized progenitor cell lines. Scheme adapted from Hong et al., 2020. **B** Experimental workflow for transduction of MIG-hu- *MYD88*^{L265P} or MIG-vector control in WT and *CXCR4*^{C1013G} Hoxb8 cell lines to generate *Myd88*^{L265P} Hoxb8 and *CXCR4*^{C1013G}; *MYD88*^{L265P} Hoxb8 cell line. **C** Validation of cell lines through quantitative real-time PCR. **D** Growth analysis using trypan blue method of *WT*, *CXCR4*^{C1013G}, *MYD88*^{L265P}, and *CXCR4*^{C1013G}; *MYD88*^{L265P} Hoxb8 cell lines (n=3). **E** Fraction of CD19+ B-cells in *WT*, *CXCR4*^{C1013G}, *MYD88*^{L265P}, and *CXCR4*^{C1013G}; *MYD88*^{L265P} Hoxb8 cell lines after B-cell differentiation (n=3).

3.12. Gain-of-function CXCR4 mutation drives plasma cell differentiation *in vitro* through CXCL12 mediated signaling pathway

The role of mutated MYD88 and gain-of-function CXCR4 mutation in the activation of humoral immune responses *in vitro* needed to be further examined to understand the mechanism underlying the increased plasma cell and plasmablast population observed in *CXCR4*^{C1013G}: *Myd88*^{L252P} mice. From previously published data, we gathered that TLR4 agonist LPS could directly stimulate the differentiation of memory B-cells into high-affinity plasma cells *in* vitro (Richard et al., 2008), and CXCR4 desensitization limits Myd88-mediated plasma cell differentiation *in vitro* and *in vivo* (Alouche et al., 2021). This study aimed to further examine the role of mutated MYD88, which is the main adaptor protein of TLR and IL-1R signaling pathway, and gain-of-function CXCR4 mutation in activation of humoral immune responses *in vitro*, delineate which of the mutation is responsible for the accumulation of plasma cells, and if they collaborate to enhance the expansion of plasma cells.

We stimulated splenic B-cells from 10-14 week-old WT, C, M-19, and CM-19 mice with TLR4 ligand LPS *in vitro* in the presence or absence of CXCR4 ligand CXCL12, and analyzed the population of plasma cells (PC) and plasmablasts (PB) (Fig. 15A). We observed an increase in the PB population in unstimulated CM-19 mice as compared to M-19 and control mice (Fig 15B). Upon LPS stimulation, we observed a profound increase of plasma cells up to 55% in mice carrying a gain-of-function mutation of CXCR4, namely C and CM-19 mice. The addition of CXCL12 in the stimulation mixture led to a slight but not significant increase in the PC population. On the contrary, stimulation by both LPS and CXCL12 showed a significant increase in splenic PC differentiation in C and CM-19 mice as compared to WT and M-19 mice, demonstrating that the gain-of-function mutation of CXCR4 plays a primary role in the progression of PC differentiation *in vitro*. This CXCL12-mediated PC differentiation was further confirmed by the reversal of this phenomenon upon the addition of CXCR4 antagonist AMD3100 to the stimulation mixture along with CXCL12. Overall, our results suggest that constitutively active CXCR4 along with *Myd88*^{L252P} plays a critical role in the activation of humoral immune responses *in vitro*, specifically in the differentiation of memory B-cells into high-affinity plasma cells.

A

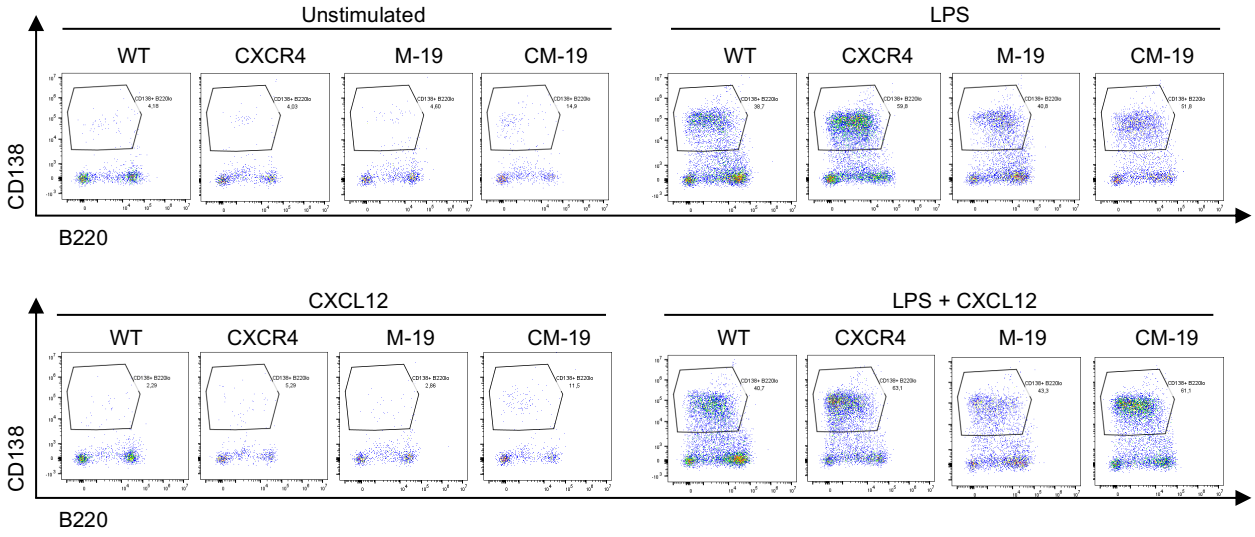

B

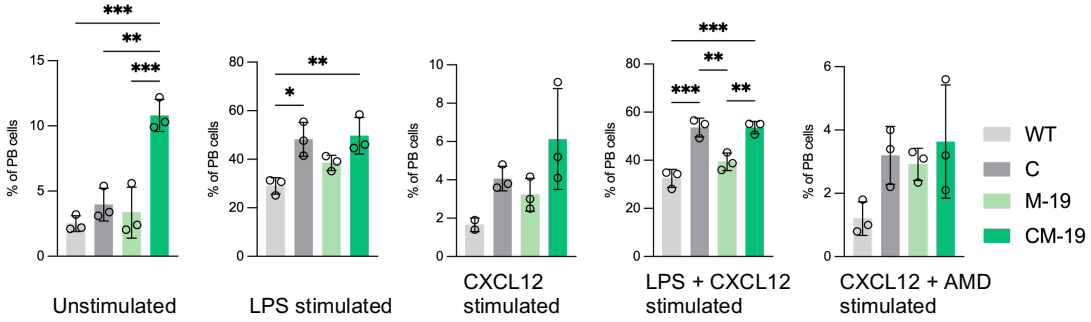

Figure 15. *CXCR4*^{C1013G} activation drives *Myd88*^{L252P} mediated plasma cell differentiation *in vitro*. A FACS plot representing the gating of CD138^{+}B220^{lo} splenic B-cell cultured in the presence of LPS, LPS^{+}CXCL12, or CXCL12 alone for 4 days. **B** Flow cytometric analysis and quantification of CD138^{+}B220^{lo} plasma cell in WT, CXCR4, M-19, and CM-19 (n=3). Statistical analyses were performed with one-way ANOVA with Tukey correction for multiple comparisons. *, $p \leq 0.05$; **, $p \leq 0.01$; ***, $p \leq 0.001$.

3.13. Activation of BTK downstream signaling by cooperative CXCR4 and Myd88 signaling contributes to lymphomagenesis in CM-19 mice

BTK is a crucial component of the Myd88 signaling cascade, and CXCR4 has been shown to play a role in activating this pathway in B cells. Previous studies have shown that *Myd88*^{L252P} can activate BTK downstream signaling, leading to the development of lymphoma (Ngo et al., 2011). To investigate whether the collaboration of mutated MYD88 and gain-of-function CXCR4 mutation can activate the BTK downstream signaling pathway, CD19-enriched splenocytes from pre-lymphoma mice were stimulated with CXCL12 in the presence or absence of AMD3100. Phosphorylation of ERK, an indicator of BTK activation, was compared against total ERK levels between CM-19 mice and respective control genotypes. Our results showed that the collaboration of *CXCR4*^{C1013G} and *Myd88*^{L252P} led to an upregulation of ERK phosphorylation (measured as phospo-ERK; total ERK) in comparison to the controls (Fig. 16A). These findings provide insights into the molecular mechanism underlying the increased plasma cell and plasmablast generation in the secondary lymphoid organs of CM-19 mice, as observed in our previous experiments. The activation of BTK downstream signaling may contribute to the development of lymphoma and could potentially serve as one of the therapeutic targets for the treatment of B-cell malignancies.

To further investigate the implications of BTK activation on the transcriptomic profile of CD19+ B-cells, we performed RNA sequencing (RNA seq) on CD19+ B-cells isolated from the bone marrow and spleen of young CM-19 mice and their respective controls. Our analysis revealed an evident clustering of the various genotypes with clear distinction, as displayed by the sample-to-sample distance (Fig. 16B). Principal component analysis (PCA) further revealed the variance of the spleen and bone marrow sample from the CD19 and CM19 mice, indicating the difference in B cell compartments (Fig. 16C). Volcano plot generated from the differentially expressed genes between CM19 and M19 showed upregulation of mature lymphocytes and immunoglobulin biomarkers including *Ighg3*, *ctse*, Ly6a, Cnn2, and CD52 (Fig. 16D). Gene set enrichment analysis (GSEA) revealed enrichment of IL6/JAK/STAT3, oxidative phosphorylation, MYC, as well as DNA repair and NF-kappaB signaling pathways in B-cells from CM19 mice, defined as the *CXCR4*^{C1013G}; *Myd88*^{L252P} signature (Fig. 16E). These results indicate that the presence of the *CXCR4*^{C1013G} mutation potentially drives the enrichment of mature B cell lymphoma gene expression signatures in CM-19 mice. These findings suggest a potential role for *CXCR4*^{C1013G} and *Myd88*^{L252P} mutations in the regulation of B-cell differentiation and lymphomagenesis.

Rupert Öllinger at TranslaTUM received isolated RNA samples for library preparation and RNASeq. Matthias Wirth further analyzed the raw data at the Charite Universitatmedizine (CBF), Department of Hematology and Oncology.

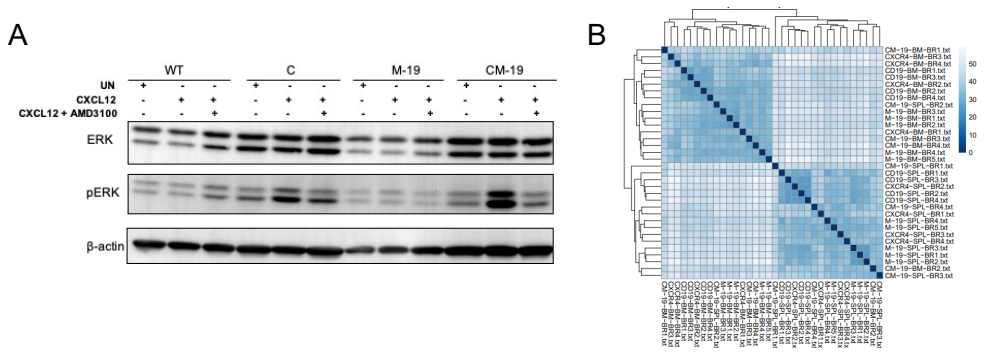

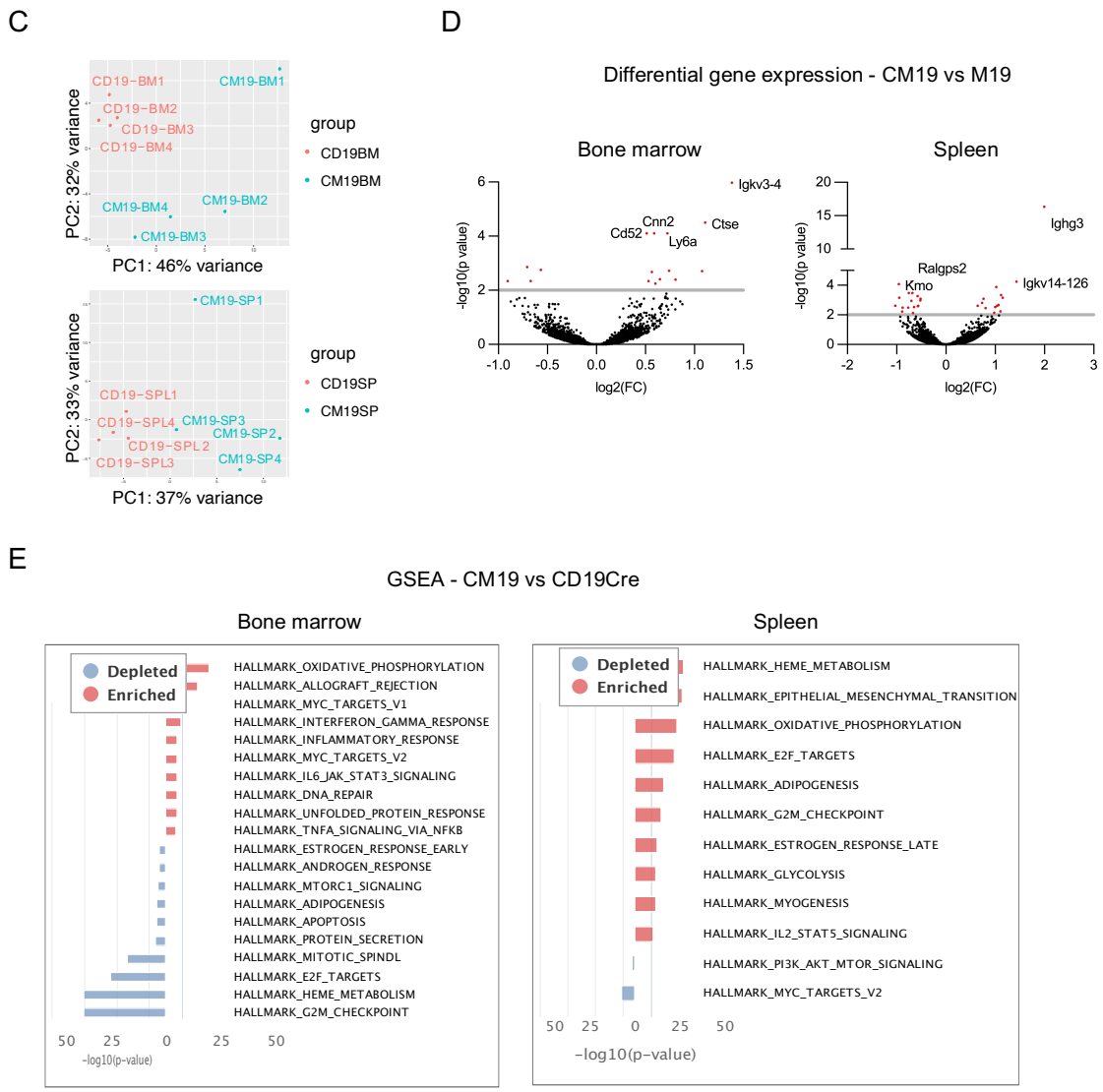

Figure 16. Expression and activity of *CXCR4*^{C1013G}; *Myd88*^{L252P} signature. A Representative image of immunoblot analysis for ERK, phospho ERK, and b actin of CD19+ splenocytes treated with/without 50nM CXCL12 and/or 10mM CXCR4 antagonist AMD3100 **B** Heat map illustrating the sample-by-sample division of all the enlisted genotypes. **C** Principal component analysis (PCA) of RNA-Seq gene expression profiles from CD19+ splenocytes of young CD19Cre (red) and CM19 (blue) mice, respectively in the bone marrow and spleen. **D** Volcano plot of the differentially expressed genes from CD19+ splenocytes of young M19 and CM19 mice in the bone marrow and spleen. **E** GSEA result of the CM19 mice versus CD19Cre mice in the bone marrow and spleen (data analysis performed by PD Matthias Wirth from AG Keller).

4. DISCUSSION

In this study, we investigated the role of the recurrent somatic mutation *MYD88*^{L265P} in the pathogenesis of Waldenström macroglobulinemia and its precursor state, IgM MGUS. Previous studies identified the presence of the *MYD88*^{L265P} mutation in patients with WM as well as those with IgM MGUS, which suggests that this mutation plays an early oncogenic role in the pathogenesis of WM. However, it is challenging to clinically distinguish between WM and IgM MGUS due to their phenotypic similarities at the premalignant stage. Whole-genome sequencing studies have reported CXCR4 mutations in ~30% of WM patients and strikingly, these mutations are exclusively concomitant with MYD88L265P mutation. To date, there has been a lack of in vivo models that accurately represent the coexistence of both mutations. Despite numerous studies examining the individual effects of MYD88 and CXCR4 mutations, there has been a gap in knowledge regarding how these mutations interact in the context of WM development.

To address these challenges, we developed a mouse model with B-cell-specific expression of the *MYD88*^{L265P} mutation and somatic mutation involving the CXCR4 receptor. This resulted in a phenotype that resembles IgM MGUS progressing towards lymphoproliferation with features of lymphoplasmacytic lymphoma. This model offers an opportunity for targeted approaches by using specific antagonists against CXCR4 or MYD88 and provides a framework for studying the downstream pathway that regulates the trafficking and dissemination of malignant cells in human WM.

Our findings have important implications for the development of targeted therapies for WM. The CXCR4 pathway has been implicated in the pathogenesis of WM and our mouse model suggests that targeting this pathway may be a promising therapeutic approach for WM. This therapeutic potential may be extended to other B-cell malignancies as well. Additionally, this study highlights the importance of understanding the molecular pathways underlying the development of WM and its precursor state, IgM MGUS. Early detection and monitoring of

patients with IgM MGUS are crucial, as the *MYD88^{L265P}* mutation plays an early oncogenic role in the pathogenesis of WM.

Overall, the findings presented in this study offer important insights into the pathogenesis of WM and its precursor state IgM MGUS. The development of a mouse model that resembles the WM precursor state opens up new avenues for the development of targeted therapies for WM and provides a framework for further study of the molecular pathways underlying the development of this disease.

4.1. Activation of highly recurring *Myd88^{L252P}* and WHIM-like *CXCR4^{C1013G}* mutation *in vivo* results in the progression toward low-grade lymphoproliferative disease

We aimed to identify the functional significance of concurrent WHIM-like mutation C1013G in CXCR4 and *MYD88^{L265P}* in WM patients. Previous studies have shown that the B-cell-specific expression of Myd88^{L252P} leads to a lymphoproliferative disorder and occasional (~30%) transformation into an aggressive lymphoma that morphologically and immunophenotypically resembles human ABC-DLBCL (Knittel et al., 2016). In this study, we specifically designated a pan B-cell Cre allele CD19^{Cre} and a Cre allele which is activated in germinal center B-cells Aid^{Cre}. This allows for the conditional introduction of the expression of *CXCR4^{C1013G}* mutation along with *Myd88^{L265P} in vivo* to mimic the state in human Waldenström macroglobulinemia.

We monitored a series of CM-Aid and CM-19 mice with their age-matched control and performed a longitudinal analysis. Our data showed reduced survival outcomes in the double transgenic mice, demonstrating that the concurrent presence of *CXCR4^{C1013G}* and *Myd88^{L252P}* transgenes in mice is associated with aggressive progression toward B-cell lymphomas. Furthermore, we observed reduced overall survival for CM-19 mice with a median survival of 67 weeks as compared to 77 weeks in CM-Aid mice. Gross histopathological assessment of CM-19 mice at necropsy revealed the presence of B220^{+} IRF4^{+} tumor cells, indicating a low-grade lymphoma with plasmacytic differentiation. As it is challenging to differentially diagnose MZL and lymphoplasmacytic lymphoma morphologically and immunophenotypically in mice,

the term low-grade B-cell lymphoma with plasmacytic differentiation is used. The lymphoma observed in our mouse model is likely to represent the LPL counterpart in humans.

Disease-bearing CM-Aid and CM-19 mice also revealed a morphological resemblance to DLBCL with a non-GC phenotype. This was in line with the finding from an earlier model of *Myd88*^{L252P} mutation *in vivo* that showed the onset of B lymphoproliferative disease and occasional ABC-DLBCL-type lymphoma (Knittel et al., 2016). We further characterized the *Myd88*^{L252P}; *CXCR4*^{C1013G} transgenic mice with IgM^{+} lymphoproliferation. We observed a few cases of serum IgM M-spike, development of predominantly extra-medullar growth pattern, splenomegaly, lymphadenopathy, and exhibition of molecular traits that overlapped with human WM.

In previous studies, Leleu and team have shown that both AKT/mTOR is activated in WM cells, and their inhibition leads to apoptotic changes, further invoking a growth-promoting role for their activation in WM (Leleu et al., 2009). The putative mechanism of action for both AKT and ERK by SDF-1a (CXCL12) in WM through the acquisition of the somatic WHIM-like CXCR4 mutation was shown by (Cao et al., 2015). In our studies with CXCR4, as well as by others who investigated CXCR4^{R334X}-related signaling (Cao et al., 2015; Lewis et al., 2021; McDermott et al., 2011), the use of the CXCR4 antagonist AMD3100 blocked SDF-1a-triggered ERK activation. These data indicate that the mice expressing *Myd88*^{L252P} and WHIM-like *CXCR4*^{C1013G} succumb to lymphoproliferation and promote the development of a polyclonal, low-grade B cell lymphoproliferative disorder of lymphoplasmacytic appearance. Our study supports the widely held belief that MYD88^{L265P} is not the only mutation needed for the development of WM (Hunter et al., 2014b; Knittel et al., 2016; Sewastianik et al., 2019). We demonstrated that the presence of *CXCR4*^{C1030G} significantly accelerated Myd88-driven lymphomagenesis. Our novel transgenic mouse models serve as compelling preclinical models for the potential development of novel therapeutic strategies and the investigation of immune surveillance for WM and other B-cell malignancies with features of plasma cell differentiation.

4.2. Immunophenotypic profile of lymphoplasmacytic lymphoma/Waldenström macroglobulinemia.

In this study, we characterized the clinical and immunophenotypic features of WM and explored the role of *CXCR4*^{C1030G} and *Myd88*^{L252P} mutation in B-cell transformation. Our findings are consistent with the established clinical criteria of WM diagnosis, which requires the presence of monoclonal serum IgM and at least 10% bone marrow involvement by lymphoplasmacytic infiltration (Schuster et al., 2010). The characteristic immunophenotypic signature of WM cells reveals surface expression of IgM+, CD5±, CD19+, CD20+, CD22+, CD79a+, CD23−, CD25+, CD27+, FMC7+, CD138+, CD103− (Kapoor et al., 2017; Konoplev et al., 2005).

Waldenström's macroglobulinemia is often described as a neoplasm of small lymphocytes, plasmacytoid lymphocytes, plasmablasts, and plasma cells, implying a common cytomorphology (Morice et al., 2009). In this study, the CM19 mice demonstrated that IgM plasma cell expansion is at the center of MYD88-dependent B-cell transformation. Indeed, by examining bone marrow and spleen in these mice, we first showed that *CXCR4*^{C1030G}; *MYD88*^{L265P} in both the models were associated with increasing CD138^{+}B220^{lo} plasmablasts (Fig. 8C) which is a characteristic of malignant WM cells. Secondly, we provided evidence for expanding MHCII^{+}CD80^{+} memory B-cells (Fig. 8D), although this phenomenon was more prominent in the CD19^{Cre} model with a higher pool of cells expressing *Myd88*^{L252P}. Memory B-cells are localized both in the bone marrow and spleen and they differentiate into plasma cells depending on CD4^{+} T helper cells (Ochsenbein et al., 2000). We recapitulated these findings in our studies where we show elevated expression of CD4^{+} T helper cells in both CM-Aid and CM-19 mice. Interestingly this observation was specific to the mice carrying *CXCR4*^{C1030G} mutation (Fig. 12C) and this reiterates the finding that CXCR4 might be a receptor used by T-cells to home to the bone marrow (Müller et al., 1999). In this study, we observed a significant increase in bone marrow localization of IgM^{+} CD138^{+}B220^{-} plasma cells in *CXCR4*^{C1030G}; *Myd88*^{L252P} mice where *Myd88*^{L252P} expression was introduced at an early developmental stage. This finding is in contrast to a recent study where they reported that switched IgG

plasma cells migrate to the bone marrow while IgM plasma cells often reside mostly in the spleen (Bohannon et al., 2016). This discrepancy raises questions regarding the factors driving bone marrow homing of WM IgM tumor B-cells. Our results suggest that the CXCR4 mutation contributes to this phenomenon. To further explore the transforming capacity of Myd88, future research could utilize the adoptive transfer of tumor B-cells resembling LPs and investigate their persistence of the lymphoplasmacytic component of the transferred tumor.

Analysis of the spleen morphology and splenic B-cell subset by flow cytometry indicated that continuous *Myd88*^{L252P} activation was associated with the early expansion of CD93^{+}B220^{+}IgM^{+}CD23^{-} transitional 1 and CD93^{+}B220^{+}IgM^{-}CD23^{+} transitional 2 B-cells (Fig. 13B). This suggests that oncogenic Myd88 enhances the germinal center transition, driving towards CD138 positive cells *in vivo* (Flümann et al., 2021). *CXCR4*^{C1030G} mice have demonstrated increased Ag-specific PCs despite splenic follicular hypoplasia. However, the number of GC B-cells was comparable between *WT* and *CXCR4*^{C1030G} mice suggesting the immune response is normal for *CXCR4*^{C1030G} mice despite the B-cell lymphopenia (Biajoux et al., 2016). In our model, we observed expansion of CD93^{-}B220^{+}CD21^{lo}CD23^{+} follicular B-cells but no difference in CD93^{-}B220^{+}CD21^{+}CD23^{-} marginal zone B-cells specifically in mice expressing oncogenic Myd88, this expansion was diminished in mice expressing both *CXCR4*^{C1030G} and *Myd88*^{L252P}, proposing the dampening effect of *CXCR4*^{C1030G} in B-cell transformation. Together our data suggest that the pro-proliferative activity of the *Myd88*^{L252P} mutation extends into later stages of B-cell differentiation.

The Hoxb8 system has been widely used to study various aspects of immune cell biology, including lymphoma development and progression. Our finding demonstrated that the *CXCR4*^{C1030G}*; MYD88*^{L265P} collaboration enhanced the differentiation of Hoxb8 cells into B-cell lineage. However, the Hoxb8 system has limitations in fully characterizing the phenotype observed in the *in vivo* model. One of the key limitations is its inability to differentiate further into the plasma cell population. This is important, as plasmacytic differentiation is a hallmark feature of low-grade B-cell lymphoma with plasmacytic differentiation. Therefore, while the

Hoxb8 system provides a valuable tool for studying lymphoma development, its use in characterizing the phenotype observed in vivo should be carefully considered. Despite its limitations, the Hoxb8 system also provides significant benefits in terms of its unlimited expansion potential, which is not possible with in vivo animal models. This allows for the generation of a large number of cells for experimentation and characterization, which is critical in understanding the underlying mechanisms of lymphoma development. Additionally, the Hoxb8 system is highly reproducible and allows for controlled experimentation in a laboratory setting. The *CXCR4*^{C1030G}*; MYD88*^{L265P} Hoxb8 and control cell lines generated in this study are very useful tools for performing high throughput drug screenings and mechanistic studies to further explore the dependency of the mutations on the synergistic engagement of the BCR, CXCL12-CXCR4 and MYD88-dependent TLR signaling.

4.3. *CXCR4*^{C1030G}; *Myd88*^{L252P} mice harbors elevated serum IgM and accelerate an early *Myd88*^{L252P} driven B-cell disorder

It remains uncertain regarding the origin of malignant clones in WM and whether the malignant B-cells in WM are unable to switch Ig isotype from IgM to a different class (IgA or IgG). It is also unclear whether neoplastic B-cell-derived clones have undergone somatic hypermutation but not isotype switching, and retain the capability of plasmacytic differentiation. (Growková et al., 2017; Sahota et al., 2002; Zojer et al., 2003). In our study, we demonstrated that the activation of the mutation by CD19^{Cre} in early B-cells caused a polyclonal, low-grade lymphoproliferative disease accompanied by plasma cell expansion and increasing serum IgM titers (Fig. 10B), whereas the activation of the mutation at the initiation of the GC stage by Aid^{Cre} caused a similar, albeit weaker, phenotype, consistent with a lower number of mutated B-cells, plasma cells, and low serum IgM titers (Fig. 9 and 10A).

Recent studies have shown that the clonal lymphoplasmacytic cell phenotype in WM is consistent with the late stage of B-cell differentiation and is most likely derived from memory B-cells that produce IgM but have not undergone an isotype switch (Kapoor et al., 2015). Moreover, the pathological WM cell population is characterized by aberrant cells of mature

stages of B-cell development as germinal center B-cells, plasmablasts, and plasma or memory cells. In line with this work, we demonstrated what appears to be a competitive advantage of IgM expressing *Myd88*^{L252P} and WHIM-like *CXCR4*^{C1030G} mutated B-cells over normal B-cells, resulting in a larger pool of germinal center B-cells, long-lived plasma cells, and memory B-cells. Previous studies have identified that *CXCR4*^{C1030G} mutation intrinsically and locally promoted germinal center response and PC differentiation (Biajoux et al., 2016). Another study reported the cooperation of oncogenic Myd88 and BCL2 in enhancing reactive splenomegaly and germinal center formation *in vivo* (Flümann et al., 2021). This observation was integrated and recapitulated in our study by the histological analysis results showing an increase in the number and size of germinal centers in CM-19 mice compared to the control genotypes (Fig. 11).

Additional research is required to determine whether the extrafollicular plasma cells that developed preferentially as a result of the engineered mutations, rather than the germinal center reaction, were the cause of the enhanced number of plasma cells observed in the CM19 mice. Further investigation using our model can be used to find the direct link between the IgM M spikes seen in the WM patient and the associated frequently detected clones through proteomics analysis.

4.4. The transcriptional profile associated with *CXCR4*^{C1030G}; *Myd88*^{L252P} mice

In this study, we conducted the first RNA sequencing-based profiling of the transcriptional program in *CXCR4*^{C1030G}*; Myd88*^{L252P} associated B-cell lymphomagenesis. We found that distinguished pathways associated with B-cell cancer biology and DNA repair were enriched, while pathways relating to apoptosis and cell cycle progression were diminished in CM19 bone marrow samples compared to CD19. Notably, spleen samples from CM19 mice showed enrichment of pathways involved in cell cycle progression and proliferation (G2M checkpoint, E2F targets, cell cycle checkpoints, myogenesis) and immune response and inflammation (IL2_STAT5), while, MYC and mTOR signaling pathways were depleted. Analysis of

transcriptomic *CXCR4*^{C1030G}; *Myd88*^{L252P} signature in spleen revealed enrichment of pathway associated with activation of CXCR4/CXCL12 axis and epithelial-mesenchymal transition (Aversa et al., 2017; Oh et al., 2020). Furthermore, the enrichment of oxidative phosphorylation, heme oxidation, and cellular stress signaling pathways observed in the spleen of CM19 mice could be influenced TLR/MYD88 pathway (Bauerfeld et al., 2012; Qi et al., 2022; Zhou et al., 2018).

In previous studies, gene-expression analysis of WM pathological alterations in humans employed healthy cells as control. A total of 171 genes were found to be differentially expressed between the two groups when comparing Waldenström′s macroglobulinemia-B-cells and normal B-cells with 109 genes downregulated in WM-BC and 62 genes upregulated (Gutiérrez et al., 2007). The transgenic mouse model generated in this study would aid in differentiating and benchmarking the WM phenotype. Further analysis should be performed by investigating if the transcriptome data derived from CM-Aid and CM-19 lymphomas co-cluster with data derived from human WM, human GCB- or ABC-DLBCL by performing a cross-species analysis.

Another study that investigated the transcriptional profile of WM cells and classified patients based on their MYD88 and CXCR4 mutational profiles found similarities between patients who had CXCR4^{WHIM} and healthy memory B and circulating B-cells. Patients with MYD88^{L265P}CXCR4^{WHIM} also exhibit diminished differentiation and correspondingly lower gene expression relevant to the conversion of memory B-cells into plasmablasts and plasma cells. Despite the *MYD88*^{L265P} mutation, these patients displayed a pattern similar to that of healthy peripheral B-cells (Hunter et al., 2016). The entire CD19+ cell population from patients and mice was employed in gene expression analysis in our study and previous studies. These analyses include WM cells as well as healthy CD19+ cells and there remains a need for the identification of the best cell population for gene expression analysis. In the future, it would be essential to conduct a gene expression profile of WM plasma cells which would help support conclusions regarding the maturation process and clonality of these cell types.

5. SUMMARY

This study aimed to establish autochthonous models of Waldenström macroglobulinemia with *CXCR4*^{C1030G} and *Myd88*^{L252P} mutations, which mimic the most prevalent mutations observed in WM. To this end, we generated two conditional mouse models to examine the disease's development mechanisms and evaluate cutting-edge therapeutic approaches. Our study primarily focused on investigating the mechanism underlying the collaboration of mutant MYD88 and CXCR4 and its impact on the signaling pathways of B-cell receptor and Toll-like receptor.

We found that the tumor sample taken from the transgenic mice was oligoclonal, suggesting that as WM develops, several cryptic clones may take part in the disease progression. This observation raises important questions regarding the processes that underlie the relevance of partner clones and the various transformation events in WM.

Furthermore, we investigated the immunophenotypic profile of the *CXCR4*^{C1030G}; *Myd88*^{L252P} mice. Our findings suggest that the plasma cell compartment is enriched throughout the transition to symptomatic WM, presenting an immature/plasmablastic phenotype with restricted isotypes of both the Ig heavy and light chains. These lymphoplasmacytic cells were discovered as having intermediate light scatters of cells with features between small B- lymphocytes and plasma cells. This subpopulation lacks high expression of B220 on the surface while expressing high levels of CD138.

Overall, our study provides important insights into the pathogenesis of WM and its precursor state, IgM monoclonal gammopathy of undetermined significance. The role played by plasma cells and plasmablasts in the pathogenesis of Waldenström's disease is less explored, and our study highlights the need for further research in this area. Our autochthonous models of WM can serve as a valuable resource in understanding the pathogenesis of the disease and the development of new therapies. These models can help to identify new therapeutic targets and test the efficacy of new drugs before they are tested in clinical trials.

6. REFERENCE

Aderem, A. U. R. J. (2000). *Toll-like receptors in the induction of the innate immune response.* www.nature.com

Agrawal, A., & Schatz, D. G. (1997). RAG1 and RAG2 Form a Stable Postcleavage Synaptic Complex with DNA Containing Signal Ends in V(D)J Recombination. In *Cell* (Vol. 89).

Akira, S. , T. K. & K. (2001). Akira, S., Takeda, K. & Kaisho. *Nat Immunol*, *2*, 675–680.

Akira Sanjo, S., Ogawa, T., Takeda, Y., Katsuaki Hoshino, K., Takeuchi, O., & Kawai, T. (1999). *Gene Product Lps the Lipopolysaccharide: Evidence for TLR4 as to (TLR4)-Deficient Mice Are Hyporesponsive Cutting Edge: Toll-Like Receptor 4*. http://www.jimmunol.org/content/162/7/3749http://www.jimmunol.org/content/162/7/3749.full#ref-list-1

Alizadeh, A. A., Eisen, M. B., Davis, R. E., Ma, C., Lossos, I. S., Rosenwald, A., Boldrick, J. C., Sabet, H., Tran, T., Yu, X., Powell, J. I., Yang, L., Marti, G. E., Moore, T., Hudson, J., Lu, L., Lewis, D. B., Tibshirani, R., Sherlock, G., … Staudt, L. M. (2000). Distinct types of diffuse large B-cell lymphoma identi®ed by gene expression pro®ling. In *NATURE* (Vol. 403). www.nature.com

Allen, C. D. C., Okada, T., & Cyster, J. G. (2007). Germinal-Center Organization and Cellular Dynamics. In *Immunity* (Vol. 27, Issue 2, pp. 190–202). https://doi.org/10.1016/j.immuni.2007.07.009

Allman, D., Lindsley, R. C., Demuth, W., Rudd, K., Shinton, S. A., & Hardy, R. R. (2001). *Resolution of Three Nonproliferative Immature Splenic B Cell Subsets Reveals Multiple Selection Points During Peripheral B Cell Maturation 1*.

Allman, D., & Pillai, S. (2008). Peripheral B cell subsets. In *Current Opinion in Immunology* (Vol. 20, Issue 2, pp. 149–157). https://doi.org/10.1016/j.coi.2008.03.014

Alouche, N., Bonaud, A., Rondeau, V., Hussein-agha, R., Nguyen, J., Bisio, V., Khamyath, M., Crickx, E., Dulphy, N., Alouche, N., Bonaud, A., Rondeau, V., Hussein-agha, R., & Nguyen, J. (2021). *Hematological disorder associated Cxcr4-gain-of-function mutation leads to uncontrolled extrafollicular immune response Short title : Cxcr4 signaling and the extrafollicular response To cite this version : HAL Id : hal-03314577*.

Anderson, S. M., Tomayko, M. M., Ahuja, A., Haberman, A. M., & Shlomchik, M. J. (2007). New markers for murine memory B cells that define mutated and unmutated subsets. *Journal of Experimental Medicine*, *204*(9), 2103–2114. https://doi.org/10.1084/jem.20062571

Antony, P., Petro, J. B., Carlesso, G., Shinners, N. P., Lowe, J., & Khan, W. N. (2004). *B-cell antigen receptor activates transcription factors NFAT (nuclear factor of activated T-cells) and NF-κB (nuclear factor κB) via a mechanism that involves diacylglycerol*.

Aref, S., Goda, T., & El-Sherbiny, M. (2003). Syndecan-1 in multiple myeloma: Relationship to conventional prognostic factors. *Hematology*, *8*(4), 221–228. https://doi.org/10.1080/1024533031000153630

Attanavanich, K., & Kearney, J. F. (2004). Marginal Zone, but Not Follicular B Cells, Are Potent Activators of Naive CD4 T Cells. *The Journal of Immunology*, *172*(2), 803–811. https://doi.org/10.4049/jimmunol.172.2.803

B H Ye, Cattoretti G, Shen Q, Z. J., Hawe N, de Waard R, Leung C, Nouri-Shirazi M, Orazi A, C. R., Rothman P, Stall AM, Pandolfi PP, & Dalla-Favera R. (1997). The BCL-6 proto-oncogene controls germinal-centre formation and Th2-type inflammation. *Nat Genet.*, *16*(2), 161–170.

Bachelerie, F., Graham, G. J., Locati, M., Mantovani, A., Murphy, P. M., Nibbs, R., Rot, A., Sozzani, S., & Thelen, M. (2014). New nomenclature for atypical chemokine receptors. In *Nature Immunology* (Vol. 15, Issue 3, pp. 207–208). https://doi.org/10.1038/ni.2812

Balabanian, K., Brotin, E., Biajoux, V., Bouchet-Delbos, L., Lainey, E., Fenneteau, O., Bonnet, D., Fiette, L., Emilie, D., & Bachelerie, F. (2012). *Proper desensitization of CXCR4 is required for lymphocyte development and peripheral compartmentalization in mice*. https://doi.org/10.1182/blood-2012

Barrera, J., Raman, D., & Richmond, A. (2001). *Involvement of chemokine receptors in breast cancer metastasis Related papers Role of chemokines in t umor growt h*. www.nature.com

Barry, M., & Bleackley, R. C. (2002). Cytotoxic T lymphocytes: All roads lead to death. In *Nature Reviews Immunology* (Vol. 2, Issue 6, pp. 401–409). European Association for Cardio-Thoracic Surgery. https://doi.org/10.1038/nri819

Bartolomé, R. A., Ferreiro, S., Miquilena-Colina, M. E., Martínez-Prats, L., Soto-Montenegro, M. L., García-Bernal, D., Vaquero, J. J., Agami, R., Delgado, R., Desco, M., Sánchez-Mateos, P., & Teixidó, J. (2009). The Chemokine Receptor CXCR4 and the Metalloproteinase MT1-MMP Are Mutually Required during Melanoma Metastasis to Lungs. *American Journal of Pathology*, *174*(2), 602–612. https://doi.org/10.2353/ajpath.2009.080636

Becker, M., Hobeika, E., Jumaa, H., Reth, M., & Maity, P. C. (2017). CXCR4 signaling and function require the expression of the IgD-class B-cell antigen receptor. *Proceedings of the National Academy of Sciences of the United States of America*, *114*(20), 5231–5236. https://doi.org/10.1073/pnas.1621512114

Biajoux, V., Natt, J., Freitas, C., Alouche, N., Sacquin, A., Hemon, P., Gaudin, F., Fazilleau, N., Espéli, M., & Balabanian, K. (2016). Efficient Plasma Cell Differentiation and Trafficking Require Cxcr4 Desensitization. *Cell Reports*, *17*(1), 193–205. https://doi.org/10.1016/j.celrep.2016.08.068

Blanchet, X., Langer, M., Weber, C., Koenen, R., & von Hundelshausen, P. (2012). Touch of chemokines. *Frontiers in Immunology*, *3*(JUL). https://doi.org/10.3389/fimmu.2012.00175

Blink, E. J., Light, A., Kallies, A., Nutt, S. L., Hodgkin, P. D., & Tarlinton, D. M. (2005). Early appearance of germinal center-derived memory B cells and plasma cells in blood after primary immunization. *Journal of Experimental Medicine*, *201*(4), 545–554. https://doi.org/10.1084/jem.20042060

Blonska, M., & Lin, X. (2009). CARMA1-mediated NF-κB and JNK activation in lymphocytes. *Immunological Reviews*, *228*(1), 199–211. https://doi.org/10.1111/j.1600-065X.2008.00749.x

Bräuninger, A., Spieker, T., Willenbrock, K., Gaulard, P., Wacker, H.-H., Rajewsky, K., Hansmann, M.-L., & Küppers, R. (2001). The Rockefeller University Press • 0022-1007. In *J. Exp. Med* (Vol. 194, Issue 7). http://www.jem.org/cgi/content/full/194/7/927

Buchner, M., & Müschen, M. (2014). Targeting the B-cell receptor signaling pathway in B lymphoid malignancies. In *Current Opinion in Hematology* (Vol. 21, Issue 4, pp. 341–349). Lippincott Williams and Wilkins. https://doi.org/10.1097/MOH.0000000000000048

Burger, J. A., & Peled, A. (2009). CXCR4 antagonists: Targeting the microenvironment in leukemia and other cancers. In *Leukemia* (Vol. 23, Issue 1, pp. 43–52). Nature Publishing Group. https://doi.org/10.1038/leu.2008.299

Burns, K., Janssens, S., Brissoni, B., Olivos, N., Beyaert, R., & Tschopp, J. (2003). Inhibition of interleukin 1 receptor/toll-like receptor signaling through the alternatively spliced, short form of MyD88 is due to its failure to recruit IRAK-4. *Journal of Experimental Medicine*, *197*(2), 263–268. https://doi.org/10.1084/jem.20021790

Cai, X., Chen, Z., Pan, X., Xia, L., Chen, P., Yang, Y., Hu, H., Zhang, J., Li, K., Ge, J., Yu, K., & Zhuang, J. (2014). Inhibition of angiogenesis, fibrosis and thrombosis by tetramethylpyrazine: Mechanisms contributing to the SDF-1/CXCR4 axis. *PLoS ONE*, *9*(2). https://doi.org/10.1371/journal.pone.0088176

Cao, Y., Hunter, Z. R., Liu, X., Xu, L., Yang, G., Chen, J., Patterson, C. J., Tsakmaklis, N., Kanan, S., Rodig, S., Castillo, J. J., & Treon, S. P. (2015). The WHIM-like CXCR4 S338X somatic mutation activates AKT and ERK, and promotes resistance to ibrutinib and other agents used in the treatment of Waldenstrom's Macroglobulinemia. *Leukemia*, *29*(1), 169–176. https://doi.org/10.1038/leu.2014.187

Cariappa, A., Chase, C., Liu, H., Russell, P., & Pillai, S. (2007a). Naive recirculating B cells mature simultaneously in the spleen and bone marrow. *Blood*, *109*(6), 2339–2345. https://doi.org/10.1182/blood-2006-05-021089

Cariappa, A., Chase, C., Liu, H., Russell, P., & Pillai, S. (2007b). Naive recirculating B cells mature simultaneously in the spleen and bone marrow. *Blood*, *109*(6), 2339–2345. https://doi.org/10.1182/blood-2006-05-021089

Cariappa, A., Mazo, I. B., Chase, C., Shi, H. N., Liu, H., Li, Q., Rose, H., Leung, H., Cherayil, B. J., Russell, P., von Andrian, U., & Pillai, S. (2005). Perisinusoidal B cells in the bone marrow participate in T-independent responses to blood-borne microbes. *Immunity*, *23*(4), 397–407. https://doi.org/10.1016/j.immuni.2005.09.004

Casola, S., Otipoby, K. L., Alimzhanov, M., Humme, S., Uyttersprot, N., Kutok, J. L., Carroll, M. C., & Rajewsky, K. (2004). B cell receptor signal strength determines B cell fate. *Nature Immunology*, *5*(3), 317–327. https://doi.org/10.1038/ni1036

Castillo, J. J., Bibas, M., & Miranda, R. N. (2015). *The biology and treatment of plasmablastic lymphoma*. https://doi.org/10.1182/blood-2014-10

Castillo, J. J., Moreno, D. F., Arbelaez, M. I., Hunter, Z. R., & Treon, S. P. (2019). CXCR4 mutations affect presentation and outcomes in patients with Waldenström macroglobulinemia: A systematic review. *Expert Review of Hematology*, 1–9. https://doi.org/10.1080/17474086.2019.1649132

Castillo, J. J., Olszewski, A. J., Kanan, S., Meid, K., Hunter, Z. R., & Treon, S. P. (2015). Overall survival and competing risks of death in patients with Waldenström macroglobulinaemia: An analysis of the Surveillance, Epidemiology and End Results database. *British Journal of Haematology*, *169*(1), 81–89. https://doi.org/10.1111/bjh.13264

Cesar Nunez, Norihiro Nishimoto, G. Larry Cartland, Linda C. Billips, Peter D. Burrows, Hiromi Kubagawa, & Max D. Cooper. (1996). *B Cells Are Generated Throughout life in Humans*. https://doi.org/10.4049/jimmunol.156.2.866

Chaplin, D. D. (2010). Overview of the immune response. *Journal of Allergy and Clinical Immunology*, *125*(2 SUPPL. 2). https://doi.org/10.1016/j.jaci.2009.12.980

Chen, K., & Cerutti, A. (2011). The function and regulation of immunoglobulin D. In *Current Opinion in Immunology* (Vol. 23, Issue 3, pp. 345–352). https://doi.org/10.1016/j.coi.2011.01.006

Cheng AM, Rowley B, Pao W, Hayday A, Bolen B J, & Pawson T. (1995). Syk tyrosine kinase required for mouse viability and B-cell development. *Nature*, *378*.

Choi, Y. H., Burdick, M. D., Strieter, B. A., Mehrad, B., & Strieter, R. M. (2014). CXCR4, but not CXCR7, discriminates metastatic behavior in non-small cell lung cancer cells. *Molecular Cancer Research*, *12*(1), 38–47. https://doi.org/10.1158/1541-7786.MCR-12-0334

Chu, V. T., Berek, C., & Batista, F. (2012). *The establishment of the plasma cell survival niche in the bone marrow*. www.immunologicalreviews.com

Chung, J. B., Silverman, M., & Monroe, J. G. (2003). Transitional B cells: Step by step towards immune competence. In *Trends in Immunology* (Vol. 24, Issue 6, pp. 342–348). Elsevier Ltd. https://doi.org/10.1016/S1471-4906(03)00119-4

Cinamon, G., Zachariah, M. A., Lam, O. M., Foss, F. W., & Cyster, J. G. (2008). Follicular shuttling of marginal zone B cells facilitates antigen transport. *Nature Immunology*, *9*(1), 54–62. https://doi.org/10.1038/ni1542

Cojoc, M., Peitzsch, C., Trautmann, F., Polishchuk, L., Telegeev, G. D., & Dubrovska, A. (2013). Emerging targets in cancer management: Role of the CXCL12/CXCR4 axis. In *OncoTargets and Therapy* (Vol. 6, pp. 1347–1361). https://doi.org/10.2147/OTT.S36109

Cooper, C. R., Pienta, K. J., & Hopkins Medicine, J. (2002). *Use of the Stromal Cell-derived Factor1/CXCR4 Pathway in Prostate Cancer Metastasis to Bone1*. http://cancerres.aacrjournals.org/content/62/6/1832

Cox, M. A., Kahan, S. M., & Zajac, A. J. (2013). Anti-viral CD8 T cells and the cytokines that they love. In *Virology* (Vol. 435, Issue 1, pp. 157–169). https://doi.org/10.1016/j.virol.2012.09.012

Dal Porto, J. M., Gauld, S. B., Merrell, K. T., Mills, D., Pugh-Bernard, A. E., & Cambier, J. (2004). B cell antigen receptor signaling 101. *Molecular Immunology*, *41*(6–7), 599–613. https://doi.org/10.1016/j.molimm.2004.04.008

de Silva, N. S., Simonetti, G., Heise, N., & Klein, U. (2012). The diverse roles of IRF4 in late germinal center B-cell differentiation. In *John Wiley & Sons A/S Immunological Reviews* (Vol. 247).

Décaillot, F. M., Kazmi, M. A., Lin, Y., Ray-Saha, S., Sakmar, T. P., & Sachdev, P. (2011). CXCR7/CXCR4 heterodimer constitutively recruits β-arrestin to enhance cell migration. *Journal of Biological Chemistry*, *286*(37), 32188–32197. https://doi.org/10.1074/jbc.M111.277038

Dillmann, F., Veldwijk, M. R., Laufs, S., Sperandio, M., Calandra, G., Wenz, F., Zeller, W. J., & Fruehauf, S. (2009). Plerixafor inhibits chemotaxis toward SDF-1 and CXCR4-mediated stroma contact in a dose-dependent manner resulting in increased susceptibility of BCR-ABL cell to Imatinib and Nilotinib. *Leukemia and Lymphoma*, *50*(10), 1676–1686. https://doi.org/10.1080/10428190903150847

Dimopoulos, M. A., Tedeschi, A., Trotman, J., García-Sanz, R., Macdonald, D., Leblond, V., Mahe, B., Herbaux, C., Tam, C., Orsucci, L., Palomba, M. L., Matous, J. v., Shustik, C., Kastritis, E., Treon, S. P., Li, J., Salman, Z., Graef, T., & Buske, C. (2018). Phase 3 Trial of Ibrutinib plus Rituximab in Waldenström's Macroglobulinemia. *New England Journal of Medicine*, *378*(25), 2399–2410. https://doi.org/10.1056/nejmoa1802917

Dutton, R. W., Bradley, L. M., & Swain, S. L. (1998). T CELL MEMORY. In *Annu. Rev. Immunol* (Vol. 16). www.annualreviews.org

Edwards, J. C. W., & Cambridge, G. (2006). B-cell targeting in rheumatoid arthritis and other autoimmune diseases. In *Nature Reviews Immunology* (Vol. 6, Issue 5, pp. 394–403). https://doi.org/10.1038/nri1838

Efremov, D. G., Turkalj, S., & Laurenti, L. (2020). Mechanisms of b cell receptor activation and responses to b cell receptor inhibitors in b cell malignancies. In *Cancers* (Vol. 12, Issue 6). MDPI AG. https://doi.org/10.3390/cancers12061396

Esencay, M., Newcomb, E. W., & Zagzag, D. (2010). HGF upregulates CXCR4 expression in gliomas via NF-κB: Implications for glioma cell migration. *Journal of Neuro-Oncology*, *99*(1), 33–40. https://doi.org/10.1007/s11060-010-0111-2

Eter, P., Elves, J. D., & Oitt, V. M. R. (2000). *THE IMMUNE SYSTEM First of Two Parts* (Vol. 343).

Flajnik, M. F. (2002). Comparative analyses of immunoglobulin genes: Surprises and portents. In *Nature Reviews Immunology* (Vol. 2, Issue 9, pp. 688–698). https://doi.org/10.1038/nri889

Flaswinkel, H., & Reth1, M. (1994). Dual role of the tyrosine activation motif of the Ig-a protein during signal transduction via the B cell antigen receptor. In *The EMBO Journal* (Vol. 13, Issue 1).

Fonseca, V. R., Ribeiro, F., & Graca, L. (2019). T follicular regulatory (Tfr) cells: Dissecting the complexity of Tfr-cell compartments. In *Immunological Reviews* (Vol. 288, Issue 1, pp. 112–127). Blackwell Publishing Ltd. https://doi.org/10.1111/imr.12739

Frassanito, M. A., Cusmai, A., Iodice, G., & Dammacco, F. (2001). *Autocrine interleukin-6 production and highly malignant multiple myeloma: relation with resistance to drug-induced apoptosis*. www.bloodjournal.org

Fu È Tterer, K., Wong, J., Grucza, R. A., Chan, A. C., & Waksman, G. (1998). *Structural Basis for Syk Tyrosine Kinase Ubiquity in Signal Transduction Pathways Revealed by the Crystal Structure of its Regulatory SH2 Domains Bound to a Dually Phosphorylated ITAM Peptide*.

Gallwitz, M., Wossning, T., Flemming, A., Schamel, W. W. A., Zü, C., & Reth, M. (2002). Amplification of B Cell Antigen Receptor Signaling by a Syk/ITAM Positive Feedback Loop. In *Molecular Cell* (Vol. 10).

Ganju, R. K., Brubaker, S. A., Meyer, J., Dutt, P., Yang, Y., Qin, S., Newman, W., & Groopman, J. E. (1998). *The-Chemokine, Stromal Cell-derived Factor-1, Binds to the Transmembrane G-protein-coupled CXCR-4 Receptor and Activates Multiple Signal Transduction Pathways**. http://www.jbc.org/

Geisberger, R., Lamers, M., & Achatz, G. (2006). The riddle of the dual expression of IgM and IgD. In *Immunology* (Vol. 118, Issue 4, pp. 429–437). https://doi.org/10.1111/j.1365-2567.2006.02386.x

Geminder, H., Sagi-Assif, O., Goldberg, L., Meshel, T., Rechavi, G., Witz, I. P., & Ben-Baruch, A. (2001). A Possible Role for CXCR4 and Its Ligand, the CXC Chemokine Stromal Cell-Derived Factor-1, in the Development of Bone Marrow Metastases in Neuroblastoma. *The Journal of Immunology*, *167*(8), 4747–4757. https://doi.org/10.4049/jimmunol.167.8.4747

Gerber, P. A., Hippe, A., Buhren, B. A., Müller, A., & Homey, B. (2009). Chemokines in tumor-associated angiogenesis. In *Biological Chemistry* (Vol. 390, Issue 12, pp. 1213–1223). https://doi.org/10.1515/BC.2009.144

Gerondakis, S., & Siebenlist, U. (2010). Roles of the NF-kappaB pathway in lymphocyte development and function. In *Cold Spring Harbor perspectives in biology* (Vol. 2, Issue 5). https://doi.org/10.1101/cshperspect.a000182

Gilbert, L. A., & Hemann, M. T. (2010). DNA damage-mediated induction of a chemoresistant niche. *Cell*, *143*(3), 355–366. https://doi.org/10.1016/j.cell.2010.09.043

Good-Jacobson, K. L., Szumilas, C. G., Chen, L., Sharpe, A. H., Tomayko, M. M., & Shlomchik, M. J. (2010). PD-1 regulates germinal center B cell survival and the formation and affinity of long-lived plasma cells. *Nature Immunology*, *11*(6), 535–542. https://doi.org/10.1038/ni.1877

Gray, P., Dunne, A., Brikos, C., Jefferies, C. A., Doyle, S. L., & O'Neill, L. A. J. (2006). MyD88 adapter-like (Mal) is phosphorylated by Bruton's tyrosine kinase during TLR2 and TLR4 signal transduction. *Journal of Biological Chemistry*, *281*(15), 10489–10495. https://doi.org/10.1074/jbc.M508892200

Grimont, C. N., Castillo Almeida, N. E., & Gertz, M. A. (2021). Current and Emerging Treatments for Waldenström macroglobulinemia. In *Acta Haematologica* (Vol. 144, Issue 2, pp. 146–157). S. Karger AG. https://doi.org/10.1159/000509286

Groves, F. D., Linet, M. S., Travis, L. B., & Devesa, S. S. (2000). *Cancer Surveillance Series: Non-Hodgkin's Lymphoma Incidence by Histologic Subtype in the United States From 1978 Through 1995*. https://academic.oup.com/jnci/article/92/15/1240/2905894

Guerrera, M. L., Tsakmaklis, N., Xu, L., Yang, G., Demos, M., Kofides, A., Chan, G. G., Manning, R. J., Liu, X., Chen, J. G., Munshi, M., Patterson, C. J., Castillo, J. J., Dubeau, T., Gustine, J., Carrasco, R. D., Arcaini, L., Varettoni, M., Cazzola, M., … Hunter, Z. R. (2018). MYD88 mutated and wild-type waldenström's macroglobulinemia: Characterization of chromosome 6q gene losses and their mutual exclusivity with mutations in CXCR4. In *Haematologica* (Vol. 103, Issue 9, pp. e408–e411). Ferrata Storti Foundation. https://doi.org/10.3324/haematol.2018.190181

Guo, F., Wang, Y., Liu, J., Mok, S. C., Xue, F., & Zhang, W. (2016). CXCL12/CXCR4: A symbiotic bridge linking cancer cells and their stromal neighbors in oncogenic communication networks. In *Oncogene* (Vol. 35, Issue 7, pp. 816–826). Nature Publishing Group. https://doi.org/10.1038/onc.2015.139

Hall, J. M., & Korach, K. S. (2003). Stromal cell-derived factor 1, a novel target of estrogen receptor action, mediates the mitogenic effects of estradiol in ovarian and breast cancer cells. *Molecular Endocrinology*, *17*(5), 792–803. https://doi.org/10.1210/me.2002-0438

Hardy, R. R., & Hayakawa, K. (2001). *B CELL DEVELOPMENT PATHWAYS*. www.annualreviews.org

Hardy, R. R., Kincade, P. W., & Dorshkind, K. (2007). The Protean Nature of Cells in the B Lymphocyte Lineage. In *Immunity* (Vol. 26, Issue 6, pp. 703–714). https://doi.org/10.1016/j.immuni.2007.05.013

Hassan, S., Buchanan, M., Jahan, K., Aguilar-Mahecha, A., Gaboury, L., Muller, W. J., Alsawafi, Y., Mourskaia, A. A., Siegel, P. M., Salvucci, O., & Basik, M. (2011). CXCR4 peptide antagonist inhibits primary breast tumor growth, metastasis and enhances the efficacy of anti-VEGF treatment or docetaxel in a transgenic mouse model. *International Journal of Cancer*, *129*(1), 225–232. https://doi.org/10.1002/ijc.25665

Hauser, A. E., Junt, T., Mempel, T. R., Sneddon, M. W., Kleinstein, S. H., Henrickson, S. E. E., von Andrian, U. H., Shlomchik, M. J., & Haberman, A. M. (2007). Definition of Germinal-Center B Cell Migration In Vivo Reveals Predominant Intrazonal Circulation Patterns. *Immunity*, *26*(5), 655–667. https://doi.org/10.1016/j.immuni.2007.04.008

Helbig, G., Christopherson, K. W., Bhat-Nakshatri, P., Kumar, S., Kishimoto, H., Miller, K. D., Broxmeyer, H. E., & Nakshatri, H. (2003). NF-κB promotes breast cancer cell migration and metastasis by inducing the expression of the chemokine receptor CXCR4. *Journal of Biological Chemistry*, *278*(24), 21631–21638. https://doi.org/10.1074/jbc.M300609200

Hernandez, P. A., Gorlin, R. J., Lukens, J. N., Taniuchi, S., Bohinjec, J., Francois, F., Klotman, M. E., & Diaz, G. A. (2003). Mutations in the chemokine receptor gene CXCR4 are associated with WHIM syndrome, a combined immunodeficiency disease. *Nature Genetics*, *34*(1), 70–74. https://doi.org/10.1038/ng1149

Herzog, S., & Jumaa, H. (2012). Self-recognition and clonal selection: Autoreactivity drives the generation of B cells. In *Current Opinion in Immunology* (Vol. 24, Issue 2, pp. 166–172). https://doi.org/10.1016/j.coi.2012.02.004

Herzog, S., Reth, M., & Jumaa, H. (2009). Regulation of B-cell proliferation and differentiation by pre-B-cell receptor signalling. In *Nature Reviews Immunology* (Vol. 9, Issue 3, pp. 195–205). https://doi.org/10.1038/nri2491

Hong, Y., Singh, N., Bamopoulos, S., Gjerga, E., Schmalbrock, L. K., Balabanian, K., Schick, M., Keller, U., & Wirth, M. (2020). Authentication of primary murine cell lines by a microfluidics-based lab-on-chip system. *Biomedicines*, *8*(12), 1–13. https://doi.org/10.3390/biomedicines8120590

Hunter, Z. R., Xu, L., Tsakmaklis, N., Demos, M. G., Kofides, A., Jimenez, C., Chan, G. G., Chen, J., Liu, X., Munshi, M., Gustine, J., Meid, K., Patterson, C. J., Yang, G., Dubeau, T., Samur, M. K., Castillo, J. J., Anderson, K. C., Munshi, N. C., & Treon, S. P. (2018). Insights into the genomic landscape of MYD88 wild-Type Waldenström macroglobulinemia. *Blood Advances*, *2*(21), 2937–2946. https://doi.org/10.1182/bloodadvances.2018022962

Hunter, Z. R., Xu, L., Yang, G., Zhou, Y., Liu, X., Cao, Y., Manning, R. J., Tripsas, C., Patterson, C. J., Sheehy, P., & Treon, S. P. (2014a). The genomic landscape of Waldenström macroglobulinemia is characterized by highly recurring MYD88 and WHIM-like CXCR4 mutations, and small somatic deletions associated with B-cell lymphomagenesis. *Blood*, *123*(11), 1637–1646. https://doi.org/10.1182/blood

Hunter, Z. R., Xu, L., Yang, G., Zhou, Y., Liu, X., Cao, Y., Manning, R. J., Tripsas, C., Patterson, C. J., Sheehy, P., & Treon, S. P. (2014b). The genomic landscape of Waldenström macroglobulinemia is characterized by highly recurring MYD88 and WHIM-like CXCR4 mutations, and small somatic deletions associated with B-cell lymphomagenesis. *Blood*, *123*(11), 1637–1646. https://doi.org/10.1182/blood-2013-09-525808

Hunter, Z. R., Yang, G., Xu, L., Liu, X., Castillo, J. J., & Treon, S. P. (2017). Genomics, signaling, and treatment of Waldenström macroglobulinemia. In *Journal of Clinical Oncology* (Vol. 35, Issue 9, pp. 994–1001). American Society of Clinical Oncology. https://doi.org/10.1200/JCO.2016.71.0814

Igarashi, H., Gregory, S. C., Yokota, T., Sakaguchi, N., & Kincade, P. W. (2002). Transcription from the RAG1 Locus Marks the Earliest Lymphocyte Progenitors in Bone Marrow expressed in multipotent, IL-3-dependent, hematopoi-etic progenitor cell lines (Cross et al., 1994). As another example, Ig (B29), a component and signal transducer. In *Immunity* (Vol. 17).

Jellusova, J., Miletic, A. v., Cato, M. H., Lin, W. W., Hu, Y., Bishop, G. A., Shlomchik, M. J., & Rickert, R. C. (2013). Context-Specific BAFF-R Signaling by the NF-κB and PI3K Pathways. *Cell Reports*, *5*(4), 1022–1035. https://doi.org/10.1016/j.celrep.2013.10.022

Jiménez, C., Sebastián, E., Chillón, M. C., Giraldo, P., Mariano Hernández, J., Escalante, F., González-López, T. J., Aguilera, C., de Coca, A. G., Murillo, I., Alcoceba, M., Balanzategui, A., Sarasquete, M. E., Corral, R., Marín, L. A., Paiva, B., Ocio, E. M.,

Gutiérrez, N. C., González, M., … García-Sanz, R. (2013). MYD88 L265P is a marker highly characteristic of, but not restricted to, Waldenström's macroglobulinemia. *Leukemia*, *27*(8), 1722–1728. https://doi.org/10.1038/leu.2013.62

Kabashima, K., Haynes, N. M., Xu, Y., Nutt, S. L., Allende, M. L., Proia, R. L., & Cyster, J. G. (2006). Plasma cell S1P1 expression determines secondary lymphoid organ retention versus bone marrow tropism. *Journal of Experimental Medicine*, *203*(12), 2683–2690. https://doi.org/10.1084/jem.20061289

Kaifi, J. T., Yekebas, E. F., Schurr, P., Obonyo, D., Wachowiak, R., Busch, P., Heinecke, A., Pantel, K., & Izbicki, J. R. (2005). Tumor-cell homing to lymph nodes and bone marrow and CXCR4 expression in esophageal cancer. *Journal of the National Cancer Institute*, *97*(24), 1840–1847. https://doi.org/10.1093/jnci/dji431

Karasuyama, H., Rollnk, A., Shinkai, Y., Young, F., Alt, F. W., & M&hers', F. (1994). The Expression of V,&5 Surrogate Light Chain in Early Bone Marrow Precursor B Cells of Normal and B Cell-Deficient Mutant Mice. In *Cell* (Vol. 77).

Kawai, T., Adachi, O., Ogawa, T., Takeda, K., & Akira, S. (1999). Unresponsiveness of MyD88-Deficient Mice to Endotoxin responses that are favorable to the host by augmenting microbicidal activities of macrophages, overactivation of macrophages by large amounts of LPS results in TLR2 binds LPS in the presence of LBP and CD14 and induces NF-B activation. Dominant-negative TLR2. In *Immunity* (Vol. 11).

Kim, S. Y., Lee, C. H., Midura, B. v., Yeung, C., Mendoza, A., Hong, S. H., Ren, L., Wong, D., Korz, W., Merzouk, A., Salari, H., Zhang, H., Hwang, S. T., Khanna, C., & Helman, L. J. (2008). Inhibition of the CXCR4/CXCL12 chemokine pathway reduces the development of murine pulmonary metastases. *Clinical and Experimental Metastasis*, *25*(3), 201–211. https://doi.org/10.1007/s10585-007-9133-3

Klein, U., & Dalla-Favera, R. (2008). Germinal centres: Role in B-cell physiology and malignancy. In *Nature Reviews Immunology* (Vol. 8, Issue 1, pp. 22–33). https://doi.org/10.1038/nri2217

Knittel, G., Liedgens, P., Korovkina, D., Seeger, J. M., Al-Baldawi, Y., Al-Maarri, M., Fritz, C., Vlantis, K., Bezhanova, S., Scheel, A. H., Wolz, O.-O., Reimann, M., Schlesner, M., Lohneis, P., R Weber, A. N., TrümperTr, L., Staudt, L. M., Ortmann, M., Pasparakis, M., … Christian Reinhardt, H. (2016). B-cell-specific conditional expression of Myd88 p.L252P leads to the development of diffuse large B-cell lymphoma in mice German International Cancer Genome Consortium Molecular Mechanisms in Malignant Lymphoma by Sequencing Project Consortium. *Blood*, *127*(22), 2732–2741. https://doi.org/10.1182/blood-2015-11

Konopleva, M. Y., & Jordan, C. T. (2011). Leukemia stem cells and microenvironment: Biology and therapeutic targeting. In *Journal of Clinical Oncology* (Vol. 29, Issue 5, pp. 591–599). https://doi.org/10.1200/JCO.2010.31.0904

Kruisbeek, A. M. (1999). Introduction: Regulation of T cell development by the thymic microenvironment. In *MMU NOLOGY* (Vol. 11).

Kurosaki, T., Shinohara, H., & Baba, Y. (2010). B cell signaling and fate decision. In *Annual Review of Immunology* (Vol. 28, pp. 21–55). https://doi.org/10.1146/annurev.immunol.021908.132541

Kwak, K., Akkaya, M., & Pierce, S. K. (2019). B cell signaling in context. In *Nature Immunology* (Vol. 20, Issue 8, pp. 963–969). Nature Publishing Group. https://doi.org/10.1038/s41590-019-0427-9

Kyewski, B., Derbinski, J., Gotter, J., & Klein, L. (2002). Review Review Review. In *TRENDS in Immunology* (Vol. 23, Issue 7). http://immunology.trends.com1471-4906/02/$-seefrontmatter

Laurens P. Kil, Marjolein J. W. de Bruijn, Menno van Nimwegen, Odilia B. J. Corneth, Jan Piet van Hamburg, Gemma M. Dingjan, Friedrich Thaiss, Guus F. Rimmelzwaan, Dirk Elewaut, Dianne Delsing, Pieter Fokko van Loo, & Rudi W. Hendriks. (2012). Btk levels set the threshold for B-cell activation and negative selection ofautoreactive B cells in mice. *Blood*, *119*(16).

Li, J., Wang, X., Zhang, F., & Yin, H. (2013). Toll-like receptors as therapeutic targets for autoimmune connective tissue diseases. In *Pharmacology and Therapeutics* (Vol. 138, Issue 3, pp. 441–451). https://doi.org/10.1016/j.pharmthera.2013.03.003

Liang, Z., Wu, H., Reddy, S., Zhu, A., Wang, S., Blevins, D., Yoon, Y., Zhang, Y., & Shim, H. (2007). Blockade of invasion and metastasis of breast cancer cells via targeting CXCR4 with an artificial microRNA. *Biochemical and Biophysical Research Communications*, *363*(3), 542–546. https://doi.org/10.1016/j.bbrc.2007.09.007

Lin, S. C., Lo, Y. C., & Wu, H. (2010). Helical assembly in the MyD88-IRAK4-IRAK2 complex in TLR/IL-1R signalling. *Nature*, *465*(7300), 885–890. https://doi.org/10.1038/nature09121

Litman, G. W., Anderson, M. K., & Rast, J. P. (1999). EVOLUTION OF ANTIGEN BINDING RECEPTORS. In *Annu. Rev. Immunol* (Vol. 17).

Liu, W., Tolar, P., Song, W., & Kim, T. J. (2020). Editorial: BCR Signaling and B Cell Activation. In *Frontiers in Immunology* (Vol. 11). Frontiers Media S.A. https://doi.org/10.3389/fimmu.2020.00045

Loder, F., Mutschler, B., Ray, R. J., Paige, C. J., Sideras, P., Torres, R., Lamers, M. C., & Carsetti, R. (1999). B Cell Development in the Spleen Takes Place in Discrete Steps and Is Determined by the Quality of B Cell Receptor-derived Signals. In *J. Exp. Med* (Vol. 190, Issue 1). http://www.jem.org

Ma, B., Osborn, M. J., Avis, S., Ouisse, L. H., Ménoret, S., Anegon, I., Buelow, R., & Brüggemann, M. (2013). Human antibody expression in transgenic rats: Comparison of chimeric IgH loci with human VH, D and JH but bearing different rat C-gene regions. *Journal of Immunological Methods*, *400–401*(1), 78–86. https://doi.org/10.1016/j.jim.2013.10.007

Maclennan, I. C. M. (1994). GERMINAL CENTERS Further ANNUAL REVIEWS. In *Annu. Rev. Immunol* (Vol. 12). www.annualreviews.org

Maity, P. C., Blount, A., Jumaa, H., Ronneberger, O., Lillemeier, B. F., & Reth, M. (2015). *B cell antigen receptors of the IgM and IgD classesare clustered in different protein islands that arealtered during B cell activation*. www.SCIENCESIGNALING.org

Maity, P. C., Datta, M., Nicolò, A., & Jumaa, H. (2018). Isotype Specific Assembly of B Cell Antigen Receptors and Synergism With Chemokine Receptor CXCR4. In *Frontiers in Immunology* (Vol. 9). Frontiers Media S.A. https://doi.org/10.3389/fimmu.2018.02988

Maroni, P., Matteucci, E., & Desiderio, M. A. (2007). HGF induces CXCR4 and CXCL12-mediated tumor invasion through Ets1 and NF-κB. *Carcinogenesis*, *28*(2), 267–279. https://doi.org/10.1093/carcin/bgl129

Matthias, P., & Rolink, A. G. (2005). Transcriptional networks in developing and mature B cells. In *Nature Reviews Immunology* (Vol. 5, Issue 6, pp. 497–508). https://doi.org/10.1038/nri1633

Melchers, F. (2015). Checkpoints that control B cell development. *Journal of Clinical Investigation*, *125*(6), 2203–2210. https://doi.org/10.1172/JCI78083

Mu È ller, A., Homey, B., Soto, H., Ge, N., Catron, D., Buchanan, M. E., McClanahan, T., Murphy, E., Yuan, W., Wagner, S. N., Luis Barrerak, J., Mohark, A., Vera Â steguik, E., & Zlotnik, A. (2001). *Involvement of chemokine receptors in breast cancer metastasis*. www.nature.com

Mukaida, N., Sasaki, S. I., & Baba, T. (2014). Chemokines in cancer development and progression and their potential as targeting molecules for cancer treatment. In *Mediators of Inflammation* (Vol. 2014). Hindawi Publishing Corporation. https://doi.org/10.1155/2014/170381

Munshi, M., Liu, X., Chen, J. G., Xu, L., Tsakmaklis, N., Demos, M. G., Kofides, A., Guerrera, M. L., Jimenez, C., Chan, G. G., Hunter, Z. R., Palomba, M. L., Argyropoulos, K. v., Meid, K., Keezer, A., Gustine, J., Dubeau, T., Castillo, J. J., Patterson, C. J., … Yang, G. (2020). SYK is activated by mutated MYD88 and drives pro-survival signaling in MYD88 driven B-cell lymphomas. *Blood Cancer Journal*, *10*(1). https://doi.org/10.1038/s41408-020-0277-6

Nagasawa Takashi, Hirota sejichi, Tachibana Kazunobu, Takakura Nobuyuki, Yoshida Nobuaki, Kikutani Hitoshi, & Kishimoto tadamitsu. (1996). Defects of B-cell lymphopoiesis and bone-marrow myelopoiesis in mice lacking the CXC chemokine PBSF/SDF-1. *Nature*, *382*, 635–638.

Nakamura, A., Ohwada, C., Takeuchi, M., Takeda, Y., Tsukamoto, S., Mimura, N., Nagisa, O. H., Sugita, Y., Tanaka, H., Wakita, H., Aotsuka, N., Matsue, K., Yokote, K., Ohara, O., Nakaseko, C., & Sakaida, E. (2019). Detection of MYD88 L265P mutation by next-generation deep sequencing in peripheral blood mononuclear cells of Waldenström's macroglobulinemia and IgM monoclonal gammopathy of undetermined significance. *PLoS ONE*, *14*(9). https://doi.org/10.1371/journal.pone.0221941

Naumann, U., Cameroni, E., Pruenster, M., Mahabaleshwar, H., Raz, E., Zerwes, H. G., Rot, A., & Thelen, M. (2010). CXCR7 functions as a scavenger for CXCL12 and CXCL11. *PLoS ONE*, *5*(2). https://doi.org/10.1371/journal.pone.0009175

Ngo, H. T., Leleu, X., Lee, J., Jia, X., Melhem, M., Runnels, J., Moreau, A. S., Burwick, N., Azab, A. K., Roccaro, A., Azab, F., Sacco, A., Farag, M., Sackstein, R., & Ghobrial, I. M. (2008). SDF-1/CXCR4 and VLA-4 interaction regulates homing in Waldenstrom macroglobulinemia. *Blood*, *112*(1), 150–158. https://doi.org/10.1182/blood-2007-12-129395

Ngo, V. N., Young, R. M., Schmitz, R., Jhavar, S., Xiao, W., Lim, K. H., Kohlhammer, H., Xu, W., Yang, Y., Zhao, H., Shaffer, A. L., Romesser, P., Wright, G., Powell, J., Rosenwald, A., Muller-Hermelink, H. K., Ott, G., Gascoyne, R. D., Connors, J. M., … Staudt, L. M. (2011). Oncogenically active MYD88 mutations in human lymphoma. *Nature*, *470*(7332), 115–121. https://doi.org/10.1038/nature09671

Niiro, H., & Clark, E. A. (2002). Regulation of B-cell fate by antigen-receptor signals. In *Nature Reviews Immunology* (Vol. 2, Issue 12, pp. 945–956). https://doi.org/10.1038/nri955

Nojima, T., Haniuda, K., Moutai, T., Matsudaira, M., Mizokawa, S., Shiratori, I., Azuma, T., & Kitamura, D. (2011). In-vitro derived germinal centre B cells differentially generate memory B or plasma cells in vivo. *Nature Communications*, *2*(1). https://doi.org/10.1038/ncomms1475

Nomiyama, H., Osada, N., & Yoshie, O. (2013). Systematic classification of vertebrate chemokines based on conserved synteny and evolutionary history. In *Genes to Cells* (Vol. 18, Issue 1, pp. 1–16). https://doi.org/10.1111/gtc.12013

Nutt, S. L., Hodgkin, P. D., Tarlinton, D. M., & Corcoran, L. M. (2015). The generation of antibody-secreting plasma cells. *Nature Reviews Immunology*, *15*(3), 160–171. https://doi.org/10.1038/nri3795

Ochiai, K., Maienschein-Cline, M., Simonetti, G., Chen, J., Rosenthal, R., Brink, R., Chong, A. S., Klein, U., Dinner, A. R., Singh, H., & Sciammas, R. (2013). Transcriptional Regulation of Germinal Center B and Plasma Cell Fates by Dynamical Control of IRF4. *Immunity*, *38*(5), 918–929. https://doi.org/10.1016/j.immuni.2013.04.009

O'Connor, B. P., Raman, V. S., Erickson, L. D., Cook, W. J., Weaver, L. K., Ahonen, C., Lin, L. L., Mantchev, G. T., Bram, R. J., & Noelle, R. J. (2004). BCMA Is Essential for the Survival of Long-lived Bone Marrow Plasma Cells. *Journal of Experimental Medicine*, *199*(1), 91–97. https://doi.org/10.1084/jem.20031330

Odendahl, M., Mei, H., Hoyer, B. F., Jacobi, A. M., Hansen, A., Muehlinghaus, G., Berek, C., Hiepe, F., Manz, R., Radbruch, A., & Dörner, T. (2005). Generation of migratory antigen-specific plasma blasts and mobilization of resident plasma cells in a secondary immune response. *Blood*, *105*(4), 1614–1621. https://doi.org/10.1182/blood-2004-07-2507

Oettinger, M. A., Schatz, D. G., Gorka, C., & Baltimore, D. (1990). *HtlAsd RAG-I1 and RAG-2, Adjacent Genes That Synergistically Activate V(D)J Recombination*. www.sciencemag.org

O'Neill, L. A. J., & Bowie, A. G. (2007). The family of five: TIR-domain-containing adaptors in Toll-like receptor signalling. In *Nature Reviews Immunology* (Vol. 7, Issue 5, pp. 353–364). https://doi.org/10.1038/nri2079

Ono, S. J., Nakamura, T., Miyazaki, D., Ohbayashi, M., Dawson, M., & Toda, M. (2003). Chemokines: Roles in leukocyte development, trafficking, and effector function. In

Journal of Allergy and Clinical Immunology (Vol. 111, Issue 6, pp. 1185–1199). Mosby Inc. https://doi.org/10.1067/mai.2003.1594

Onoue T, Uchida D, Begum NM, Tomizuka Y, Yoshida H, & Sato M. (2006). *Epithelial-mesenchymal transition induced by the stromal cell-derived factor-1/CXCR4 system in oral squamous cell carcinoma cells*.

Otipoby, K. L., Waisman, A., Derudder, E., Srinivasan, L., Franklin, A., & Rajewsky, K. (2015). The B-cell antigen receptor integrates adaptive and innate immune signals. *Proceedings of the National Academy of Sciences of the United States of America*, *112*(39), 12145–12150. https://doi.org/10.1073/pnas.1516428112

Ouk, C., Roland, L., Gachard, N., Poulain, S., Oblet, C., Rizzo, D., Saintamand, A., Lemasson, Q., Carrion, C., & Thomas, M. (2021). Continuous MYD88 Activation Is Associated With Expansion and Then Transformation of IgM Differentiating Plasma Cells. *Frontiers in Immunology*, *12*. https://doi.org/10.3389/fimmu.2021.641692ï

Owen, R. G., Treon, S. P., Al-Katib, A., Fonseca, R., Greipp, P. R., McMaster, M. L., Morra, E., Pangalis, G. A., San Miguel, J. F., Branagan, A. R., & Dimopoulos, M. A. (2003). Clinicopathological definition of Waldenstrom's macroglobulinemia: Consensus panel recommendations from the Second International Workshop on Waldenstrom's Macroglobulinemia. *Seminars in Oncology*, *30*(2), 110–115. https://doi.org/10.1053/sonc.2003.50082

Parekh, S., Ziegenhain, C., Vieth, B., Enard, W., & Hellmann, I. (2016). The impact of amplification on differential expression analyses by RNA-seq. *Scientific Reports*, *6*. https://doi.org/10.1038/srep25533

Patton, D. T., Plumb, A. W., & Abraham, N. (2014). The Survival and Differentiation of Pro-B and Pre-B Cells in the Bone Marrow Is Dependent on IL-7Rα Tyr 449 . *The Journal of Immunology*, *193*(7), 3446–3455. https://doi.org/10.4049/jimmunol.1302925

Perez-Andres, M., Paiva, B., Nieto, W. G., Caraux, A., Schmitz, A., Almeida, J., Vogt, R. F., Marti, G. E., Rawstron, A. C., van Zelm, M. C., van Dongen, J. J. M., Johnsen, H. E., Klein, B., & Orfao, A. (2010). Human peripheral blood B-Cell compartments: A crossroad in B-cell traffic. In *Cytometry Part B - Clinical Cytometry* (Vol. 78, Issue SUPPL. 1). https://doi.org/10.1002/cyto.b.20547

Perlot, T., & Penninger, J. M. (2012). Development and Function of Murine B Cells Lacking RANK. *The Journal of Immunology*, *188*(3), 1201–1205. https://doi.org/10.4049/jimmunol.1102063

Pillai S, & Baltimore D. (1987). Formation of disulphide-linked μ2ω2 tetramers in pre-B cells by the 18K ω-immunoglobulin light chain. *Nature*, *329*, 172–174.

Pillai, S., & Cariappa, A. (2009). The follicular versus marginal zone B lymphocyte cell fate decision. In *Nature Reviews Immunology* (Vol. 9, Issue 11, pp. 767–777). https://doi.org/10.1038/nri2656

Pohl, T., Gugasyan, R., Grumont, R. J., Strasser, A., Metcalf, D., Tarlinton, D., Sha, W., Baltimore, D., & Gerondakis, S. (2002). *The combined absence of NF-B1 and c-Rel reveals that overlapping roles for these transcription factors in the B cell lineage are restricted to the activation and function of mature cells*. www.pnas.org

Poltorak, A., He, X., Smirnova, I., Liu, M. Y., van Huffel, C., Du, X., Birdwell, D., Alejos, E., Silva, M., Galanos, C., Freudenberg, M., Ricciardi-Castagnoli, P., Layton, B., & Beutler, B. (1998). Defective LPS signaling in C3H/HeJ and C57BL/10ScCr mice: Mutations in Tlr4 gene. *Science*, *282*(5396), 2085–2088. https://doi.org/10.1126/science.282.5396.2085

Profitós-Pelejà, N., Santos, J. C., Marín-Niebla, A., Roué, G., & Ribeiro, M. L. (2022). Regulation of B-Cell Receptor Signaling and Its Therapeutic Relevance in Aggressive B-Cell Lymphomas. In *Cancers* (Vol. 14, Issue 4). MDPI. https://doi.org/10.3390/cancers14040860

Redecke, V., Wu, R., Zhou, J., Finkelstein, D., Chaturvedi, V., High, A. A., & Häcker, H. (2013). Hematopoietic progenitor cell lines with myeloid and lymphoid potential. *Nature Methods*, *10*(8), 795–803. https://doi.org/10.1038/nmeth.2510

Richard, K., Pierce, S. K., & Song, W. (2008). The Agonists of TLR4 and 9 Are Sufficient to Activate Memory B Cells to Differentiate into Plasma Cells In Vitro but Not In Vivo. *The Journal of Immunology*, *181*(3), 1746–1752. https://doi.org/10.4049/jimmunol.181.3.1746

Rickert, R. C. (2013). New insights into pre-BCR and BCR signalling with relevance to B cell malignancies. In *Nature Reviews Immunology* (Vol. 13, Issue 8, pp. 578–591). https://doi.org/10.1038/nri3487

Rickert, R. C., Roes, J., & Rajewsky, K. (1997). B lymphocyte-specific, Cre-mediated mutagenesis in mice. In *Nucleic Acids Research* (Vol. 25, Issue 6). Oxford University Press.

Ridderstad, A., & Tarlinton, D. M. (1998). Population as Revealed by CD38 Expression Kinetics of Establishing the Memory B Cell. In *J Immunol References*. http://www.jimmunol.org/content/160/10/46881998;160:4688-4695;;http://www.jimmunol.org/content/160/10/4688.full#ref-list-1

Riera Romo, M., Pérez-Martínez, D., & Castillo Ferrer, C. (2016). Innate immunity in vertebrates: An overview. *Immunology*, *148*(2), 125–139. https://doi.org/10.1111/imm.12597

Rip, J., de Bruijn, M. J. W., Appelman, M. K., Singh, S. P., Hendriks, R. W., & Corneth, O. B. J. (2019). Toll-like receptor signaling drives Btk-mediated autoimmune disease. *Frontiers in Immunology*, *10*(JAN). https://doi.org/10.3389/fimmu.2019.00095

Robbiani, D. F., Bothmer, A., Callen, E., Reina-San-Martin, B., Dorsett, Y., Difilippantonio, S., Bolland, D. J., Chen, H. T., Corcoran, A. E., Nussenzweig, A., & Nussenzweig, M. C. (2008). AID Is Required for the Chromosomal Breaks in c-myc that Lead to c-myc/IgH Translocations. *Cell*, *135*(6), 1028–1038. https://doi.org/10.1016/j.cell.2008.09.062

Romain, B., Hachet-Haas, M., Rohr, S., Brigand, C., Galzi, J.-L., Gaub, M.-P., Pencreach, E., & Guenot, D. (2014). *Hypoxia differentially regulated CXCR4 and CXCR7 signaling in colon cancer*. http://www.molecular-cancer.com/content/13/1/58

Rowley RB, Burkhardt AL, Chao HG, Matsueda GR, & Bolen JB. (1995). Syk protein-tyrosine kinase is regulated by tyrosine-phosphorylated Ig alpha/Ig beta immunoreceptor tyrosine activation motif binding and autophosphorylation. *J Biol Chem*, *270*(19).

Rumfelt, L. L., Zhou, Y., Rowley, B. M., Shinton, S. A., & Hardy, R. R. (2006). Lineage specification and plasticity in CD19- early B cell precursors. *Journal of Experimental Medicine*, *203*(3), 675–687. https://doi.org/10.1084/jem.20052444

Saba, N. F., Wang, Y., Fu, H., Koenig, L., Khuri, F. R., Shin, D. M., & Chen, Z. (Georgia). (2017). Association of Cytoplasmic CXCR4 With Loss of Epithelial Marker and Activation of ERK1/2 and AKT Signaling Pathways in Non–Small-Cell Lung Cancer. *Clinical Lung Cancer*, *18*(3), e203–e210. https://doi.org/10.1016/j.cllc.2016.12.005

Samitas, K., Lötvall, J., & Bossios, A. (2010). B Cells: From early development to regulating allergic diseases. In *Archivum Immunologiae et Therapiae Experimentalis* (Vol. 58, Issue 3, pp. 209–225). https://doi.org/10.1007/s00005-010-0073-2

Sanchez, M., Misulovin, Z., Burkhardt, A. L., Mahajan, S., Costa, T., Franke, R., Bolen, J. B., & Nussenzweig, M. (1993). *Signal Transduction by Immunoglobulin Is Mediated Through Igc~ and Ig~*. http://rupress.org/jem/article-pdf/178/3/1049/1394760/1049.pdf

Sander, S., Calado, D. P., Srinivasan, L., Köchert, K., Zhang, B., Rosolowski, M., Rodig, S. J., Holzmann, K., Stilgenbauer, S., Siebert, R., Bullinger, L., & Rajewsky, K. (2012). Synergy between PI3K Signaling and MYC in Burkitt Lymphomagenesis. *Cancer Cell*, *22*(2), 167–179. https://doi.org/10.1016/j.ccr.2012.06.012

Satpathy, S., Wagner, S. A., Beli, P., Gupta, R., Kristiansen, T. A., Malinova, D., Francavilla, C., Tolar, P., Bishop, G. A., Hostager, B. S., & Choudhary, C. (2015). Systems-wide analysis of BCR signalosomes and downstream phosphorylation and ubiquitylation . *Molecular Systems Biology*, *11*(6), 810. https://doi.org/10.15252/msb.20145880

Schatz, D. G., & Ji, Y. (2011). Recombination centres and the orchestration of V(D)J recombination. In *Nature Reviews Immunology* (Vol. 11, Issue 4, pp. 251–263). https://doi.org/10.1038/nri2941

Schweighoffer, E., Vanes, L., Nys, J., Cantrell, D., McCleary, S., Smithers, N., & Tybulewicz, V. L. J. (2013). The BAFF Receptor Transduces Survival Signals by Co-opting the B Cell

Receptor Signaling Pathway. *Immunity*, *38*(3), 475–488. https://doi.org/10.1016/j.immuni.2012.11.015

Song, H. H., & Cerny, J. (2003). Functional Heterogeneity of Marginal Zone B Cells Revealed by Their Ability to Generate Both Early Antibody-forming Cells and Germinal Centers with Hypermutation and Memory in Response to a T-dependent Antigen. *Journal of Experimental Medicine*, *198*(12), 1923–1935. https://doi.org/10.1084/jem.20031498

Sprent, J., & Surh, C. D. (2002). T cell memory. In *Annual Review of Immunology* (Vol. 20, pp. 551–579). https://doi.org/10.1146/annurev.immunol.20.100101.151926

St´, S., Poulain, S., Roumier, C., Decambron, A., Renneville, A., Herbaux, C., Bertrand, E., Tricot, S., Daudignon, A., Galì Egue-Zouitina, S., Soenen, V., Theisen, O., Grardel, N., Nibourel, O., Roche-Lestienne, C., Quesnel, B., Duthilleul, P., Preudhomme, C., & Leleu, X. (2013). MYD88 L265P mutation in Waldenstrom macroglobulinemia. *Blood*, *121*(22), 4504–4511. https://doi.org/10.1182/blood-2012-06

Sugiyama, T., Kohara, H., Noda, M., & Nagasawa, T. (2006). Maintenance of the Hematopoietic Stem Cell Pool by CXCL12-CXCR4 Chemokine Signaling in Bone Marrow Stromal Cell Niches. *Immunity*, *25*(6), 977–988. https://doi.org/10.1016/j.immuni.2006.10.016

Sun, Y., Cheng, Z., Ma, L., & Pei, G. (2002). β-arrestin2 is critically involved in CXCR4-mediated chemotaxis, and this is mediated by its enhancement of p38 MAPK activation. *Journal of Biological Chemistry*, *277*(51), 49212–49219. https://doi.org/10.1074/jbc.M207294200

Takahashi, Y., Ohta, H., & Takemori, T. (2001). Fas Is Required for Clonal Selection in Germinal Centers and the Subsequent Establishment of the Memory B Cell Repertoire controlled, at least in part, by several antiapoptotic and proapoptotic molecules. Transgenic mice overexpress-ing Bcl-xL and Bcl-2 show an accumulation of low-affin-ity or autoreactive B cells in either the long-lived AFC or the memory compartment, indicating that those types As previously reported (Oliver et al., 1997), more than. In *Immunity* (Vol. 14).

Takemori, T., Kaji, T., Takahashi, Y., Shimoda, M., & Rajewsky, K. (2014). Generation of memory B cells inside and outside germinal centers. In *European Journal of Immunology* (Vol. 44, Issue 5, pp. 1258–1264). Wiley-VCH Verlag. https://doi.org/10.1002/eji.201343716

Tangye, S. G., & Tarlinton, D. M. (2009). Memory B cells: Effectors of long-lived immune responses. In *European Journal of Immunology* (Vol. 39, Issue 8, pp. 2065–2075). Wiley-VCH Verlag. https://doi.org/10.1002/eji.200939531

ten Hacken, E., Gounari, M., Ghia, P., & Burger, J. A. (2019). The importance of B cell receptor isotypes and stereotypes in chronic lymphocytic leukemia. In *Leukemia* (Vol. 33, Issue 2, pp. 287–298). Nature Publishing Group. https://doi.org/10.1038/s41375-018-0303-x

Tomayko, M. M., Steinel, N. C., Anderson, S. M., & Shlomchik, M. J. (2010). Cutting Edge: Hierarchy of Maturity of Murine Memory B Cell Subsets. *The Journal of Immunology*, *185*(12), 7146–7150. https://doi.org/10.4049/jimmunol.1002163

Treon, S. P. (2009). How I treat Waldenström macroglobulinemia. In *Blood* (Vol. 114, Issue 12, pp. 2375–2385). American Society of Hematology. https://doi.org/10.1182/blood-2009-05-174359

Treon, S. P., Gustine, J., Xu, L., Manning, R. J., Tsakmaklis, N., Demos, M., Meid, K., Guerrera, M. L., Munshi, M., Chan, G., Chen, J., Kofides, A., Patterson, C. J., Yang, G., Liu, X., Severns, P., Dubeau, T., Hunter, Z. R., & Castillo, J. J. (2018). MYD88 wild-type Waldenstrom Macroglobulinaemia: differential diagnosis, risk of histological transformation, and overall survival. *British Journal of Haematology*, *180*(3), 374–380. https://doi.org/10.1111/bjh.15049

Treon, S. P., Hunter, Z. R., Branagan, A. R., & Castillo, J. J. (2019). Genomic landscape of Waldenström's macroglobulinemia. *HemaSphere*, *3*, 58–61. https://doi.org/10.1097/HS9.0000000000000228

Treon, S. P., Xu, L., Guerrera, M. L., Jimenez, C., Hunter, Z. R., Liu, X., Demos, M., Gustine, J., Chan, G., Munshi, M., Tsakmaklis, N., Chen, J. G., Kofides, A., Sklavenitis-Pistofidis,

R., Bustoros, M., Keezer, A., Meid, K., Patterson, C. J., Sacco, A., … Castillo, J. J. (2020). Genomic landscape of Waldenström macroglobulinemia and its impact on treatment strategies. *Journal of Clinical Oncology*, *38*(11), 1198–1208. https://doi.org/10.1200/JCO.19.02314

Treon, S. P., Xu, L., Luisa Guerrera, M., Jimenez, C., Hunter, Z. R., Liu, X., Demos, M., Gustine, J., Chan, G., Munshi, M., Tsakmaklis, N., Chen, J. G., Kofides, A., Sklavenitis-Pistofidis, R., Bustoros, M., Keezer, A., Meid, K., Patterson, C. J., Sacco, A., … Castillo, J. J. (2020). Genomic Landscape of WaldenströmWaldenstr¨Waldenström macroglobulinemia and Its Impact on Treatment Strategies. *J Clin Oncol*, *38*. https://doi.org/10.1200/JCO.19

Treon, S. P., Xu, L., Yang, G., Zhou, Y., Liu, X., Cao, Y., Sheehy, P., Manning, R. J., Patterson, C. J., Tripsas, C., Arcaini, L., Pinkus, G. S., Rodig, S. J., Sohani, A. R., Harris, N. L., Laramie, J. M., Skifter, D. A., Lincoln, S. E., & Hunter, Z. R. (2012). MYD88 L265P Somatic Mutation in Waldenström's Macroglobulinemia. *New England Journal of Medicine*, *367*(9), 826–833. https://doi.org/10.1056/nejmoa1200710

Treon SP, Xu L, & Yang G. (2012). MYD88 L265P Somatic Mutation in IgM MGUS. *New England Journal of Medicine*, *367*(23), 2253–2255. https://doi.org/10.1056/nejmc1212050

Varettoni, M., Zibellini, S., Arcaini, L., Boveri, E., Rattotti, S., Pascutto, C., Mangiacavalli, S., Gotti, M., Pochintesta, L., Paulli, M., & Cazzola, M. (2013). MYD88 (L265P) mutation is an independent risk factor for progression in patients with IgM monoclonal gammopathy of undetermined significance. In *Blood* (Vol. 122, Issue 13, pp. 2284–2285). https://doi.org/10.1182/blood-2013-07-513366

Victora, G. D., & Nussenzweig, M. C. (2012). Germinal centers. In *Annual Review of Immunology* (Vol. 30, pp. 429–457). https://doi.org/10.1146/annurev-immunol-020711-075032

Wang, B., Wang, W., Niu, W., Liu, E., Liu, X., Wang, J., Peng, C., Liu, S., Xu, L., Wang, L., & Niu, J. (2014). SDF-1/CXCR4 axis promotes directional migration of colorectal cancer cells through upregulation of integrin αvß6. *Carcinogenesis*, *35*(2), 282–291. https://doi.org/10.1093/carcin/bgt331

Willis, S. N., Good-Jacobson, K. L., Curtis, J., Light, A., Tellier, J., Shi, W., Smyth, G. K., Tarlinton, D. M., Belz, G. T., Corcoran, L. M., Kallies, A., & Nutt, S. L. (2014). Transcription Factor IRF4 Regulates Germinal Center Cell Formation through a B Cell–Intrinsic Mechanism. *The Journal of Immunology*, *192*(7), 3200–3206. https://doi.org/10.4049/jimmunol.1303216

Xu, L., Hunter, Z. R., Yang, G., Zhou, Y., Cao, Y., Liu, X., Morra, E., Trojani, A., Greco, A., Arcaini, L., Varettoni, M., Brown, J. R., Tai, Y. T., Anderson, K. C., Munshi, N. C., Patterson, C. J., Manning, R. J., Tripsas, C. K., Lindeman, N. I., & Treon, S. P. (2013a). MYD88 L265P in Waldenström macroglobulinemia, immunoglobulin M monoclonal gammopathy, and other B-cell lymphoproliferative disorders using conventional and quantitative allele-specific polymerase chain reaction. *Blood*, *121*(11), 2051–2058. https://doi.org/10.1182/blood-2012-09-454355

Xu, L., Hunter, Z. R., Yang, G., Zhou, Y., Cao, Y., Liu, X., Morra, E., Trojani, A., Greco, A., Arcaini, L., Varettoni, M., Brown, J. R., Tai, Y.-T., Anderson, K. C., Munshi, N. C., Patterson, C. J., Manning, R. J., Tripsas, C. K., Lindeman, N. I., & Treon, S. P. (2013b). MYD88 L265P in Waldenström macroglobulinemia, immunoglobulin M monoclonal gammopathy, and other B-cell lymphoproliferative disorders using conventional and quantitative allele-specific polymerase chain reaction. *Blood*, *121*(11), 2051–2058. https://doi.org/10.1182/blood

Yang, G., Zhou, Y., Liu, X., Xu, L., Cao, Y., Manning, R. J., Patterson, C. J., Buhrlage, S. J., Gray, N., Tai, Y.-T., Anderson, K. C., Hunter, Z. R., & Treon, S. P. (2013). A mutation in MYD88 (L265P) supports the survival of lymphoplasmacytic cells by activation of Bruton tyrosine kinase in Waldenström macroglobulinemia. *Blood*, *122*(7), 1222–1232. https://doi.org/10.1182/blood-2012-12

Yang, Q., Bell, J. J., & Bhandoola, A. (2010). T-cell lineage determination. In *Immunological Reviews* (Vol. 238).

Young, R. M., & Staudt, L. M. (2013). Targeting pathological B cell receptor signalling in lymphoid malignancies. In *Nature Reviews Drug Discovery* (Vol. 12, Issue 3, pp. 229–243). https://doi.org/10.1038/nrd3937

Yu, T., Liu, K., Wu, Y., Fan, J., Chen, J., Li, C., Yang, Q., & Wang, Z. (2014). MicroRNA-9 inhibits the proliferation of oral squamous cell carcinoma cells by suppressing expression of CXCR4 via the Wnt/β-catenin signaling pathway. *Oncogene*, *33*(42), 5017–5027. https://doi.org/10.1038/onc.2013.448

Zagzag, D., Krishnamachary, B., Yee, H., Okuyama, H., Chiriboga, L., Ali, M. A., Melamed, J., & Semenza, G. L. (2005). *Stromal Cell-Derived Factor-1A and CXCR4 Expression in Hemangioblastoma and Clear Cell-Renal Cell Carcinoma: von Hippel-Lindau Loss-of-Function Induces Expression of a Ligand and Its Receptor*. www.aacrjournals.org

Zeng, Z., Shi, Y. X., Samudio, I. J., Wang, R. Y., Ling, X., Frolova, O., Levis, M., Rubin, J. B., Negrin, R. R., Estey, E. H., Konoplev, S., Andreeff, M., & Konopleva, M. (2009). Targeting the leukemia microenvironment by CXCR4 inhibition overcomes resistance to kinase inhibitors and chemotherapy in AML. *Blood*, *113*(24), 6215–6224. https://doi.org/10.1182/blood-2008-05-158311

Zhang, Y., Garcia-Ibanez, L., & Toellner, K.-M. (2016). *Regulation of germinal center B-cell differentiation*.

Zheng, W., Xu, Q., Zhang, Y., Xiaofei, E., Gao, W., Zhang, M., Zhai, W., Rajkumar, R. S., & Liu, Z. (2020). Toll-like receptor-mediated innate immunity against herpesviridae infection: a current perspective on viral infection signaling pathways. In *Virology Journal* (Vol. 17, Issue 1). BioMed Central Ltd. https://doi.org/10.1186/s12985-020-01463-2

Zlotnik, A., Burkhardt, A. M., & Homey, B. (2011). Homeostatic chemokine receptors and organ-specific metastasis. In *Nature Reviews Immunology* (Vol. 11, Issue 9, pp. 597–606). https://doi.org/10.1038/nri3049

Zotos, D., & Tarlinton, D. M. (2012). Determining germinal centre B cell fate. In *Trends in Immunology* (Vol. 33, Issue 6, pp. 281–288). https://doi.org/10.1016/j.it.2012.04.003

7. LIST OF TABLES

8. LIST OF FIGURES

9. ACKNOWLEDGMENT

First and foremost, I would like to express my sincere gratitude to Prof. Dr. Ulrich Keller for providing me with the opportunity to work in his group and for his invaluable guidance, counsel, and unwavering support throughout my Ph.D. studies. I am deeply grateful for his patience, motivation, and constructive feedback that has helped me to grow both personally and scientifically, especially during some challenging periods.

I would like to thank Dr. med. Stefan Habringer for his time, support, and discussions that have contributed to the advancement of the project. I am also thankful to Prof. Dr. Robert Oostendorp for accepting me as a graduate student under his supervision and for his valuable feedback and suggestions during the committee meetings.

I am grateful to Prof. Dr. Dirk Haller and Dr. Maike Buchner for accepting to be part of my Ph.D. committee and for their insightful comments and advice on the project. I would like to acknowledge the significant contributions of Prof. Dr. Leticia Quintanilla-Fend, Dr. Irene Gonzalez-Menendez, Dr. Rupert Öllinger, Dr. Markus Thaler, and Dr. Matthias Wirth. Additionally, I express my gratitude to Prof. Karl Balabanian and Prof. Christian Reinhardt for providing the mouse strains, and Prof. Dr. Marc Schmidt-Supprian for generously sharing essential plasmids and cell lines.

I would like to express my gratitude to the members of the animal facility for their excellent care of the mice used in the study. Special thanks go to Veronika Schulze and all the members of AG Keller, past and present, for their support, scientific discussions, and friendly working environment.

I would like to express my gratitude to my friends Yuen Lam Dora Ng, Josephina Doffo, and Stavriani Litsiou for making this journey unforgettable in so many ways and for their unwavering support throughout the Ph.D. program.

Finally, I would like to acknowledge my parents, Prabhakar Prasad Singh and Mridula Singh, and my siblings for their unconditional love, support, and encouragement that have allowed me to pursue my dreams and achieve my goals.